UNIVERSITY OF CALIFORNIA,

IRVINE

Genetic and Chemical Alterations Affecting the Activity of Nitrogenase

DISSERTATION

submitted in partial satisfaction of the requirements for the degree of

DOCTOR OF PHILOSOPHY

in Biological Sciences

by

Jasper Liedtke

Dissertation Committee:

Prof. Dr. Yilin Hu, Chair
Prof. Dr. Markus W. Ribbe
Prof. Dr. Sheryl Tsai

2020

Dedicated to

Science

(as we all are)

Table of Contents

List of figures

List of tables

List of abbreviations

µL	microliter
µM	micromolar
5'-dA	5'-desoxyadenosine
Å	Ångström
ADP	adenosine diphosphate
AlF_4^-	aluminium tetrafluoride
Ar	argon
Arg	arginine
atm	standard atmosphere
ATP	adenosine triphosphate
Av	*Azotobacter vinelandii*
C_2H_2	acetylene
C_2H_4	ethylene
C_3H_6	propene
C_3H_8	propane
C_4H_{10}	butane
C_4H_8	butene
Cit	citrate
CN^-	cyanide
CO	carbon monoxide
CODH	CO dehydrogenase
COS	carbonyl sulphide
Cys	cysteine
DFT	density functional theory
DMF	Dimethylformamide
DT	dithionite
e^-	electron
EPR	electron paramagnetic resonance

Eu^{II}-DTPA	europium (II) diethylenetriaminepentaacetic acid
eV	electronvolt
EXAFS	Extended X-Ray Absorption Fine Structure
FMN	flavin mononucleotide
GC-FID	gas chromatograph-flame ionization detector
GHz	gigahertz
Gly	glycine
h	hours
H^+	proton
H_2	hydrogen
H_2O	water
H_2SO_4	sulfuric acid
HCl	hydrochloric acid
His	histidine
HNO_3	nitric acid
ICP-OES	inductively coupled plasma optical emission spectroscopy
ID	inner diameter
IDS	indigo sulfonate
IPTG	Isopropyl β-D-1-thiogalactopyranoside
Isocit	isocitrate
K	Kelvin
kcal	kilocalories
kDa	kilo Dalton
kHz	kilohertz
kJ	kilojoule
L	liter
Ma	*Methanosarcina acetivorans*
mg	milligram
$MgCl_2$	magnesium chloride
Min	minute
mV	millivolt

mW	milliwatt
N_2	dinitrogen
N_2H_2	diazene
N_2H_4	hydrazine
NH_3	ammonia
NH_4^+	ammonium
Nif/*nif*	nitrogen fixation
nm	nanometre
nmol	nanomol
OD	optical density
PDB	protein data bank
P_i	inorganic phosphate
ppm	parts per million
RMSD	root-mean-square deviation
rpm	rotations per minute
SAH	*S*-adenosyl-homocysteine
SAM	S-adenosyl-methionine
SDS-PAGE	sodium dodecyl sulphate–polyacrylamide gel electrophoresis
Ser	serine
TON	turnover number
V	volt
vol	volume
WT	wildtype
XAS	X-ray Absorption Spectroscopy

Acknowledgments

First, I would like to thank my research advisor Prof. Dr. Yilin Hu for providing me with the opportunity to work on such exciting research projects in her lab as well as her financial support during my time at UC Irvine. I would also like to thank Prof. Dr. Ribbe for the initial opportunity to come to Irvine and work in his lab, his efforts to getting me started as a Ph.D. student at UC Irvine, and his scientific advice throughout my studies on nitrogenase.

This work was funded by the National Science Foundation (NSF) CAREER grant, award number CHE-1651398 to Prof. Dr. Yilin Hu, the Department of Energy (DOE) BES grants DE-SC0016510 and DE-SC0014470 to Prof. Dr. Yilin Hu and Prof. Dr. Markus Ribbe, and the University of California, Irvine.

I would also like to thank my third dissertation committee member, Prof. Dr. Sheryl Tsai, who also served on my advancement committee along with Prof. Dr. Melissa Lodoen and Prof. Dr. Michael Mulligan. I am also grateful to Prof. Dr. Melanie Cocco and Prof. Dr. Celia Goulding, who served on my preliminary exam committee. All their scientific advices have also greatly benefitted me throughout my studies at UC Irvine. Furthermore, I would like to thank all professors at UC Irvine who taught me about their respective fields in the classes I took with them. This has further broadened my knowledge and gave me the opportunity to think in different ways about science. Special thanks go to Prof. Dr. Peter Donovan, who also gave me advice outside the classroom. Yoh!

Next, I would like to thank my former advisors at TU Braunschweig, PD Dr. Florian Bittner, who provided me with my first experiences in his lab and has been very supportive of my scientific career from then on, and Prof. Dr. Klemens Rottner, who provided me with the opportunity to work on a fascinating project in his lab, using cutting edge technologies. I also thank Dr. Georgi Dimchev, who was an amazing mentor during my time in Prof. Dr. Rottner's lab and a friend ever since.

A big thank you goes to my past and present co-workers in the Hu and Ribbe labs. Special thanks to Dr. Johannes Rebelein, who first taught me in the lab and welcomed me to UC Irvine, Dr. Martin Stiebritz, who gave me advice on many different topics during countless conversations, Dr. Kazuki Tanifuji, who taught me a lot about chemistry and was always willing to help me with any problem I encountered, Dr. Andrew Jasniewski, who also taught me about

science in general and helped me with all my writing, Dr. Lee Rettberg, who was always a haven of tranquillity and a great friend outside the lab as well, and Dr. Megan Newcomb, who kept me sane and motivated over the last years.

I am also incredibly grateful for all my friends in Irvine, the US, Germany and now around the world. You cannot imagine how much you all helped me along this journey. A special shout out to Andrew, Rachel and Zane, who were an awesome support in so many ways throughout grad school. My biggest gratitude goes to Zippy. You got me into, through and out of this. I could not have done it without you. Love you.

Traditionally, I also thank Arsenal FC at the end of my theses. So thanks for getting me up at 4 AM on Saturdays for disappointing losses, last minute wins and an overall distraction from the world outside. Always Forward.

Finally, I would like to thank my family at home, Annette, Thomas, Felix, Oma, Opa, and Omi. Your continuous support was incredible and always gave me a goal to work towards to.

Curriculum vitae

Jasper Liedtke

Education

September 2016 - December 2020	PhD in Biochemistry at the University of California, Irvine Focus Area: Enzyme production, characterization, and optimization Thesis prepared in the Department of Molecular Biology and Biochemistry
October 2014 - September 2016	Master of Science in Biology at TU Braunschweig Focus Areas: Biochemistry and Cell Biology Thesis prepared at the Zoological Institute, Group of Molecular Cell Biology
October 2015 - February 2016	Internship at the University of California Irvine, Department of Molecular Biology and Biochemistry
October 2011 - August 2014	Bachelor of Science in Biology at TU Braunschweig Thesis prepared at the Institute of Plant Biology, Group of Molecular- and Cell biology

Research Experience

Graduate Researcher September 2016 - present	- Genetic modification of *Escherichia coli* and *Azotobacter vinelandii* strains - Bacterial fermentation at scales up to 200 L - Purification and biochemical characterisation of enzymes - Introduced chemical modifications to enzymes to alter activity and product profiles - Managed multiple research projects in collaboration with other scientists, resulting in scientific publications - Produced organized, detailed laboratory records
Research Assistant March – September 2016	- Successful generation of a B16-F1 knock-out cell line using CRISPR/Cas9 - Characterisation of the mutant cell line using fluorescence and bright-field microscopy
Research Assistant April – August 2014	- Heterologous expression of an enzyme from *Arabidopsis thaliana* in *Escherichia coli* - Purification and biochemical characterisation of the enzyme - Creation of DNA-plasmids for transformation of *Arabidopsis thaliana* with subsequent plant transformation

Publications

Liedtke J, Lee CC, Tanifuji K, Jasniewski A, Ribbe MW, Hu Y. Characterization of a Mo-nitrogenase variant containing a citrate-substituted cofactor. Chembiochem. 2020 Sep 12. doi:10.1002/cbic.202000598

Rettberg LA, Kang W, Stiebritz MT, Hiller CJ, Lee CC, Liedtke J, Ribbe MW, Hu Y. Structural Analysis of a Nitrogenase Iron Protein from Methanosarcina acetivorans: Implications for CO_2 Capture by a Surface-Exposed [Fe_4S_4] Cluster. *mBio*. 2019;10(4):e01497-19. doi:10.1128/mBio.01497-19

Lee CC, Tanifuji K, Newcomb M, Liedtke J, Hu Y, Ribbe MW. A Comparative Analysis of the CO-Reducing Activities of MoFe Proteins Containing Mo- and V-Nitrogenase Cofactors. *Chembiochem*. 2018;19(7):649-653. doi:10.1002/cbic.201800035

Hiller CJ, Stiebritz MT, Lee CC, Liedtke J, Hu Y. Tuning Electron Flux through Nitrogenase with Methanogen Iron Protein Homologues. *Chemistry*. 2017;23(64):16152-16156. doi:10.1002/chem.201704378

Newcomb MP, Lee CC, Tanifuji K, Jasniewski AJ, Liedtke J, Ribbe MW, Hu Y. A V-Nitrogenase Variant Containing a Citrate-Substituted Cofactor. *Chembiochem*. 2020;21(12):1742-1748. doi:10.1002/cbic.201900654

Awards and Certificates

2019	Edward Steinhaus Teaching Award (UC Irvine)
2018	Effective Communication for Scientists (UC Irvine)

Concomitant Activities

September 2019 - August 2020	Organiser for weekly seminars within the Department of Molecular Biology and Biochemistry (UC Irvine)
January 2017 - May 2020	Coordinator for „Science Saturday“ (Outreach program at UC Irvine)
April 2016 - September 2016 and April 2015 - September 2015	Member of the project group „GENau nachgefragt!“ (TU Braunschweig)
October 2013 - March 2014	Mentor for first year biology students (TU Braunschweig)

Teaching Experience

Microbiology UC Irvine, 5 quarters total	Assisted the instructors with creation and grading of exams and gave weekly review presentations
Experimental Microbiology UC Irvine, 6 quarters total	Led labs of 20 students, coordinated their work on various microbiology experiments and graded lab reports
AIDS Fundamentals UC Irvine, 2 quarters total	Assisted instructors with grading of exams and provided weekly office hours for students
Molecular Biology UC Irvine, 1 quarter	Assisted instructor with grading of exams and gave weekly review presentations

Abstract of the Dissertation

Genetic and Chemical Alterations Affecting the Activity of Nitrogenase

By

Jasper Liedtke

Doctor of Philosophy in Biology

University of California, Irvine, 2020

Prof. Dr. Yilin Hu, Chair

The bacterial enzyme nitrogenase regularly catalyses the reduction of dinitrogen (N_2) to ammonia (NH_3), thereby forming bioavailable nitrogen. The same enzyme can also reduce carbon monoxide (CO) to short chain hydrocarbons, turning pollutant gas into biofuel. For both reactions the catalytic NifDK relies on electron supply from the reductase NifH. The electron transfer is mediated by a Fe_4S_4 cluster on NifH, which also enables the reductase protein to perform catalysis of carbon dioxide (CO_2) to CO and short chain hydrocarbons. NifDK utilizes a $MoFe_7S_9C$-(*R*)-homocitrate cluster, termed M-cluster, within its active site for reduction of the respective substrates.

Reduction of CO_2 by NifH from *Methanosarcina acetivorans* was investigated here. For this investigation, the protein was heterologously expressed in *Escherichia coli* and assessed for its ability to reduce CO_2. In contrast to the NiH homologue from *Azotobacter vinelandii*, the most well-studied nitrogenase expressing bacterium, NifH from *M. acetivorans* reduced CO_2 beyond CO to hydrocarbons. To further investigate this advanced catalysis by this NifH protein, specific point mutations of conserved arginine residues in close proximity to the active site on NifH were created. Assessment of the CO_2-reduction capability of these mutant proteins highlighted the need for hydrogen-bonding and proton-donating residues in close proximity to the active site on NifH.

In a different project, the role of (*R*)-homocitrate of the M-cluster of NifDK was investigated. By creating a genetic knockout of the homocitrate-synthase in *A. vinelandii*, (*R*)-homocitrate was made unavailable to the cell. This caused citrate to be integrated during the M-cluster synthesis as the

organic ligand, which led to a lower N_2-reduction but a higher CO-reduction rate by the NifDK^{Cit} protein. *In vitro* maturation of the M-cluster additionally allowed for the integration of isocitrate as the organic ligand of the M-cluster. Upon reconstitution of M-cluster-deficient NifDK with M-cluster^{Isocit}, the enzyme also showed a lower N_2-reduction but an even higher CO-reduction rate than NifDK reconstituted with regular M-cluster or M-cluster^{Cit}.

Chapter 1: Introduction to Nitrogenase

1.1 Overview of Nitrogenase

At 78 %, dinitrogen (N_2) makes up the largest portion of the atmosphere on Earth [1]. While nitrogen is an important cellular component for making nucleic acids and amino acids, it cannot be incorporated into these molecules as N_2 gas due to its strong, relatively inert triple-bond. A conversion is required to turn dinitrogen into a bioavailable form such as ammonia (NH_3), and this requires large amounts of energy to break the triple bond of dinitrogen (945.41 kJ/mol) [2]. In the industrial Haber-Bosch process, dinitrogen is converted into ammonia for fertilizer production, among other things, and this energy is provided as heat and pressure. This results in relatively high costs for the process, which corresponds to about 2 % of the world's energy consumption each year [3]. Billions of years prior to the invention of the Haber-Bosch process, bacteria evolved to carry out the same conversion of dinitrogen to ammonia at ambient conditions by utilizing the enzyme nitrogenase. These diazotrophic bacteria appear freely in the soil or as rhizobia symbionts to plants in legumes, but they can also be found in more extreme habitats in the case of archaea [4]–[6].

Through nitrogen fixation, diazotrophic organisms not only provide themselves with bioavailable nitrogen, they also can supply plants with reduced nitrogen species, especially in the case of symbiotic rhizobia. But this amount of natural fertilizer is not enough to fulfil the demand needed for industrial agricultural crops, and so large quantities of synthetic nitrogen species are required. This makes nitrogenase an interesting research topic, as it provides a biological alternative to the energy-intensive Haber-Bosch process.

The most well studied nitrogenase is the Mo-nitrogenase (short for molybdenum-dependent nitrogenase) from the bacterium *Azotobacter vinelandii* (*A. vinelandii*), named for the molybdenum atom found in its active site cofactor [7], [8]. In addition to this,

molybdenum-independent nitrogenases have also been discovered. These alternative nitrogenases utilize vanadium or iron instead of molybdenum in their cofactor and are therefore termed V-nitrogenase and Fe-nitrogenase, respectively [5], [9], [10].

1.2 Mo-Nitrogenase

The following section provides more information about the well-established Mo-nitrogenase, including the general structure of the nitrogenase machinery and catalytic abilities of the nitrogenase enzyme.

The nitrogenase enzyme consists of two proteins: the catalytic component, NifDK, and the reductive component, NifH. The catalytic nitrogenase protein is a $\alpha_2\beta_2$ heterotetramer, encoded by the *nifD* (55 kDa polypeptide monomer) and *nifK* (50 kDa polypeptide monomer) genes, respectively (Figure 1.1). The active site of the NifDK enzyme binds the M-cluster which is named for the Mo atom contained within the $MoFe_7S_9C$ core and is therefore also referenced as FeMo-cofactor. Furthermore, a Fe_8S_7-cluster called the P-cluster, sits at the interface of the α- and β- subunits. The nitrogenase reductase protein NifH is a homodimer that is encoded by the *nifH* gene (31.5 kDa polypeptide monomer). NifH utilizes a solvent-exposed Fe_4S_4-cluster for electron transfer that is localized at the interface of the two protein monomers, and is held in place by two cysteine residues from each subunit (Cys-97 and Cys-132 in *A. vinelandii*) [11]. Each NifH monomer also binds one molecule of ATP or ADP at the opposite side from the Fe_4S_4-cluster [12]. The binding and hydrolysis of ATP is a required step

in the electron transfer process from the Fe_4S_4-cluster within NifH to the P-cluster inside NifDK [13], [14].

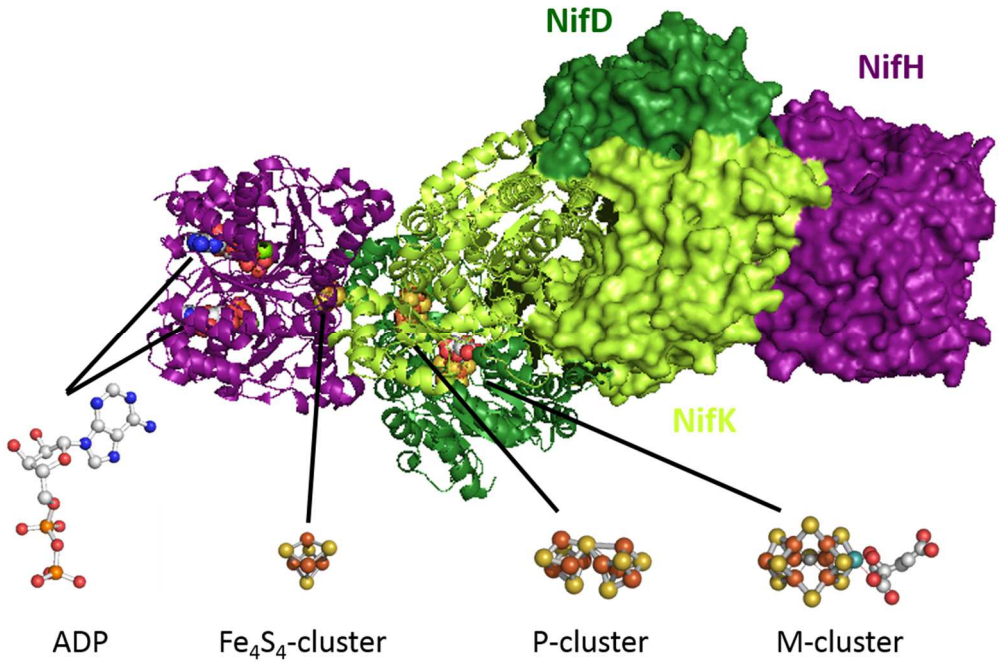

Figure 1.1 Nitrogenase structure: *Displayed is the structure of the nitrogenase complex consisting of the catalytic NifD (forest green) and NifK (lime) subunits and the reductase NifH (purple). The right side is represented as a surface model, while the proteins are presented as cartoons on the left. The cofactors and their locations within the protein complex are shown underneath (carbon (grey), nitrogen (blue), oxygen (red), phosphorous (orange), sulphur (yellow), iron (dark orange) molybdenum (teal)). (PDB: 4WZA)*

For the conversion of N_2 into NH_3, nitrogenase requires protons, a supply of electrons, and ATP. At the same time, hydrogen is generated as by-product. The reaction has the following stoichiometry [15]:

$$N_2 + 8\ e^- + 8\ H^+ + 16\ ATP \rightarrow 2\ NH_3 + H_2 + 16\ ADP + 16\ P_i \qquad \text{(Equation 1.1)}$$

In addition to N_2, nitrogenase is also capable of reducing other small molecules with a triple bond such as carbon monoxide (CO) and acetylene (C_2H_2) [16], [17]. Carbon monoxide

is reduced to short-chain hydrocarbons and water, showing a potential to produce biofuels from pollutant gas. Acetylene is reduced to ethylene (C_2H_4) and this reaction is commonly used to assess the activity of nitrogenase enzymes as quantifying C_2H_4 is easier than quantifying NH_3. During both reactions, protons are reduced to hydrogen as a by-product. The stoichiometry for these substrates has been studied in the past, however the exact stoichiometry for the reduction of CO to hydrocarbons has not been thoroughly established. As with the conversion of N_2 to NH_3, the reduction of CO to hydrocarbons requires electrons, protons, and ATP [16]. This reaction resembles the Fischer-Tropsch process, which forms hydrocarbons and water from CO and hydrogen gas [18].

With the M-cluster buried within the protein, multiple scenarios have been proposed for substrate, proton and electron movement towards the active site. The models for substrate influx are based on molecular dynamic models and experimental inclusion of small molecules, therefore these models only provide suggestions for the enzyme function [19], [20]. A computationally proposed directed proton channel made of water molecules appears to plausibly supply protons for the different catalytic reactions at the M-cluster [21]. This chain of water molecules is stabilized by various residues within NifDK active site as well as the (*R*)-homocitrate of the M-cluster itself.

1.3 Electron Transfer by NifH

NifH receives the electrons through ferredoxin and flavodoxin proteins, the latter also encoded within the *nif*-operon as *nifF*. For the electron transfer, NifF (20 kDa polypeptide) deploys flavin mononucleotide (FMN) and ferredoxin uses Fe_4S_4 clusters [22], [23]. While the loss of one of these two electron donors does not prevent the diazotrophic growth of *A.*

vinelandii cultures *in vivo*, the loss of NifF reduces the nitrogenase activity *in vivo* [24], [25]. A genetic knockout of both, ferredoxin and flavodoxin, led to reduced growth rates of *A. vinelandii* cultures under diazotrophic conditions as well as with NH_4^+ supplied to the medium [26]. This indicates that the loss of one can be partially compensated by the other protein. However, the loss of both proteins appears to affect the general metabolism of the cells rather than only the nitrogen fixation capability. The electron transfer from ferredoxin and flavodoxin to nitrogenase has also been confirmed *in vitro*, using *R. capsulatus* and *K. pneumoniae*, respectively [27], [28]. For the interaction with NifH, both proteins utilize the same binding interface that is employed for the binding of NifH and NifDK during the electron transfer from the Fe_4S_4 cluster on NifH to the P-cluster on NifDK [29]. The interaction of NifH and NifF depends on the nucleotide that is bound. While the distance between Fe_4S_4 cluster and FMN is calculated to be about 9 Å with ATP-bound NifH, this distance decreases to 6.4 Å in ADP-bound NifH. This results in the formation of a more stable complex between NifH-ADP and NifF than NifH-ATP and NifF [30].

As previously described, NifH facilitates the one-electron transfer through its Fe_4S_4 cluster. This Fe_4S_4 cluster is located between the two NifH subunits, ligated by four cysteine residues, and is highly solvent exposed [11]. The solvent exposure of the Fe_4S_4 cluster depends on the nucleotide state of NifH: in the ATP-bound state, the Fe_4S_4 cluster is more exposed and can be chelated easily [31]. With ADP bound, the chelation is less effective because the Fe_4S_4 cluster is less solvent exposed [31]. The Fe_4S_4 cluster on NifH can support three oxidation states: 2+, 1+ and 0 (also termed the all-ferrous state) [32], [33]. The 2+/1+ redox couple is thought to be physiologically relevant, with a redox potential of -300 mV in the nucleotide-free, -400 mV in the ATP-bound, and -490 mV in the ADP-bound state [34], [35]. The 1+/0 redox couple on the contrary has two different reported redox potentials: while it has been

determined to -460 mV by Watt and colleagues [32], [36], others measure the redox potential to be -790 mV and thereby questioning if it is physiologically possible to obtain [37]. Upon formation of a NifH and NifDK complex (Figure 1.2), the redox potential of the Fe_4S_4 cluster decreases by about 200 mV to -620 mV. This is likely caused by the exclusion of water between the two proteins, contributing to the desolvation of the Fe_4S_4 cluster [38], [39].

The binding geometry of NifH towards NifDK is also dependent on nucleotide binding [12]. The binding of ATP-bound NifH to NifDK results in a conformation which places the Fe_4S_4 cluster on NifH and the P-cluster on NifDK about 23 Å apart. At the same time, Lys10 and Asp129 of NifH get within close proximity with the nucleotides of the opposing half within NifH, facilitating the hydrolysis of ATP to ADP + P_i [40]. The ADP-bound NifH then takes a slightly different conformation, bringing the Fe_4S_4 cluster to a closer proximity of about 18 Å with the P-cluster [12]. This reduced distance between the two FeS clusters is proposed to improve the electron transfer from Fe_4S_4 cluster on NifH to the P-cluster on NifDK by making it faster. The interaction between NifH and NifDK is concluded by the release of P_i, which has been determined to be the rate-limiting step in electron transfer [41]. Afterwards, NifH dissociates from NifDK and is regenerated by the reduction by NifF and the exchange of ADP for ATP.

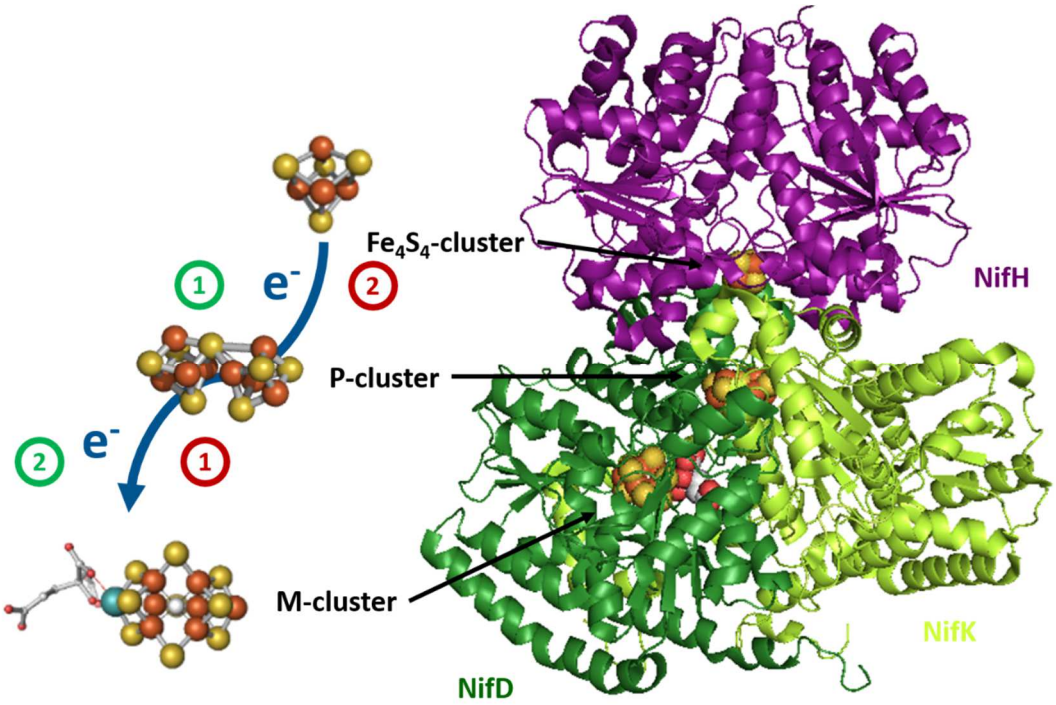

Figure 1.2 Electron transport within the nitrogenase complex: *Displayed is one half of the tetrameric NifDK (forest green and lime, respectively) in complex with NifH (purple). Additionally, ball and stick models of the clusters involved in electron transport are shown on the left (carbon (grey), nitrogen (blue), oxygen (red), phosphorous (orange), sulphur (yellow), iron (dark orange) molybdenum (teal)). Green numbers: The Fe_4S_4 cluster of NifH transfers an electron to the P-cluster within NifDK. From the P-cluster the electron is further passed on to the M-cluster at the active site of the enzyme. Red numbers: In the deficit spending model, the P-cluster first transfers one electron to the M-cluster. In the second step, the P-cluster then receives an electron from the Fe_4S_4 cluster* [42]*. (PDB: 4WZA)*

1.4 Electron Transport Within NifDK

The subsequent section describes the electron transfer from the P-cluster to the M-cluster with in NifDK as well as the step-wise electron acquisition of the M-cluster leading up to the substrate reduction.

The P-cluster functions as a mediator for electron transport from the Fe_4S_4 cluster on NifH to the eventual destination, the M-cluster, on NifDK. For this purpose, the P-cluster on NifDK can occupy different oxidations states: P^N, P^{1+}, P^{2+} and P^{3+}. The P^N/P^{1+} and P^{1+}/P^{2+} redox couples display very similar midpoint potentials around -307 mV which further decreases by -

80 mV upon complex formation of NifDK and NifH. The P^{3+} state displays a redox potential of +90 mV, but it is not clear whether this state is relevant during catalysis [38], [43]. The P-cluster is bound by six cysteine residues (Cys-α62, Cys-α88 and Cys-α154 and Cys-β70, Cys-β95 and Cys-β153 in *A. vinelandii*) and a serine residue (Ser-β188) in the oxidized state (Figure 1.3). Under this condition, the P-cluster resembles the shape of a standard Fe_4S_4-cubane and a deformed Fe_4S_3-unit. The reduction of the P-cluster results in dissociation of two Fe atoms from Cys-α88 and Ser-β188 and a subsequent conformational change which results in fusion of the two Fe_4S_4-cubane clusters through a common S atom [44], [45]. From this reduced state, the P-cluster can transfer one electron to the M-cluster over a distance of about 14 Å.

Two different models for the order in which the P-cluster receives electrons from the Fe_4S_4 cluster and donates them to the M-cluster have been proposed. The "sequential" model describes electron transfer, first from the Fe_4S_4 cluster on NifH to the P-cluster on NifDK, and in a second step from the P-cluster to the M-cluster (Figure 1.2, green numbers). However, this model would require the reduction of the P-cluster in the resting P^N state beyond the ferrous oxidation state to a P^S state. This P^S state has not yet been observed, which raises questions about the validity of the sequential model [46], [47]. The "deficit spending" model describes a process in which the P-cluster first transfers an electron to the M-cluster, and then receives an electron from the Fe_4S_4 cluster on NifH (Figure 1.2, red number). In the deficit spending model, the first electron transfer from P- to M-cluster is supposed to occur at a lower rate, making this electron transfer the rate-limiting step of the electron transport to the M-cluster [42].

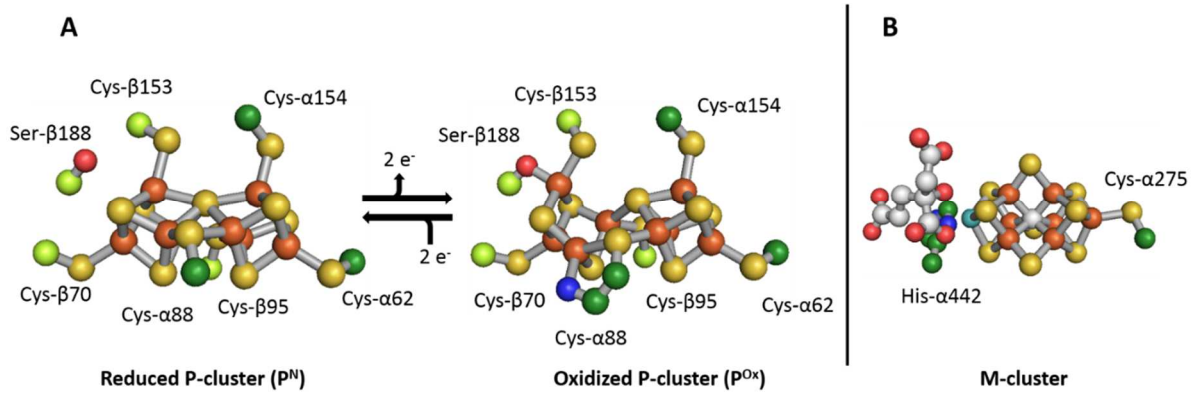

Figure 1.3 P-cluster and M-cluster coordination by surrounding amino acids: *A – The P-cluster within NifDK is displayed together with the amino acids holding it in place (Cys-α62, Cys-α88, Cys-α154 (all in forest green), Cys-β70, Cys-β95, Cys-β153 and Ser-β188 (all in lime)) (reduced P-cluster: PDB: 4WZA; oxidized P-cluster: PDB: 2MIN). B – The M-cluster within NifDK is ligated by His-α442 and Cys-α275. (PDB: 4WZA)*

The M-cluster is located 10 Å beneath the surface of the α-subunit [44]. The full composition of the M-cluster is $MoFe_7S_9C$-(*R*)-homocitrate, where the inorganic cluster displays the major part of the cluster and the organic (*R*)-homocitrate is only coordinated to the molybdenum atom. A histidine residue (His-α442) ligates the M-cluster on one side to the molybdenum atom and a cysteine residue (Cys-α275) ligates the terminal Fe atom on the opposite side (Figure 1.3, right half) [48]–[51]. The M-cluster displays a midpoint potential of -42 mV, which changes to -290 mV and -490 mV in a step-wise reduction of the M-cluster [43], [52].

Each docking event by NifH delivers one electron to the catalytic NifDK (Figure 1.2). These electrons are directed to the M-cluster at the active site of the enzyme. As shown in equation 1, eight electrons are required to fully convert N_2 to two NH_3 and produce an H_2 molecule. A model for the stepwise accumulation of electrons and the reduction of N_2 as well as H^+ has been developed by Lowe and Thorneley [53]–[57]. In this model, the step-wise accumulation of the first four electrons is accompanied by the recruitment of one H^+ per

electron. The results are intermediate states (E_n, where n = number of e^- and H^+ acquired), which can fall back two steps by the release of H_2, for example from the E_3 to the E_1 state (Figure 1.4). After the acquisition of four electrons and H^+ (E_4 state), the so-called Janus-state is formed which can either fall back two steps through the release of H_2 (to the E_2 state) or accept a N_2 molecule to start NH_3-formation [58]. When N_2 binds it also causes the release of one H_2 molecule and is reduced to diazene (N_2H_2). With the addition of further four electrons and protons, two NH_3 molecules are formed which are released from the active site. Two models are plausible for the release of NH_3: Either the two nitrogen atoms get simultaneously reduced, forming hydrazine (N_2H_4) as an intermediate and released as NH_3 after the addition of the 7^{th} and 8^{th} electron and proton (Figure 1.4, (A)). Or one nitrogen atom is fully reduced and released after the addition of the 5^{th} electron and proton before the second nitrogen atom is reduced and released as NH_3 after the addition of the 8^{th} electron and proton (Figure 1.4, (B)). Releasing the second NH_3 brings the enzyme back to the starting point of the Lowe-Thorneley model.

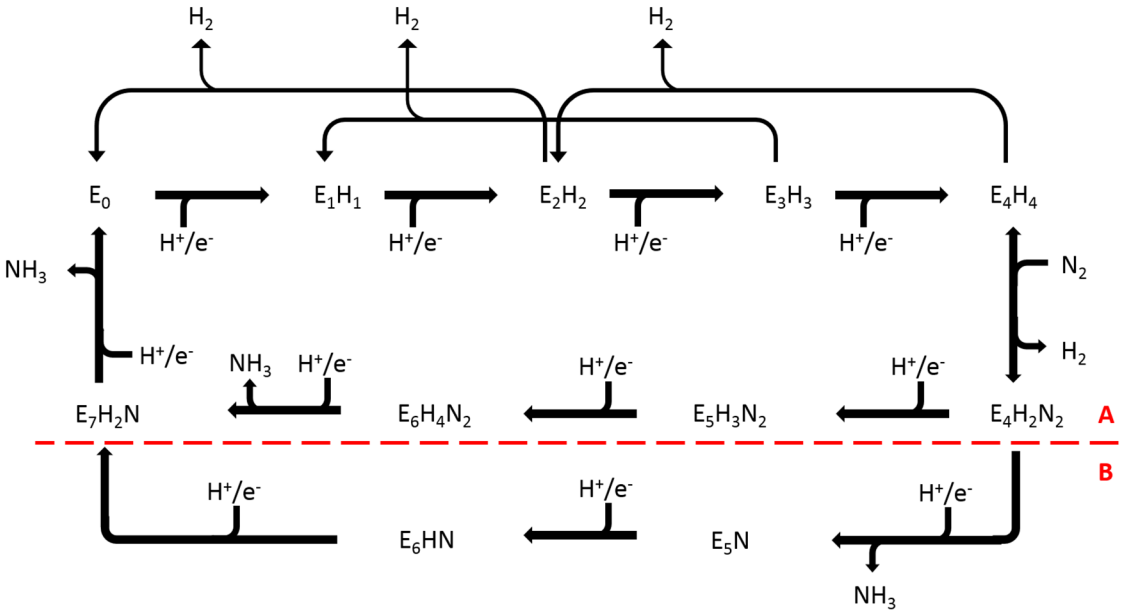

Figure 1.4 Lowe-Thorneley model: *Displayed is the electron and proton accumulation after Lowe and Thorneley. Here, electrons and protons are added in a step-wise manner until four electrons and protons are accumulated at the E_4-state. Next, the addition of nitrogen displaces two protons, which are released as H_2. Two models of nitrogen release are possible from this stage on. (A) Either both nitrogen atoms get reduced simultaneously, which leads to release of ammonia after the E_6 and after the E_7 state. (B) Or one nitrogen atom gets fully reduced and released as ammonia first (after the E_4 state) before the second nitrogen atom gets reduced and released after the E_7 state. During the acquisition of the first four electrons and protons, two protons together with two electrons can be released in the form of H_2, which sets back the model by two steps.*

1.5 Cluster Biosynthesis

The complex cofactors utilized by the nitrogenase system are unique to this enzyme and require a unique assembly machinery.

Iron-sulphur clusters are commonly used in a range of proteins throughout all kinds of organisms [59]. Within the nitrogenase system, iron-sulphur clusters also serve as precursors for the P- and M-cluster located inside NifDK. Therefore, diazotrophic bacteria evolved to have an extra set of iron-sulphur cluster genes within the *nif* operon. These proteins are termed NifU (33 kDa polypeptide) and NifS (44 kDa polypeptide) and are the first parts of a complex cluster biosynthesis pathway. NifS possess cysteine-desulfurase activity, enabling it to cleave

sulphur off cysteine, converting it into alanine [60]. The sulphur obtained is used on NifU together with iron to form Fe_4S_4-clusters [61], [62] (Figure 1.5). While NifU was shown to be crucial for diazotrophic growth in *A. vinelandii,* deletion of NifS resulted in reduced bacterial growth, which was also observed in *Klebsiella pneumoniae* (*K. pneumoniae*). *In vitro* studies confirmed this, by showing a ~95 % reduction of NifH activity and ~75 % reduction of NifDK activity for the loss of either *nifU* or *nifS* genes. The loss of both genes together almost completely eliminated NifH activity and reduced NifDK activity to 10 % [63]–[65]. Beside these iron-sulphur cluster forming proteins, the bacteria also encode a different iron-sulphur cluster assembly machinery, termed ISC (for iron-sulphur cluster), which supplies enzymes for general metabolism with such cofactors [66]. The nomenclature for these homologues is similar to the *nif* genes, where IscS is a desulfurase and IscU assembles FeS-clusters. Although NifS and IscS both display desulfurase activity, they are not capable of compensating the loss of the other, assessed by the ability of a strain to grow under diazotrophic conditions. Physiological levels of NifU and IscU were also not enough to restore the loss of the respective other protein. Only under overexpressing conditions was a partial rescue by NifU or IscU possible [67], [68]. This shows a necessity and specificity of the NifU and NifS proteins for the assembly of a functional nitrogenase complex

The P-cluster on NifDK also originates from two Fe_4S_4-clusters, but no direct evidence for the supply by NifU and NifS has been reported yet. P-cluster formation takes place *in situ* on the NifDK enzyme and is proposed to start with two Fe_4S_4 clusters, the so-called P*-state [69], [70]. This state can be confirmed by the presence of a $S = 1/2$ EPR-signal in perpendicular mode ($g = 2$), which is characteristic for Fe_4S_4 clusters [71]. Interestingly, addition of isolated M-cluster to apo-NifDK in the P*-state is not sufficient to activate the enzyme for substrate reduction. Instead the assistance of NifH is required to mature the P*-cluster into the

functional P-cluster [72], [73] (Figure 1.5). This can be monitored by the change of the *S* = 1/2 EPR-signal in perpendicular mode (*g* = 2) to a EPR-signal in parallel mode (*g* = 11.8) [71]. Furthermore, the P-cluster maturation results in an increased surface exposure of Cys-α275, which facilitates the incorporation of the M-cluster, and also a conformational change of the NifDK protein, bringing the α- and β-subunits into a more compact conformation [74], [75]. For this maturation, NifH must hydrolyse ATP, while the presence of a functional Fe_4S_4-cluster on NifH appears not to be essential for the formation of P-cluster [76], [77]. In addition to this, the chaperone protein NifZ (18 kDa polypeptide), encoded by the *nifZ* gene, is required for maturation of both P-clusters on NifDK. Strains lacking the *nifZ* gene produce a heterogeneous NifDK, displaying the regular P-cluster EPR-signal in parallel mode as well as the *S* =1/2 signal in perpendicular mode, indicative of two separate Fe_4S_4 clusters [78], [79]. This led to the model of a stepwise P-cluster formation in which NifZ precedes NifH in the maturation of the second P-cluster (Figure 1.5) [80].

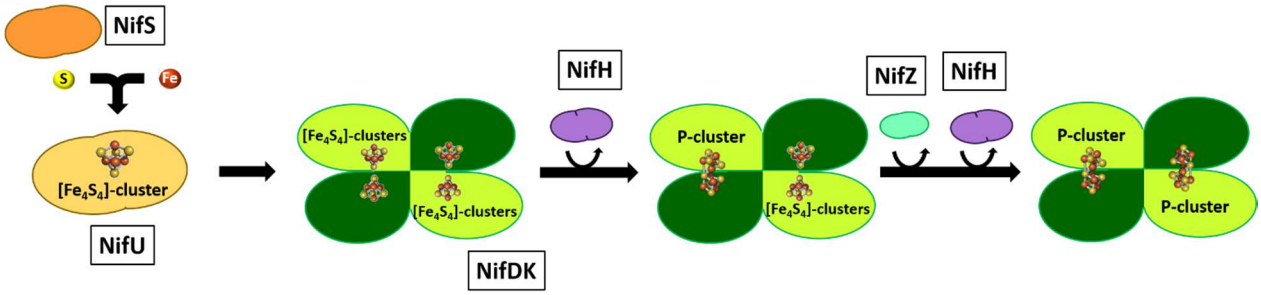

Figure 1.5 P-cluster Formation: *Presented is a schematic representation of the first steps in synthesis of nitrogenase-related FeS-clusters. NifU (light orange) receives sulphur (S) from NifS (orange) and iron (Fe) to form Fe_4S_4 clusters. These Fe_4S_4 clusters can be passed on to NifDK (forest green and lime) to form the P-cluster. NifH and NifZ support the maturation of the Fe_4S_4 clusters to P-clusters.*

The Fe_4S_4 clusters formed by NifU and NifS are also used in the synthesis of the M-cluster by NifB (54 kDa polypeptide) [81], [82]. This protein, encoded by the *nifB* gene, is an important part of M-cluster biosynthesis, as its absence results in M-cluster-deficient NifDK

[83], [84]. For this biosynthesis, NifB combines two Fe_4S_4-clusters, termed the K1- and K2-clusters, an additional sulphur and a carbide to form the L-cluster (Fe_8S_9C), also termed NifB-co, which can stably be extracted from NifB [82], [85] (Figure 1.6). The carbide originates from a methyl group of SAM (*S*-adenosyl-methionine) molecule. During the L-cluster formation, NifB transfers a methyl group from a SAM molecule onto the K2-cluster, producing SAH (*S*-adenosyl-homocysteine) as a by-product. In a second step, proton abstraction from the methyl group onto 5'-dA (5'-desoxyadenosine)-radical creates 5'dAH and incorporates the carbon atom into the intermediate L*-cluster. For this step, a third Fe_4S_4-cluster, termed the SAM-cluster, is required to facilitate the transfer of the methyl group from SAM to the K2-cluster [82], [86], [87]. This carbon is the central atom of the complete M-cluster, which can be traced from the L-cluster on NifB to the M-cluster on NifDK [49], [50], [86], [88]. Because the two K-clusters only provide eight sulphur atoms, a ninth sulphur is required to form the complete [Fe_8S_9C] L-cluster (Figure 1.6). An *in vitro* study indicated that sulphite is the only sulphur source that can be used by NifB during this step, which occurs separately after the carbon insertion [89]. After formation, the L-cluster can already be incorporated by NifDK, which enables the enzyme to reduce C_2H_2 as well as H^+ to C_2H_4 and H_2, respectively, at a reduced rate compared to NifDK containing M-cluster [90]. However, conversion of N_2 to NH_3 could not be observed under these conditions [90]. For complete nitrogenase activity, further modifications of the L-cluster are necessary.

These additional modifications of the L-cluster take place on NifEN. NifEN is a heterotetrameric protein, encoded by *nifE* (52 kDa polypeptide monomer) and *nifN* (49 kDa polypeptide monomer), which displays about 50 % similarity to NifDK [91]–[94]. In line with this similarity, NifEN also has a binding pocket for the M-cluster or its precursor, the L-cluster. It has been proposed that in contrast to NifDK, the M-cluster on NifEN is only held in place by

a cysteine residue (Cys-α25) and is located in closer proximity to the protein surface, shielded only by a stretch of several amino acids (α14-α24). A Fe_4S_4-cluster, termed the O-cluster, on NifEN is analogous to the P-cluster of NifDK. The O-cluster is ligated by four cysteine residues (Cys-α37, Cys-α62, Cys-α124 and Cys-β44) at the interface of the α- and β-subunits [95]. Despite the structural similarity to NifDK, NifEN is not capable of ATP-dependent substrate turnover when incubated with NifH [96].

NifEN is able to receive the L-cluster from NifB [97] (Figure 1.6). This transfer has been proposed to be mediated *in vivo* by NifX, which can bind the L-cluster, but NifX is not required for *in vitro* formation of M-cluster, starting with L-cluster-bound NifB [98], [99]. The first modification of the L-cluster is the replacement of one terminal Fe by Mo, creating an asymmetric construct. The molybdenum is obtained by the cell from the environment in the form of molybdate (MoO_4^{2-}) by utilizing special siderophore compounds. However, this scavenging of Mo can be impaired by tungsten, which can also bind and partially outcompete Mo, and it results in lower nitrogenase activities as shown in *R. capsulatus* [100]. *A. vinelandii*, on the other hand, has evolved to distinguish between the two elements, enabling it to selectively take up molybdate when tungstate is also supplied to the media [101]. *A. vinelandii* then uses a hexameric ($(\alpha\beta)_3$) Mo storage protein, called MoSto, which can bind more than 100 Mo atoms per hexamer [102]. This molybdenum storage occurs even in the presence of NH_4^+ in the media and can stock up to 25 times more Mo than it would be required to efficiently supply nitrogenase with functional M-cluster [103]. To bring Mo to NifEN, diazotrophic organisms potentially use the protein NifQ (22 kDa polypeptide), encoded by *nifQ* [104]. Evidence comes from *nifQ* mutant strains, which show reduced nitrogenase activity. This deficit could be compensated by adding 1000 fold extra Mo to the media [105]. Furthermore, NifQ purportedly carries a $MoFe_3S_4$-cluster that could function as the

intermediate form of Mo during transport to NifEN [106]. During this transport, the molybdenum atom could also be adjusted to the necessary oxidation state in the M-cluster: while molybdenum exists in the form of molybdate (Mo^{6+}) in the environment, it takes a Mo^{3+} state in the M-cluster [107].

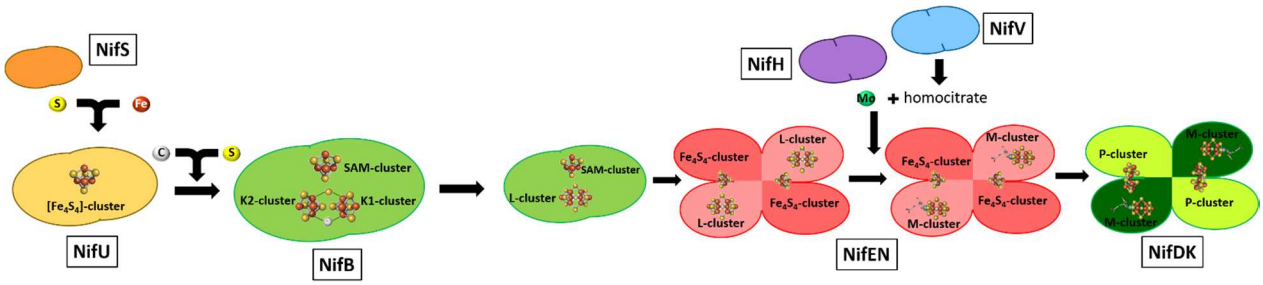

Figure 1.6 M-cluster Formation: *The steps of the M-cluster biosynthesis are schematically presented. NifS (orange) provides sulphur (S) for NifU (light orange), which uses the sulphur and iron (Fe) to form Fe_4S_4-clusters. NifB (green) receives these Fe_4S_4-clusters from NifU as well as a carbide (C) and a sulphur (S) atom to form the L-cluster. The L-cluster is then passed on to NifEN (red and rosé). With the help of NifH (purple) NifEN incorporates a molybdenum (Mo) and (R)-homocitrate, formed by NifV (blue) into the L-cluster to form the final M-cluster. The M-cluster is then passed on to the catalytic NifDK (forest green and lime).*

The second modification of the L-cluster is the addition of (*R*)-homocitrate. The organic ligand was first proposed to be part of the M-cluster by NMR analysis and later confirmed by crystallographic studies of nitrogenase [48], [108]. (*R*)-homocitrate is coordinated to the Mo atom of the cluster via its C2 hydroxyl and carboxyl oxygen atoms. A homocitrate synthase, in addition to the one utilized in leucine biosynthesis and regulated together with other *nif* genes, is responsible for the formation of (*R*)-homocitrate (Figure 1.6). This protein, termed NifV (42 kDa polypeptide), is encoded by the *nifV* gene and plays a crucial role for the activity of the nitrogenase enzyme. Mutant strains lacking a functional *nifV* gene (Δ*nifV*) displayed reduced nitrogenase activity as well as a reduced growth rate under NH_4^+-limiting conditions in *K. pneumoniae* and *A. vinelandii* [64], [109], [110]. Further investigations of Δ*nifV* strains

discovered that citric acid, or citrate, replaces (*R*)-homocitrate on the M-cluster and that addition of (*R*)-homocitrate to the media can rescue the described Δ*nifV* phenotype [111], [112]. *In vitro* studies of L-cluster maturation indicate that NifH could be responsible for delivering (*R*)-homocitrate to NifEN, potentially together with Mo [113]. Further evidence for delivery by one protein comes from another study that indicates that a simultaneous delivery of Mo and (*R*)-homocitrate is required to form a functional M-cluster which can be transferred to NifDK [114].

The formation of the M-cluster can also be facilitated *in vitro*. While initial experiments were performed by using cell extracts of strains lacking NifB or NifE [115], increased understanding of the process has led to a defined composition of proteins and important components such as Mo, reductant, ATP or (*R*)-homocitrate. The reaction can be set up to start with L-cluster formation on NifB, containing Fe_4S_4-cluster reconstituted NifB, apo-NifEN, apo-NifDK, NifH, Mo, (*R*)-homocitrate, SAM, ATP and a reducing agent. The NifB-dependency can also be bypassed with a composition containing either apo-NifEN and isolated L-cluster or holo-NifEN with bound L-cluster together with apo-NifDK, NifH, Mo, (*R*)-homocitrate, ATP-regenerating system and a reducing agent. It is also possible to reconstitute apo-NifDK directly by providing it with isolated M-cluster [99], [113]. The previously mentioned NifQ might only have relevance *in vivo*, as regular *in vitro* maturation of M-cluster does not require NifQ in the solution to produce functional M-cluster. This led to the hypothesis that NifH, present in *in vitro* maturation experiments, functions as a Mo-insertase to NifEN. This was further strengthened by the ability of NifH, isolated from an incubation with molybdenum, to support the *in vitro* M-cluster formation in the absence of added molybdenum to the reaction [113].

Interestingly, the complete M-cluster on NifEN shows a different EPR spectrum compared to M-cluster bound to NifDK, indicating a different spin state of the M-cluster [116]. This goes along with the observed lack of substrate reduction by NifEN containing M-cluster. In order to pass the M-cluster from NifEN to NifDK, diazotrophic microbes use chaperone proteins similar to NifX, which facilitates the transfer of L-cluster from NifB to NifEN [117]. In *K. pneumoniae*, NifY was found to bind to apo-NifDK and the loss of the respective gene, *nifY*, together with the knockout of *nifB,* resulted in a cofactor-deficient NifDK which showed lower activities upon reconstitution with isolated M-cluster. Once NifDK receives the M-cluster, NifY dissociates from the NifDK [118], [119]. A similar chaperone protein was later found in *A. vinelandii*, termed NafY, where naf stands for "nitrogenase associated factor". The loss of this protein only mildly impaired the growth of *A. vinelandii* cultures under regular nitrogen-fixing conditions but caused a stronger growth-related phenotype when no molybdenum source was added to the media. Furthermore, combined loss of *nafY* and *nifB* resulted in an apo-NifDK protein which also showed lower activities upon reconstitution with M-cluster, similar to observations made in *K. pneumoniae* with loss of *nifY* [120]. NafY can bind the M-cluster via its His121-residue and can also interact with Cys-α275 of NifDK, which is responsible for binding the M-cluster on NifDK [121], [122]. However, *in vitro* reconstitution of apo-NifDK does not depend on addition of either chaperone. *In vivo* processes require the assistance of chaperones potentially due to the oxidative lability of the M-cluster, which is less vulnerable in controlled reductive conditions *in vitro*.

1.6 Alternative Nitrogenases

As stated earlier, nitrogenase has alternative, molybdenum-independent variants called V-nitrogenase and Fe-nitrogenase. Similar to the catalytic NifDK protein, the vanadium-

dependent (VnfDGK) and iron-only (AnfDGK) have a heterotetrameric composition, with the addition of a δ-subunit (VnfG or AnfG, respectively). Both alternative nitrogenases share about 30 % sequence similarity to the molybdenum-dependent nitrogenase [123], [124], while VnfDGK and AnfDGK share about 55 % sequence identity [123], [125], [126]. VnfDK and AnfDK also have their respective reductase proteins, named VnfH and AnfH. VnfH shows about 90 % identity to NifH and both VnfH and NifH show about 60 % identity to AnfH [125], [127]. The reductases thereby display a higher level of conservation than their catalytic partners NifDK, VnfDK and AnfDK. In addition to these natural alternative nitrogenases, efforts have been made to incorporate other metals within the active site cofactor. Tungsten was supplied to *A. vinelandii* or *Rhodobacter capsulatus* (*R. capsulatus*) cells and W-incorporation was confirmed in the purified nitrogenase proteins. Although, W-containing nitrogenase can reduce C_2H_2 to C_2H_4 and H^+ to H_2 (in Ar atmosphere) at reduced rates compared to Mo-containing nitrogenase, W-containing nitrogenase cannot reduce N_2 to NH_3 [100], [128].

Both alternative nitrogenases react differently with substrates such as N_2, CO and C_2H_2. The vanadium nitrogenase reduces N_2 at a lower rate than the molybdenum nitrogenase but demonstrates improved production of hydrocarbons from CO. The V-nitrogenase can also make longer hydrocarbons from CO than Mo-nitrogenase [16], [129], [130]. The iron-only nitrogenase fixes N_2 at rates even lower than the vanadium nitrogenase, and no data for CO-reduction have been reported [131].

1.7 Catalytic activities

The last section broaches the issue of the catalytic activity of nitrogenases. Because the Fe-nitrogenase has not been studied to the same extent as the Mo- and V-nitrogenase, only the activities of the latter two are discussed comparatively in more detail in the following paragraph.

The Mo-nitrogenase was discovered as the first of all three nitrogenases and was also found to be the most reactive with respect to the reduction of N_2 to NH_3 with a rate of about 520 nmol NH_3 x min^{-1} x mg $protein^{-1}$ [129]. The V-nitrogenase and Fe-nitrogenase reduce N_2 to NH_3 at lower rates, with 330 and 38 nmol NH_3 x min^{-1} x mg $protein^{-1}$, respectively, if the same ratios of reductase (NifH/VnfH/AnfH) to catalytic unit (NifDK/VnfDK/AnfDK) are utilized. [129], [132]. A reason for this lower NH_3 formation rate is the relative use of electrons directed towards this specific product. While Mo-nitrogenase uses about 80 % of the electrons to form NH_3 and only 20 % to reduce H^+ to H_2, the V-nitrogenase 63 % of the electrons for NH_3 and 37 % for H_2 formation The Fe-nitrogenase uses 50 % of the electrons for each product, making it the most inefficient of the three in terms of NH_3 formation from N_2 [133]. Another difference in the reactivity towards N_2 is the formation of hydrazine (N_2H_4) as a product by V-nitrogenase [134]. This compound can be further reduced to NH_3 by the Mo-nitrogenase, but not by V-nitrogenase, if supplied as the substrate [135], [136].

As stated earlier, in the absence of any substrate, nitrogenase reduces H^+ to H_2. This can be carried out in an Argon atmosphere to assess the general reductive capability of the enzyme. Under these conditions, Mo-nitrogenase forms about 2200 nmol H_2 x min^{-1} x mg $protein^{-1}$, V-nitrogenase about 1400 nmol H_2/min/mg protein and Fe-nitrogenase 253 nmol H_2 x min^{-1} x mg $protein^{-1}$ [129], [131]. These values confirm the trend already described for the

reduction of N_2 to NH_3, where Mo-nitrogenase is the most active and Fe-nitrogenase the least active of the three variants.

Table 1.1 Specific activity values of established reactions catalysed by nitrogenase: *Presented are the products (in nmol x min^{-1} x mg $protein^{-1}$) from the reduction of N_2, H^+ (in Ar atmosphere) and C_2H_2 by Mo-, V-, and Fe-nitrogenase from A. vinelandii. Activity assays were conducted containing a ratio of reductase to catalytic subunit of 10:1 and incubated at 30°C* [129], [131], [132], [137], [138]

Substrate gas	N_2	Ar	C_2H_2	
Product	NH_3	H_2	C_2H_4	C_2H_6
$NifDK^{Av}$	520	2200	2000	not detected
$VnfDGK^{Av}$	330	1400	220	5
$AnfDGK^{Av}$	38	253	28	26

When C_2H_2 is supplied as a substrate, the Mo-nitrogenase has the highest rate for reduction of C_2H_2 to C_2H_4 with 2000 nmol C_2H_4 x min^{-1} x mg $protein^{-1}$, compared to V-nitrogenase (220 nmol C_2H_4/min/mg protein) and Fe-nitrogenase (28 nmol C_2H_4/min/mg protein), when the same protein ratios are used [129], [131]. In contrast to Mo-nitrogenase, the V-nitrogenase and Fe-nitrogenase are capable of reducing C_2H_2 further to C_2H_6 at rates of about 5 nmol C_2H_6 x min^{-1} x mg $protein^{-1}$ and 26 nmol C_2H_6 x min^{-1} x mg $protein^{-1}$, respectively [137], [138]. However, C_2H_4 cannot be utilized as a substrate for C_2H_6 formation, at least by V-nitrogenase [139]. During the reduction of C_2H_2, Mo-nitrogenase uses about 90 % of the supplied electrons to form C_2H_4 and only 10 % for the reduction of H^+ to H_2, similar to the ratio during N_2 reduction [7]. V-nitrogenase uses 35 % of electrons to reduce C_2H_2 and 65 % for H_2 formation, Fe-nitrogenase 15 % and 85 %, respectively [132], [140]. Overall, these ratios show a similar trend to the N_2 reduction, where the three enzymes can be ranked from highest to lowest efficiency as Mo-nitrogenase, V-nitrogenase, Fe-nitrogenase.

CO is another substrate for nitrogenase, which can also function as an inhibitor during N_2 or C_2H_2 reduction [7]. For a long time CO had solely been used as an inhibitor of nitrogenase

catalysis, until Lee *et al.* discovered the ability of V-nitrogenase to reduce CO to various hydrocarbons in a reaction similar to the Fischer-Tropsch process [16]. The most abundant products are C_2H_4 and C_2H_6, formed at rates of 32 nmol x min^{-1} x mg $protein^{-1}$ and 1 nmol x min^{-1} x mg $protein^{-1}$, respectively, but also products up to C_4H_8 and C_4H_{10} have been observed [130]. The Mo-nitrogenase on the other hand is not capable of reducing CO to hydrocarbons to the same extent: C_2H_4 (0.025 nmol/min/mg protein) and C_2H_6 are the most abundant products but are formed at much lower rates than by the V-nitrogenase. Furthermore, the variety of products is restricted to C_3-molecules with C_3H_6 and C_3H_8 being the largest formed hydrocarbons [16], [130]. The Fe-nitrogenase has not been assessed for its reactivity towards CO in detail, but it was shown that high CO partial pressure during C_2H_2 reduction shifts the product distribution from C_2H_4 towards C_2H_6, indicating an influence of CO on the catalysis by Fe-nitrogenase in general [141].

Table 1.2 Specific activity values for CO-reduction by nitrogenase: *Listed are the products (in nmol x min^{-1} x mg $protein^{-1}$) formed by Mo- and V-nitrogenase from A. vinelandii with CO as a substrate. Activity assays were conducted containing a ratio of reductase to catalytic subunit of 10:1 and incubated at 30°C* [16], [130] *(n. d. = not detected).*

Substrate gas	CO							
Product	CH_4	C_2H_4	C_2H_6	C_3H_6	C_3H_8	C_4H_8	C_4H_{10}	H_2
$NifDK^{Av}$	n. d.	0.025	0.013	0.0029	0.0059	n. d.	n. d.	1700
$VnfDGK^{Av}$	0.51	32	1	0.043	0.56	0.0021	0.0033	540

1.8 Aims of Dissertation

The heterologous expression of nitrogenase in non-diazotrophic organisms has long been of interest, with the eventual goal of stable nitrogenase expression in crops to circumvent the addition of an artificial nitrogen source through fertilizer. In an attempt to determine the

minimum set of *nif* genes required for a functional nitrogenase, the reductase NifH from *Methanosarcina acetivorans* was selected for heterologous expression in *Escherichia coli*. One potential hurdle of this project could be the missing oxygen protection that nitrogenase proteins usually get in their native, diazotrophic host organisms [7] In addition to this, NifH from *A. vinelandii* has been shown to reduce CO_2 to CO by itself [142]. One goal of this dissertation is to heterologously express NifH and assess it for its biochemical abilities.

While homocitrate, coordinated to Mo on the M-cluster of nitrogenase, has been shown to be a crucial part for nitrogenase activity [113], its role has only been speculated about in the past [21], [112], [143], [144]. For this dissertation, the effect that the organic ligand has on the catalysis of nitrogenase is under investigation. In a previous attempt, the loss of the homocitrate synthase NifV has been investigated, finding that citrate replaces homocitrate in its absence [145]. With new insights into the catalytic abilities of nitrogenase, the change of nitrogenase's organic ligand can provide further knowledge about the reactions catalysed by nitrogenase.

Specific Aim 1: Heterologous expression of nitrogenase reductase NifH from *Methanosarcina acetivorans* in *Escherichia coli*

The diazotrophic archaea *M. acetivorans* possess a nitrogenase system. The reductase NifH from *M. acetivorans* was selected for a heterologous expression in *E. coli* to assess the expression of nitrogenase proteins in non-diazotrophic organisms. Furthermore, the cross-compatibility of reductase and catalytic nitrogenase subunits from bacterial and archaeal origins was investigated.

Specific Aim 2: Investigation of the catalytic properties of the nitrogenase reductase, NifH

The nitrogenase reductase protein, NifH, has been shown to possess adventitious catalytic properties towards the conversion of CO_2 into CO and hydrocarbons. Arginine residues near the Fe_4S_4-cluster are proposed to be involved with this reaction, therefore are of interest. Arginine100 will be selectively mutated and the protein characterised to gain insight into the mechanism of catalysis.

Specific Aim 3: The effect of the organic ligand of the nitrogenase cofactor on catalysis

3.1 *In vivo* investigation: Knocking out the organic ligand synthase in the bacterial strain

A new strain of *Azotobacter vinelandii* will be generated that deletes the gene that encodes the homocitrate synthase called NifV. This should alter the resultant nitrogenase purified from the strain, as homocitrate will not be present.

3.2 *In vitro* investigation: Insertion of isocitrate into the cofactor biosynthesis

An *in vitro* approach can be used to generate a nitrogenase protein with the cofactor having alternative organic cofactor ligand. The properties of the resulting enzyme will be compared to the wild type and *in vivo* altered enzymes.

1.9 References

[1] R. A. Minzner *et al.*, “NASA Technical Report - Defining Constants, Equations, and Abbreviated Tables of the 1975 U.S. Standard Atmosphere,” 1975.

[2] N. N. Greenwood and A. Earnshaw, “Nitrogen,” in *Chemistry of the Elements*, 2nd ed., Elsevier, 1997, pp. 406–415.

[3] R. Schlögl, “Catalytic synthesis of ammonia - A ‘never-ending story’?,” *Angewandte Chemie - International Edition*, vol. 42, no. 18. John Wiley & Sons, Ltd, pp. 2004–2008, 09-May-2003.

[4] E. S. Boyd, A. D. Anbar, S. Miller, T. L. Hamilton, M. Lavin, and J. W. Peters, “A late methanogen origin for molybdenum-dependent nitrogenase,” *Geobiology*, vol. 9, no. 3, pp. 221–232, May 2011.

[5] Raymond J., Siefert J. L., Staples C. R., and Blankenship R. E., “The Natural History of Nitrogen Fixation,” *Mol. Biol. Evol.*, vol. 21, no. 3, pp. 541–554, 2004.

[6] P. R. Hardoim *et al.*, “The Hidden World within Plants: Ecological and Evolutionary Considerations for Defining Functioning of Microbial Endophytes,” 2015.

[7] B. K. Burgess and D. J. Lowe, “Mechanism of molybdenum nitrogenase,” *Chem. Rev.*, vol. 96, no. 7, pp. 2983–3011, Nov. 1996.

[8] G. D. Watt and A. Burns, “Kinetics of Dithionite Ion Utilization and ATP Hydrolysis for Reactions Catalyzed by the Nitrogenase Complex from Azotobacter vinelandii,” *Biochemistry*, vol. 16, no. 2, pp. 264–270, Jan. 1977.

[9] R. D. Joerger, P. E. Bishop, and H. J. Evans, “Bacterial alternative nitrogen fixation systems,” *Crit. Rev. Microbiol.*, vol. 16, no. 1, pp. 1–14, 1988.

[10] E. S. Boyd and J. W. Peters, “New insights into the evolutionary history of biological nitrogen fixation,” *Front. Microbiol.*, vol. 4, no. AUG, p. 201, Aug. 2013.

[11] M. M. Georgiadis, H. Komiya, P. Chakrabarti, D. Woo, J. J. Kornuc, and D. C. Rees, “Crystallographic structure of the nitrogenase iron protein from Azotobacter vinelandii,” *Science (80-.).*, vol. 257, no. 5077, pp. 1653–1659, 1992.

[12] F. A. Tezcan, J. T. Kaiser, D. Mustafi, M. Y. Walton, J. B. Howard, and D. C. Rees, “Nitrogenase complexes: Multiple docking sites for a nucleotide switch protein,” *Science (80-.).*, vol. 309, no. 5739, pp. 1377–1380, Aug. 2005.

[13] W. A. Bulen and J. R. LeComte, “The nitrogenase system from Azotobacter: two-enzyme requirement for N2 reduction, ATP-dependent H2 evolution, and ATP hydrolysis.,” *Proc. Natl. Acad. Sci.*, 1966.

[14] H. L. Rutledge and F. A. Tezcan, “Electron Transfer in Nitrogenase,” *Chem. Rev.*, vol. 120, no. 12, pp. 5158–5193, 2020.

[15] F. B. Simpson and R. H. Burris, “A nitrogen pressure of 50 atmospheres does not prevent evolution of hydrogen by nitrogenase,” *Science (80-.).*, 1984.

[16] C. C. Lee, Y. Hu, and M. W. Ribbe, “Vanadium nitrogenase reduces CO,” *Science*. 2010.

[17] M. J. Dilworth, “Acetylene reduction by nitrogen-fixing preparations from Clostridium pasteurianum,” *BBA - Gen. Subj.*, vol. 127, no. 2, pp. 285–294, Oct. 1966.

[18] A. de Klerk, “Fischer-Tropsch Process,” in *Kirk-Othmer Encyclopedia of Chemical Technology*, Hoboken, NJ, USA: John Wiley & Sons, Inc., 2013, pp. 1–20.

[19] C. N. Morrison, J. A. Hoy, L. Zhang, O. Einsle, and D. C. Rees, “Substrate Pathways in the nitrogenase MoFe protein by experimental identification of small molecule binding sites,” *Biochemistry*, vol. 54, no. 11, pp. 2052–2060, Mar. 2015.

[20] D. Smith, K. Danyal, S. Raugei, and L. C. Seefeldt, “Substrate Channel in Nitrogenase Revealed by a Molecular Dynamics Approach,” 2014.

[21] I. Dance, “The controlled relay of multiple protons required at the active site of nitrogenase,” *Dalt. Trans.*, vol. 41, no. 25, pp. 7647–7659, Jul. 2012.

[22] J. Kluglist, J. Voorberg, H. Haaker, and C. Veeger, “Characterization of three different flavodoxins from Azotobacter vinelandii,” *Eur. J. Biochem.*, vol. 155, no. 1, pp. 33–40, Feb. 1986.

[23] B. Shen, D. R. Jolliet, T. C. Diller, C. D. Stout, P. J. Stephenst, and B. K. Burgess, “Site-directed mutagenesis of Azotobacter vinelandii ferredoxin I: Cysteine ligation of the [4Fe-4S1 cluster with protein rearrangement is preferred over serine ligation,” 1995.

[24] T. V. Morgan, D. J. Lundell, and B. K. Burgess, “Azotobacter vinelandii Ferredoxin I: Cloning, Sequencing, and Mutant Analysis,” 1988.

[25] L. T. Bennett, M. R. Jacobson, and D. R. Dean, “Isolation, Sequencing, and Mutagenesis of the nifF Gene Encoding Flavodoxin from Azotobacter vinelandii,” 1988.

[26] A. E. Martin, B. K. Burgess, S. E. Iismaa, C. T. Smartt, M. R. Jacobson, and D. R. Dean2, “Construction and Characterization of an Azotobacter vinelandii Strain with Mutations in the Genes Encoding Flavodoxin and Ferredoxin It,” 1989.

[27] I. Naud, C. Meyer, L. David, J. Breton, J. Gaillard, and Y. Jouanneau, “Identification of Residues of Rhodobacter capsulatus Ferredoxin I Important for Its Interaction with Nitrogenase,” *Eur. J. Biochem.*, vol. 237, no. 2, pp. 399–405, Apr. 1996.

[28] J. Deistung, F. C. Cannon, M. C. Cannon, S. Hill, and R. N. Thorneley, “Electron transfer to nitrogenase in Klebsiella pneumoniae: NifF gene cloned and the gene product, a flavodoxin, purified,” *Biochem. J.*, vol. 231, no. 3, pp. 743–753, Nov. 1985.

[29] H. M. Segal, T. Spatzal, M. G. Hill, A. K. Udit, and D. C. Rees, “Electrochemical and structural characterization of Azotobacter vinelandii flavodoxin II,” *Protein Sci.*, vol. 26, no. 10, pp. 1984–1993, Oct. 2017.

[30] N. Pence *et al.*, “Unraveling the interactions of the physiological reductant flavodoxin with the different conformations of the Fe protein in the nitrogenase cycle,” 2017.

[31] G. A. Walker and L. E. Mortenson, “Effect of Magnesium Adenosine 5’-Triphosphate on the Accessibility of the Iron of Clostridial Azoferredoxin, a Component of Nitrogenase,” *Biochemistry*, vol. 13, no. 11, pp. 2382–2388, May 1974.

[32] G. D. Watt and K. R. N. Reddy, “Formation of an all ferrous Fe4S4 cluster in the iron

protein component of Azotobacter vinelandii nitrogenase," *J. Inorg. Biochem.*, vol. 53, no. 4, pp. 281–294, Mar. 1994.

[33] H. C. Angove, S. J. Yoo, B. K. Burgess, and E. Münck, "Mössbauer and EPR evidence for an all-ferrous Fe4S4 cluster with S = 4 in the Fe protein of nitrogenase," *J. Am. Chem. Soc.*, vol. 119, no. 37, pp. 8730–8731, 1997.

[34] G. D. Watt, R. R. Knotts, and Z. C. Wang, "Redox Reactions of and Nucleotide Binding to the Iron Protein of Azotobacter vinelandii," *Biochemistry*, vol. 25, no. 25, pp. 8156–8162, 1986.

[35] T. V. Morgan, R. C. Prince, and L. E. Mortenson, "Electrochemical titration of the S = 3/2 and S = ½ states of the iron protein of nitrogenase," *FEBS Lett.*, vol. 206, no. 1, pp. 4–8, Sep. 1986.

[36] T. J. Lowery *et al.*, "Flavodoxin hydroquinone reduces Azotobacter vinelandii Fe protein to the all-ferrous redox state with a S = 0 spin state," *Proc. Natl. Acad. Sci. U. S. A.*, vol. 103, no. 46, pp. 17131–17136, Nov. 2006.

[37] M. Guo, F. Sulc, M. W. Ribbe, P. J. Farmer, and B. K. Burgess, "Direct assessment of the reduction potential of the [4Fe-4S]1+/0 couple of the Fe protein from Azotobacter vinelandii," *J. Am. Chem. Soc.*, vol. 124, no. 41, pp. 12100–12101, Oct. 2002.

[38] W. N. Lanzilotta and L. C. Seefeldt, "Changes in the midpoint potentials of the nitrogenase metal centers as a result of iron protein-molybdenum-iron protein complex formation," *Biochemistry*, vol. 36, no. 42, pp. 12976–12983, Oct. 1997.

[39] I. V. Kurnikov, A. K. Charnley, and D. N. Beratan, "From ATP to electron transfer: Electrostatics and free-energy transduction in nitrogenase," *J. Phys. Chem. B*, vol. 105, no. 23, pp. 5359–5367, Jun. 2001.

[40] H. Schindelin, C. Kisker, J. L. Schlessman, J. B. Howard, and D. C. Rees, "Structure of ADP·AlF4/--stabilized nitrogenase complex and its implications for signal transduction," *Nature*, vol. 387, no. 6631, pp. 370–376, May 1997.

[41] Z. Y. Yang *et al.*, "Evidence That the Pi Release Event Is the Rate-Limiting Step in the Nitrogenase Catalytic Cycle," *Biochemistry*, vol. 55, no. 26, pp. 3625–3635, Jul. 2016.

[42] K. Danyal, D. R. Dean, B. M. Hoffman, and L. C. Seefeldt, "Electron transfer within nitrogenase: Evidence for a deficit-spending mechanism," *Biochemistry*, vol. 50, no. 43, pp. 9255–9263, Nov. 2011.

[43] A. J. Pierik, H. Wassink, H. Haaker, and W. R. Hagen, "Redox properties and EPR spectroscopy of the P clusters of Azotobacter vinelandii MoFe protein," *Eur. J. Biochem.*, vol. 212, no. 1, pp. 51–61, Feb. 1993.

[44] J. Kim and D. C. Rees, "Structural models for the metal centers in the nitrogenase molybdenum-iron protein," *Science (80-.).*, 1992.

[45] J. W. Peters, M. H. B. Stowell, S. M. Soltis, M. G. Finnegan, M. K. Johnson, and D. C. Rees, "Redox-dependent structural changes in the nitrogenase P-cluster," *Biochemistry*, vol. 36, no. 6, pp. 1181–1187, Feb. 1997.

[46] P. A. Lindahl, V. Papaefthymiou, W. H. Orme-Johnson, and E. Münck, "Mössbauer

studies of solid thionin-oxidized MoFe protein of nitrogenase.," *J. Biol. Chem.*, vol. 263, no. 36, pp. 19412–19418, 1988.

[47] S. J. Yoo, H. C. Angove, V. Papaefthymiou, B. K. Burgess, and E. Münck, "Mossbauer study of the MoFe protein of nitrogenase from Azotobacter vinelandii using selective 57Fe enrichment of the M-centers," *J. Am. Chem. Soc.*, vol. 122, no. 20, pp. 4926–4936, May 2000.

[48] T. R. Hoover, J. Imperial, P. W. Ludden, and V. K. Shah, "Homocitrate Is a Component of the Iron-Molybdenum Cofactor of Nitrogenase," *Biochemistry*, 1989.

[49] K. M. Lancaster *et al.*, "X-ray emission spectroscopy evidences a central carbon in the nitrogenase iron-molybdenum cofactor," *Science (80-.).*, 2011.

[50] T. Spatzal *et al.*, "Evidence for interstitial carbon in nitrogenase FeMo cofactor," *Science*, vol. 334, no. 6058. American Association for the Advancement of Science, p. 940, 18-Nov-2011.

[51] N. S. Sickerman, M. W. Ribbe, and Y. Hu, "Nitrogenase Cofactor Assembly: An Elemental Inventory," *Acc. Chem. Res.*, vol. 50, no. 11, pp. 2834–2841, 2017.

[52] T. V. Morgan, L. E. Mortenson, J. W. McDonald, and G. D. Watt, "Comparison of redox and EPR properties of the molybdenum iron proteins of Clostridium pasteurianum and Azotobacter vinelandii nitrogenases," *J. Inorg. Biochem.*, vol. 33, no. 2, pp. 111–120, Jun. 1988.

[53] R. N. F. Thorneley and D. J. Lowe, "Nitrogenase of Klebsiella pneumoniae Kinetics of the dissociation of oxidized iron protein from molybdenum-iron protein: Identification of the rate-limiting step for substrate reduction," 1983.

[54] R. N. F. Thorneley and D. J. Lowe, "The mechanism of Klebsiella pneumoniae nitrogenase action Simulation of the dependences of H2-evolution rate on component-protein concentration and ratio and sodium dithionite concentration," 1984.

[55] D. J. Lowe, K. Fisher, and R. N. F. Thorneley, "Klebsiella pneumoniae nitrogenase: pre-steady-state absorbance changes show that redox changes occur in the MoFe protein that depend on substrate and component protein ratio; a role for P-centres in reducing dinitrogen ?," 1993.

[56] D. J. Lowe and R. N. Thorneley, "The mechanism of Klebsiella pneumoniae nitrogenase action. The determination of rate constants required for the simulation of the kinetics of N2 reduction and H2 evolution.," *Biochem. J.*, vol. 224, no. 3, pp. 895–901, Dec. 1984.

[57] D. J. Lowe and R. N. Thorneley, "The mechanism of Klebsiella pneumoniae nitrogenase action. Pre-steady-state kinetics of H2 formation.," *Biochem. J.*, vol. 224, no. 3, pp. 877–886, Dec. 1984.

[58] B. M. Hoffman, D. Lukoyanov, D. R. Dean, and L. C. Seefeldt, "Nitrogenase: A draft mechanism," *Acc. Chem. Res.*, vol. 46, no. 2, pp. 587–595, Feb. 2013.

[59] C. Wachnowsky and J. A. Cowan, "In Vitro Studies of Cellular Iron–Sulfur Cluster

Biosynthesis, Trafficking, and Transport," in *Methods in Enzymology*, vol. 595, Academic Press Inc., 2017, pp. 55–82.

[60] L. Zheng, R. H. White, V. L. Cash, R. F. Jack, and D. R. Dean, "Cysteine desulfurase activity indicates a role for NIFS in metallocluster biosynthesis," *Proc. Natl. Acad. Sci. U. S. A.*, vol. 90, no. 7, pp. 2754–2758, Apr. 1993.

[61] A. D. Smith *et al.*, "NifS-mediated assembly of [4Fe-4S] clusters in the N- and C-terminal domains of the NifU Scaffold protein," *Biochemistry*, vol. 44, no. 39, pp. 12955–12969, Oct. 2005.

[62] P. C. Dos Santos, A. D. Smith, J. Frazzon, V. L. Cash, M. K. Johnson, and D. R. Dean, "Iron-sulfur cluster assembly: NifU-directed activation of the nitrogenase Fe protein," *J. Biol. Chem.*, vol. 279, no. 19, pp. 19705–19711, May 2004.

[63] M. R. Jacobson *et al.*, "Physical and genetic map of the major nif gene cluster from Azotobacter vinelandii.," *J. Bacteriol.*, vol. 171, no. 2, pp. 1017–1027, Feb. 1989.

[64] M. R. Jacobson, V. L. Cash, M. C. Weiss, N. F. Laird, W. E. Newton, and D. R. Dean, "Biochemical and genetic analysis of the nifUSVWZM cluster from Azotobacter vinelandii," *MGG Mol. Gen. Genet.*, vol. 219, no. 1–2, pp. 49–57, Oct. 1989.

[65] G. P. Roberts, T. MacNeil, D. MacNeil, and W. J. Brill, "Regulation and characterization of protein products coded by the nif (nitrogen fixation) genes of Klebsiella pneumoniae," *J. Bacteriol.*, vol. 136, no. 1, pp. 267–279, Oct. 1978.

[66] L. Zheng, V. L. Cash, D. H. Flint, and D. R. Dean, "Assembly of iron-sulfur clusters. Identification of an iscSUA-hscBA-fdx gene cluster from Azotobacter vinelandii," *J. Biol. Chem.*, vol. 273, no. 21, pp. 13264–13272, May 1998.

[67] D. C. Johnson, P. C. Dos Santos, and D. R. Dean, "NifU and NifS are required for the maturation of nitrogenase and cannot replace the function of isc-gene products in Azotobacter vinelandii," in *Biochemical Society Transactions*, 2005, vol. 33, no. 1, pp. 90–93.

[68] P. C. Dos Santos, D. C. Johnson, B. E. Ragle, M. C. Unciuleac, and D. R. Dean, "Controlled expression of nif and isc iron-sulfur protein maturation components reveals target specificity and limited functional replacement between the two systems," *J. Bacteriol.*, vol. 189, no. 7, pp. 2854–2862, Apr. 2007.

[69] R. B. Broach *et al.*, "Variable-temperature, variable-field magnetic circular dichroism spectroscopic study of the metal clusters in the ΔnifB and ΔnifH MoFe proteins of nitrogenase from Azotobacter vinelandii," *Biochemistry*, vol. 45, no. 50, pp. 15039–15048, Dec. 2006.

[70] M. C. Corbett, Y. Hu, F. Naderi, M. W. Ribbe, B. Hedman, and K. O. Hodgson, "Comparison of iron-molybdenum cofactor-deficient nitrogenase MoFe proteins by x-ray absorption spectroscopy. Implications for P-cluster biosynthesis," *J. Biol. Chem.*, vol. 279, no. 27, pp. 28276–28282, Jul. 2004.

[71] Y. Hu *et al.*, "Nitrogenase reactivity with P-cluster variants," *Proc. Natl. Acad. Sci. U. S. A.*, vol. 102, no. 39, pp. 13825–13830, Sep. 2005.

[72] A. C. Robinson, T. W. Chun, J. G. Li, and B. K. Burgess, “Iron-molybdenum cofactor insertion into the apo-MoFe protein of nitrogenase involves the iron protein-MgATP complex,” *J. Biol. Chem.*, vol. 264, no. 17, pp. 10088–10095, 1989.

[73] M. W. Ribbe, Y. Hu, M. Guo, B. Schmid, and B. K. Burgess, “The Femoco-deficient MoFe protein produced by a nifH deletion strain of Azotobacter vinelandii shows unusual P-cluster features,” *J. Biol. Chem.*, vol. 277, no. 26, pp. 23469–23476, Jun. 2002.

[74] M. C. Corbett *et al.*, “Conformational differences between Azotobacter vinelandii nitrogenase MoFe proteins as studied by small-angle X-ray scattering,” *Biochemistry*, vol. 46, no. 27, pp. 8066–8074, Jul. 2007.

[75] J. K. Magnuson *et al.*, “Nitrogenase iron-molybdenum cofactor binding site: Protein conformational changes associated with cofactor binding,” in *Tetrahedron*, 1997, vol. 53, no. 35, pp. 11971–11984.

[76] Y. Hu, A. W. Fay, C. L. Chi, and M. W. Ribbe, “P-cluster maturation on nitrogenase MoFe protein,” *Proc. Natl. Acad. Sci. U. S. A.*, vol. 104, no. 25, pp. 10424–10429, Jun. 2007.

[77] P. Rangaraj, V. K. Shah, and P. W. Ludden, “ApoNifH functions in iron-molybdenum cofactor synthesis and apodinitrogenase maturation,” *Proc. Natl. Acad. Sci. U. S. A.*, vol. 94, no. 21, pp. 11250–11255, Oct. 1997.

[78] Y. Hu, A. W. Fay, P. C. Dos Santos, F. Naderi, and M. W. Ribbe, “Characterization of Azotobacter vinelandii nifZ deletion strains: Indication of stepwise MoFe protein assembly,” *J. Biol. Chem.*, vol. 279, no. 52, pp. 54963–54971, Dec. 2004.

[79] M. S. Cotton *et al.*, “VTVH-MCD study of the δnifB δnifZ MoFe protein from azotobacter vinelandii,” *J. Am. Chem. Soc.*, vol. 131, no. 13, pp. 4558–4559, Apr. 2009.

[80] C. C. Lee *et al.*, “Stepwise formation of P-cluster in nitrogenase MoFe protein,” *Proc. Natl. Acad. Sci. U. S. A.*, vol. 106, no. 44, pp. 18474–18478, Nov. 2009.

[81] D. Zhao, L. Curatti, and L. M. Rubio, “Evidence for nifU and nifS participation in the biosynthesis of the iron-molybdenum cofactor of nitrogenase,” *J. Biol. Chem.*, vol. 282, no. 51, pp. 37016–37025, Dec. 2007.

[82] L. A. Rettberg *et al.*, “Probing the coordination and function of Fe4S4 modules in nitrogenase assembly protein NifB,” *Nat. Commun.*, vol. 9, no. 1, pp. 1–8, Dec. 2018.

[83] G. Martínez-Noël, L. Curatti, J. A. Hernandez, and L. M. Rubio, “NifB and NifEN protein levels are regulated by ClpX2 under nitrogen fixation conditions in Azotobacter vinelandii,” *Mol. Microbiol.*, vol. 79, no. 5, pp. 1182–1193, Mar. 2011.

[84] H. H. Nagatani, V. K. Shah, and W. J. Brill, “Activation of inactive nitrogenase by acid-treated component I.,” *J. Bacteriol.*, vol. 120, no. 2, pp. 697–701, Nov. 1974.

[85] V. K. Shah, J. R. Allen, N. J. Spangler, and P. W. Ludden, “In vitro synthesis of the iron-molybdenum cofactor of nitrogenase. Purification and characterization of NifB cofactor, the product of NIFB protein,” *J. Biol. Chem.*, vol. 269, no. 2, pp. 1154–1158, 1994.

[86] J. A. Wiig, Y. Hu, C. C. Lee, and M. W. Ribbe, “Radical SAM-dependent carbon insertion into the nitrogenase M-cluster,” *Science (80-.).*, vol. 337, no. 6102, pp. 1672–1675, Sep. 2012.

[87] J. A. Wiig, Y. Hu, and M. W. Ribbe, “NifEN-B complex of Azotobacter vinelandii is fully functional in nitrogenase FeMo cofactor assembly,” *Proc. Natl. Acad. Sci. U. S. A.*, vol. 108, no. 21, pp. 8623–8627, May 2011.

[88] K. M. Lancaster, Y. Hu, U. Bergmann, M. W. Ribbe, and S. Debeer, “X-ray spectroscopic observation of an interstitial carbide in NifEN-bound FeMoco precursor,” *J. Am. Chem. Soc.*, vol. 135, no. 2, pp. 610–612, Jan. 2013.

[89] K. Tanifuji *et al.*, “Tracing the ‘ninth sulfur’ of the nitrogenase cofactor via a semi-synthetic approach.,” *Nat. Chem.*, vol. 10, no. 5, pp. 568–572, 2018.

[90] B. Soboh, E. S. Boyd, D. Zhao, J. W. Peters, and L. M. Rubio, “Substrate specificity and evolutionary implications of a NifDK enzyme carrying NifB-co at its active site,” *FEBS Lett.*, vol. 584, no. 8, pp. 1487–1492, Apr. 2010.

[91] T. D. Paustian, V. K. Shah, and G. P. Roberts, “Purification and characterization of the nifN and nifE gene products from Azotobacter vinelandii mutant UW45.,” *Proc. Natl. Acad. Sci. U. S. A.*, vol. 86, no. 16, pp. 6082–6086, Aug. 1989.

[92] D. R. Dean and K. E. Brigle, “Azotobacter vinelandii nifD- and nifE-encoded polypeptides share structural homology,” *Proc. Natl. Acad. Sci. U. S. A.*, vol. 82, no. 17, pp. 5720–5723, 1985.

[93] K. E. Brigle, M. C. Weiss, W. E. Newton, and D. R. Dean, “Products of the iron-molybdenum cofactor-specific biosynthetic genes, nifE and nifN, are structurally homologous to the products of the nitrogenase molybdenum-iron protein genes, nifD and nifK,” *J. Bacteriol.*, vol. 169, no. 4, pp. 1547–1553, 1987.

[94] R. Fani, R. Gallo, and P. Liò, “Molecular Evolution of Nitrogen Fixation: The Evolutionary History of the nifD, nifK, nifE, and nifN Genes,” *J. Mol. Evol.*, 2000.

[95] J. T. Kaiser, Y. Hu, J. A. Wiig, D. C. Rees, and M. W. Ribbe, “Structure of precursor-bound NifEN: A nitrogenase FeMo cofactor maturase/insertase,” *Science (80-.).*, vol. 331, no. 6013, pp. 91–94, Jan. 2011.

[96] A. W. Fay *et al.*, “Assembly scaffold NifEN: A structural and functional homolog of the nitrogenase catalytic component,” *Proc. Natl. Acad. Sci. U. S. A.*, vol. 113, no. 34, pp. 9504–9508, Aug. 2016.

[97] R. M. Allen, R. Chatterjee, P. W. Ludden, and V. K. Shah, “Incorporation of iron and sulfur from NifB cofactor into the iron- molybdenum cofactor of dinitrogenase,” *J. Biol. Chem.*, vol. 270, no. 45, pp. 26890–26896, Nov. 1995.

[98] P. Rangaraj, C. Rüttimann-Johnson, V. K. Shah, and P. W. Ludden, “Accumulation of 55Fe-Labeled Precursors of the Iron-Molybdenum Cofactor of Nitrogenase on NifH and NifX of Azotobacter vinelandii,” *J. Biol. Chem.*, vol. 276, no. 19, pp. 15968–15974, May 2001.

[99] L. Curatti, J. A. Hernandez, R. Y. Igarashi, B. Soboh, D. Zhao, and L. M. Rubio, “In vitro

synthesis of the iron-molybdenum cofactor of nitrogenase from iron, sulfur, molybdenum, and homocitrate using purified proteins," *Proc. Natl. Acad. Sci. U. S. A.*, vol. 104, no. 45, pp. 17626–17631, Nov. 2007.

[100] S. Siemann, K. Schneider, M. Oley, and A. Müller, "Characterization of a tungsten-substituted nitrogenase isolated from Rhodobacter capsulatus," *Biochemistry*, vol. 42, no. 13, pp. 3846–3857, Apr. 2003.

[101] T. Wichard, J. P. Bellenger, A. Loison, and A. M. L. Kraepiel, "Catechol siderophores control tungsten uptake and toxicity in the nitrogen-fixing bacterium Azotobacter vinelandii," *Environ. Sci. Technol.*, vol. 42, no. 7, pp. 2408–2413, Apr. 2008.

[102] B. Kowalewski *et al.*, "Natures polyoxometalate chemistry: X-ray structure of the Mo storage protein loaded with discrete polynuclear Mo-O clusters," *J. Am. Chem. Soc.*, vol. 134, no. 23, pp. 9768–9774, Jun. 2012.

[103] P. T. Pienkos and W. J. Brill, "Molybdenum accumulation and storage in Klebsiella pneumoniae and Azotobacter vinelandii," *J. Bacteriol.*, vol. 145, no. 2, pp. 743–751, Feb. 1981.

[104] R. D. Joerger and P. E. Bishop, "Nucleotide sequence and genetic analysis of the nifB-nifQ region from Azotobacter vinelandii.," *J. Bacteriol.*, vol. 170, no. 4, pp. 1475–1487, Apr. 1988.

[105] F. Rodriguez-Quinones, R. Bosch, and J. Imperial, "Expression of the nifBfdxNnifOQ region of Azotobacter vinelandii and its role in nitrogenase activity," *J. Bacteriol.*, vol. 175, no. 10, pp. 2926–2935, May 1993.

[106] J. A. Hernandez, L. Curatti, C. P. Aznar, Z. Perova, R. D. Britt, and L. M. Rubio, "Metal trafficking for nitrogen fixation: NifQ donates molybdenum to NifEN/NifH for the biosynthesis of the nitrogenase FeMo-cofactor," *Proc. Natl. Acad. Sci. U. S. A.*, vol. 105, no. 33, pp. 11679–11684, Aug. 2008.

[107] T. Spatzal *et al.*, "Nitrogenase FeMoco investigated by spatially resolved anomalous dispersion refinement," *Nat. Commun.*, vol. 7, no. 1, pp. 1–7, Mar. 2016.

[108] M. K. Chan, J. Kim, and D. C. Rees, "The nitrogenase FeMo-cofactor and P-cluster pair: 2.2 Å resolution structures," *Science (80-.).*, vol. 260, no. 5109, pp. 792–794, May 1993.

[109] P. A. McLean and R. A. Dixon, "Requirement of nifV gene for production of wild-type nitrogenase enzyme in Klebsiella pneumoniae," *Nature*, vol. 292, no. 5824, pp. 655–656, 1981.

[110] P. A. McLean, B. E. Smith, and R. A. Dixon, "Nitrogenase of Klebsiella pneumoniae nifV mutants.," *Biochem. J.*, vol. 211, no. 3, pp. 589–597, Jun. 1983.

[111] J. Liang, M. Madden, V. K. Shah, and R. H. Burris, "Citrate Substitutes for Homocitrate in Nitrogenase of a nifV Mutant of Klebsiella pneumoniae," *Biochemistry*, vol. 29, no. 37, pp. 8577–8581, Sep. 1990.

[112] T. R. Hoover, J. Imperial, P. W. Ludden, and V. K. Shah, "Homocitrate cures the NifV-phenotype in Klebsiella pneumoniae.," *J. Bacteriol.*, vol. 170, no. 4, pp. 1978–1979,

1988.

[113] Y. Hu *et al.*, “Nitrogenase Fe protein: A molybdate/homocitrate insertase,” *Proc. Natl. Acad. Sci.*, 2006.

[114] A. W. Fay *et al.*, “Formation of a homocitrate-free iron-molybdenum cluster on NifEN: Implications for the role of homocitrate in nitrogenase assembly,” *Dalt. Trans.*, vol. 39, no. 12, pp. 3124–3130, Mar. 2010.

[115] V. K. Shah, J. Imperial, R. A. Ugalde, P. W. Ludden, and W. J. Brill, “In vitro synthesis of the iron-molybdenum cofactor of nitrogenase,” *Proc. Natl. Acad. Sci. U. S. A.*, vol. 83, no. 6, pp. 1636–1640, Mar. 1986.

[116] Y. Hu *et al.*, “FeMo cofactor maturation on NifEN,” *Proc. Natl. Acad. Sci. U. S. A.*, vol. 103, no. 46, pp. 17119–17124, Nov. 2006.

[117] J. A. Hernandez *et al.*, “NifX and NifEN exchange NifB cofactor and the VK-cluster, a newly isolated intermediate of the iron-molybdenum cofactor biosynthetic pathway,” *Mol. Microbiol.*, vol. 63, no. 1, pp. 177–192, Jan. 2007.

[118] T. C. White, G. S. Harris, and W. H. Orme-Johnson, “Electrophoretic studies on the assembly of the nitrogenase molybdenum- iron protein from the Klebsiella pneumoniae nifD and nifK gene products,” *J. Biol. Chem.*, vol. 267, no. 33, pp. 24007–24016, 1992.

[119] M. J. Homer, T. D. Paustian, V. K. Shah, and G. P. Roberts, “The nifY product of Klebsiella pneumoniae is associated with apodinitrogenase and dissociates upon activation with the iron-molybdenum cofactor,” *J. Bacteriol.*, vol. 175, no. 15, pp. 4907–4910, Aug. 1993.

[120] L. M. Rubio, P. Rangaraj, M. J. Homer, G. P. Roberts, and P. W. Ludden, “Cloning and mutational analysis of the γ gene from Azotobacter vinelandii defines a new family of proteins capable of metallocluster binding and protein stabilization,” *J. Biol. Chem.*, vol. 277, no. 16, pp. 14299–14305, Apr. 2002.

[121] E. Jimenez-Vicente *et al.*, “Sequential and differential interaction of assembly factors during nitrogenase MoFe protein maturation,” *J. Biol. Chem.*, vol. 293, no. 25, pp. 9812–9823, Jun. 2018.

[122] L. M. Rubio, S. W. Singer, and P. W. Ludden, “Purification and Characterization of NafY (Apodinitrogenase γ Subunit) from Azotobacter vinelandii,” *J. Biol. Chem.*, vol. 279, no. 19, pp. 19739–19746, May 2004.

[123] R. R. Eady, “Structure-function relationships of alternative nitrogenases,” *Chem. Rev.*, vol. 96, no. 7, pp. 3013–3030, 1996.

[124] K. Schüddekopf, S. Hennecke, U. Liese, M. Kutsche, and W. Klipp, “Characterization of anf genes specific for the alternative nitrogenase and identification of nif genes required for both nitrogenases in Rhodobacter capsulatus,” *Mol. Microbiol.*, vol. 8, no. 4, pp. 673–684, May 1993.

[125] R. D. Joerger, M. R. Jacobson, R. Premakumar, E. D. Wolfinger, and P. E. Bishop, “Nucleotide sequence and mutational analysis of the structural genes (anfHDGK) for

the second alternative nitrogenase from Azotobacter vinelandii.," *J. Bacteriol.*, vol. 171, no. 2, pp. 1075–1086, 1989.

[126] D. Sippel and O. Einsle, "The structure of vanadium nitrogenase reveals an unusual bridging ligand," *Nat. Chem. Biol.*, vol. 13, no. 9, pp. 956–960, Sep. 2017.

[127] R. D. Joerger, T. M. Loveless, R. N. Pau, L. A. Mitchenall, B. H. Simon, and P. E. Bishop, "Nucleotide sequences and mutational analysis of the structural genes for nitrogenase 2 of Azotobacter vinelandii," *J. Bacteriol.*, vol. 172, no. 6, pp. 3400–3408, 1990.

[128] B. J. Hales and E. E. Case, "Nitrogen fixation by Azotobacter vinelandii in tungsten-containing medium.," *J. Biol. Chem.*, vol. 262, no. 33, pp. 16205–11, Nov. 1987.

[129] B. J. Hales, E. E. Case, J. E. Morningstar, M. F. Dzeda, and L. A. Mauterer, "Isolation of a New Vanadium-Containing Nitrogenase from Azotobacter vinelandii," *Biochemistry*, vol. 25, no. 23, pp. 7251–7255, 1986.

[130] Y. Hu, C. C. Lee, and M. W. Ribbe, "Extending the carbon chain: Hydrocarbon formation catalyzed by vanadium/molybdenum nitrogenases," *Science (80-.).*, 2011.

[131] J. R. Chisnell, R. Premakumar, and P. E. Bishop, "Purification of a second alternative nitrogenase from a nifHDK deletion strain of Azotobacter vinelandii.," *J. Bacteriol.*, vol. 170, no. 1, pp. 27–33, Jan. 1988.

[132] D. F. Harris *et al.*, "Mechanism of N 2 Reduction Catalyzed by Fe-Nitrogenase Involves Reductive Elimination of H 2," *Cite This Biochem.*, vol. 57, p. 710, 2018.

[133] A. J. Jasniewski, C. C. Lee, M. W. Ribbe, and Y. Hu, "Reactivity, Mechanism, and Assembly of the Alternative Nitrogenases," 2020.

[134] M. J. Dilworth and R. R. Eadyt, "Hydrazine is a product of dinitrogen reduction by the vanadium-nitrogenase from Azotobacter chroococcum," 1991.

[135] R. N. F. Thorneley, R. R. Eady, and D. J. Lowe, "Biological nitrogen fixation by way of an enzyme-bound dinitrogen-hydride intermediate," *Nature*, vol. 272, no. 5653, pp. 557–558, 1978.

[136] B. K. Burgess, S. Wherland, W. E. Newton, and E. I. Stiefel, "Nitrogenase Reactivity: Insight into the Nitrogen-Fixing Process through Hydrogen-Inhibition and HD-Forming Reactions," *Biochemistry*, vol. 20, no. 18, pp. 5140–5146, 1981.

[137] R. N. Pau, M. E. Eldridge, D. J. Lowe, L. A. Mitchenall, and R. R. Eady, "Molybdenum-independent nitrogenases of Azotobacter vinelandii: A functional species of alternative nitrogenase-3 isolated from a molybdenum-tolerant strain contains an iron-molybdenum cofactor," *Biochem. J.*, vol. 293, no. 1, pp. 101–107, Jul. 1993.

[138] D. Sippel *et al.*, "Production and isolation of vanadium nitrogenase from Azotobacter vinelandii by molybdenum depletion," *J. Biol. Inorg. Chem.*, vol. 22, no. 1, pp. 161–168, Jan. 2017.

[139] M. J. Dilworth, R. R. Eady, and M. E. Eldridge, "The vanadium nitrogenase of Azotobacter chroococcum. Reduction of acetylene and ethylene to ethane.," *Biochem. J.*, vol. 249, no. 3, pp. 745–751, Feb. 1988.

[140] C. C. Lee, Y. Hu, and M. W. Ribbe, “Unique features of the nitrogenase VFe protein from Azotobacter vinelandii,” *Proc. Natl. Acad. Sci. U. S. A.*, vol. 106, no. 23, pp. 9209–9214, Jun. 2009.

[141] A. Müller, K. Schneider, U. Gollan, E. Krahn, and M. Dröttboom, “Characterization of the ‘iron only’ nitrogenase from Rhodobacter capsulatus,” *J. Inorg. Biochem.*, vol. 59, no. 2–3, p. 551, Aug. 1995.

[142] J. G. Rebelein, M. T. Stiebritz, C. C. Lee, and Y. Hu, “Activation and reduction of carbon dioxide by nitrogenase iron proteins.,” *Nat. Chem. Biol.*, vol. 13, no. 2, pp. 147–149, 2017.

[143] I. Dance, “The pathway for serial proton supply to the active site of nitrogenase: Enhanced density functional modeling of the Grotthuss mechanism,” *Dalt. Trans.*, vol. 44, no. 41, pp. 18167–18186, Oct. 2015.

[144] T. R. Hoover *et al.*, “Identification of the V factor needed for synthesis of the iron-molybdenum cofactor of nitrogenase as homocitrate,” *Nature*, vol. 329, no. 6142, pp. 855–857, 1987.

[145] J. Liang, M. Madden, V. K. Shah, and R. H. Burris, “Citrate Substitutes for Homocitrate in Nitrogenase of a nifV Mutant of Klebsiella pneumoniaet,” 1990.

Chapter 2: Heterologous Expression of NifH in *Escherichia coli*

2.1 Introduction

Nitrogenase's ability to convert inert N_2 to bioavailable NH_3 makes it potentially valuable for the production of bio-fertilizer [1]. If agricultural crops could express a functional nitrogenase and produce their own NH_3, less supplemented fertilizer would be required for their growth. To accomplish this long-term goal, various efforts have been made in the past to heterologously express a functional nitrogenase in non-diazotrophic prokaryotic and eukaryotic organisms [2]–[6]. Moreover, heterologous expression of nitrogenase can also facilitate the expression and analysis of nitrogenase proteins from other organisms which usually grow under conditions that complicate a large-scale cultivation. One example is methanogenic archaea, which thrive in anaerobic, high-salinity, and high-temperature environments [7]–[9]. Here, we heterologously co-expressed the NifH protein from *Methanosarcina acetivorans* (*M. acetivorans*) in *Escherichia coli* (*E. coli*) together with the FeS-cluster assembly machinery IscSUA. We suspect NifH is a good candidate protein for heterologous expression of the nitrogenase machinery due to its rather simple homodimeric architecture and relatively small size of 60 kDa [10]. Additionally, NifH contains a Fe_4S_4 cluster, which bridges the two monomers and is held in place by four cysteine residues. This Fe_4S_4 cluster makes the protein susceptible to oxygen exposure. Successful expression of functional, active NifH protein in *E. coli* would be a proof of concept for the potential expression of the entire nitrogenase machinery in different host organisms.

NifH has multiple functions within the nitrogenase machinery. NifH facilitates the formation of the Fe_8S_7 P-cluster on NifDK as well as the insertion of molybdenum and homocitrate into the M-cluster during the M-cluster maturation on NifEN [11]–[13]. Furthermore, NifH functions as an ATP-dependent reductase during catalysis, delivering electrons to the catalytic NifDK [1]. The electron transfer is mediated by NifH's Fe_4S_4 cluster

to the P-cluster on NifDK and from there to the M-cluster at the active site of the enzyme. The Fe_4S_4 cluster has been described in the oxidation states 2+, 1+ and 0, among which the 2+/1+ redox couple is considered physiological relevant for electron transfer to NifDK [14], [15]. An ATP binding site is found within each NifH monomer [10]. The state of the bound nucleotide has a direct effect on the position of the Fe_4S_4 cluster as well as the redox potential: in the ATP-bound state the Fe_4S_4 cluster is more solvent exposed than in the ADP-bound state [16]. In the nucleotide-free state the redox potential of NifH is -300 mV, which is lowered by ATP binding to -400 mV and even further to -490 mV by ATP-hydrolysis to ADP [17], [18]. During the transfer process of one electron from the Fe_4S_4 cluster on NifH to the P-cluster on NifDK, two ATP are hydrolysed to ADP [1].

The catalytic nitrogenase complex NifDK relies on a constant supply of electrons from NifH during substrate reduction. By varying the ratio of NifH:NifDK, the electron flux can be altered, resulting in different activity rates of NifDK [19]. Another potential way to influence the electron flux towards NifDK is the use of NifH proteins from different organisms. The NifH proteins from *M. acetivorans* and *A. vinelandii* share 59 % sequence identity and 72 % sequence homology. This close relationship could allow for binding of NifH from *M. acetivorans* to NifDK from *A. vinelandii* and an electron transfer from the Fe_4S_4 cluster to the P-cluster, but at slower rates compared to the natural NifH from *A. vinelandii*. A slightly reduced compatibility between NifH and NifDK could give insights into binding energetics as well as electron transfer efficiencies, which could also lead to substrates or intermediate products being trapped at the active site.

Furthermore, the NifH protein from *A. vinelandii* has been shown to reduce CO_2 to CO [20]. This ability of a rather simple protein containing a Fe_4S_4 cluster to convert CO_2 suggests the possibility of new pathways to deal with this pollutant gas. The ability of nitrogenase to

reduce CO to hydrocarbons [21], [22] could be coupled with the CO_2 reduction by NifH, creating a two-step process to eventually convert CO_2 to hydrocarbons. Therefore, the study of conversion of CO_2 to CO by NifH homologues from different organisms is of interest to better understand and potentially improve this reaction.

2.2 Materials and Methods

Reagents and chemicals were purchased from Sigma-Aldrich and Fisher Scientific, unless stated otherwise. Protein work was performed in an argon atmosphere, with an oxygen concentration of < 5 ppm.

Cell growth and protein purification

Escherichia coli (*E. coli*) strain expressing $NifH^{Ma}$ (strain YM135EE) was constructed by co-transforming a plasmid carrying *iscSUA* and a pet-14b vector carrying the *nifH* of *Methanosarcina acetivorans* (*M. acetivorans*) into *E. coli* strain BL21(DE3). The strain was grown in 10 L batched in Difco LB medium containing 100 mg/L ampicillin (BD Biosciences) and 34 mg/L chloramphenicol in a BIOFLO 415 fermenter (New Brunswick Scientific). At 37 °C with 200 rpm agitation and 10 L/min airflow. Growth rates were monitored by measuring cell density at 600 nm using a Spectronic 20 Genesys spectrometer (Spectronic Instruments). When OD_{600} reached 0.5, the temperature was lowered to 25 °C before expression of $NifH^{Ma}$ was induced by addition of 25 µM IPTG. Expression of protein was allowed to continue for 16 h before cells were harvested by centrifugation using a Thermo Fisher Scientific Legend XTR centrifuge. Subsequently, His-tagged $NifH^{Ma}$ was purified by immobilized metal affinity chromatography (IMAC) using methods adapted from the purification of His-tagged nitrogenase proteins [23], [24]. *Azotobacter vinelandii* (*A. vinelandii*) strains expressing

NifDK^{Av}, NifH^{Av} and VnfDGK^{Av} proteins were grown at 30 °C in 180 L batches in a 200 L fermenter (New Brunswick Scientific) in Burke's minimal medium supplemented with 2 mM ammonium acetate. Growth rates were monitored by measuring cell density at 436 nm. Cells were harvested once OD_{436} reached 1.0 by a flow-through centrifugal harvester (Cepa). Published methods were used to purify these proteins [23], [24].

SDS-PAGE Analysis and Molecular Mass Determination

SDS-PAGE analysis was performed using a 4-20 % Mini-PROTEAN TGX precast gel (BioRad), which was run at 100 V in a TGX running buffer for 1 h, followed by staining with Coomassie Brilliant Blue (BioRad). The native molecular mass of NifH^{Ma} was determined by gel filtration on a column packed with Ultrogel ACA 34 (Pall Life Science; ID: 1.5 cm, length: 1.4 m) at a flow rate of 0.5 mL/min. Protein standards (GE Healthcare) used for molecular mass determination were carbonic anhydrase (29 kDa), ovalbumin (43 kDa), albumin (66 kDa), catalase (232 kDa) and ferritin (440 kDa).

Iron Determination

The iron (Fe) content of NifH^{Ma} was determined by inductively coupled plasma optical emission spectroscopy (ICP-OES) using a Thermo Scientific iCAP7000. Stock solutions of elemental Fe (1 mg/mL, Thermo Fisher Scientific) were diluted to make standard solutions for calibration. Each protein sample was mixed with 100 µL concentrated sulfuric acid (H_2SO_4) and 100 µL concentrated nitric acid (HNO_3) and heated at 250 °C for 30 min. This procedure was repeated until the solutions became colourless. Subsequently, the solutions were cooled to room temperature, diluted to a total volume of 7.5 mL with 2 % HNO_3 (vol/vol), and subjected to sample analysis.

EPR Analysis

The electron paramagnetic resonance (EPR) samples were prepared in a Vacuum Atmosphere glove box with less than 5 ppm O_2 and flash frozen in liquid nitrogen prior to analysis. The dithionite (DT)-reduced samples contained 10 mg/mL of $NifH^{Ma}$ or $NifH^{Av}$, 25 mM Tris-HCl (pH 8.0), 10 % (vol/vol/ glycerol, 250 mM imidazole, 2 mM DT ($Na_2S_2O_4$) and, in some cases, 5.4 mM ATP or ADP. The indigo disulfonate (IDS)-oxidized samples were prepared by incubating the DT-reduced samples with excess IDS for 5 min, followed by removal of excess IDS using a G25 desalting column. The super-reduced, all-ferrous samples were prepared by incubating the DT-reduced sample with 20 mM europium (II) diethylenetriaminepentaacetic acid (Eu^{II}-DTPA) for 5 min, followed by removal of excess Eu^{II}-DTPA using a G25 desalting column.

P-cluster Maturation Assay

This assay contained, in a total volume of 1 mL, 25 mM Tris-HCl (pH 8.0), 20 mM $Na_2S_2O_4$, 0.45 mg Δ*nifH* $NifDK^{Av}$, 0.21 mg $NifH^{Av}$ or $NifH^{Ma}$, 0.8 mM ATP, 1.6 mM $MgCl_2$, 10 mM creatine phosphate, 8 units creatine kinase and 8 nmol isolated M-cluster (cofactor) from the Mo-nitrogenase. This mixture was then incubated at 30 °C for 60 min, followed by determination of enzymatic activities.

Enzymatic Assays

Enzymatic assays were conducted as previously described [24], [25]. The assay contained, in a total volume of 1 mL, 0.27 mg $NifDK^{Av}$ or $VnfDGK^{Av}$, 0.15 mg $NifH^{Av}$ or $NifH^{Ma}$, 20 mM $Na_2S_2O_4$, 0.8 mM ATP, 1.6 mM $MgCl_2$, 10 mM creatine phosphate and 8 units creatine kinase. For CO-, C_2H_2-, H^+- and N_2-reduction assays, 1 atm CO, 0.1 atm C_2H_2, 1 atm Ar and 1 atm N_2, respectively, were added to the headspace of samples. Determination of H_2, C_2H_4 and NH_3 were performed as described previously [26], [27]. Hydrocarbon products were quantified by a gas-chromatograph-flame ionization detector (GC-FID), where 250 µL

headspace of each sample was injected onto a Grace 5664PC column (3.2 mm diameter, 1.5 m length), held at 55 °C for 1 min, heated to 180 °C at 12.5 °C/min and held at 180 °C for 2.6 min prior to the determination of hydrocarbon products by GC-FID.

Docking Analyses

Docking calculations were performed to define the affinity and specificity markers of the nitrogenase complexes that could be used for correlation with the experimentally determined activities of the catalytic and assembly complexes of nitrogenase.

Catalytic complexes

To this end, homology models of NifH^{Ma} were generated with SWISS-MODEL [28]–[30] using the crystal structure of the ADP·AlF_4^-stabilized, transition state Mo-nitrogenase complex (NifH^{Av}/NifDK^{Av}) [PDB entry: 1M34] as a template [31]. The ADP·AlF_4^-stabilized, transition-state V-nitrogenase complex (VnfH^{Av}/VnfDGK^{Av}) was generated using the same template and the crystal structure of VnfDGK^{Av} [PDB entry: 5M6Y] [32].

Based on the homology models, ensembles of possible protein-protein complexes between the Fe proteins (NifH^{Av} and NifH^{Ma}) and the catalytic components of Mo- and V-nitrogenase (NifDK^{Av} and VnfDGK^{Av}) were created with the ClusPro server [33]–[36] and binding energies of all these complexes were calculated with FoldX [37]–[39] in a process automised by Bash and Pearl scripting. As no parameters for FeS clusters were provided in the FoldX force field, the reported binding energies did not include contributions from these clusters. Given the mediation of protein-protein interactions by surface residues, and an overall high degree of structural conservation of the proteins considered (especially with regard to the locations of the cluster sites), the comparative docking approach used in this study should not be negatively impacted by this omission, as it focuses on the relative

differences in binding affinity and, therefore, will not be affected by the distinct, yet mostly constant, systematic deviation due to the high spatial conservation of cluster sites. A more refined approach, however, would include force-field descriptions for all clusters present in the proteins in order to offset the constant, systematic deviation generated by the omission of the clusters. For further analysis (see below), all in silico low-energy docking models determined by ClusPro were considered for all coefficients of the scoring energy term. However, different numbers of docking solutions were used for further analysis of individual nitrogenase complexes/hybrids due to a variation of the number of docking models fulfilling the final energy screening of ClusPro.

To evaluate the affinity between the two components in each complex, an energy landscape was first generated by arranging the binding energies of all docking models, from the left to the right, in the order of energetically most favourable (exothermic) to the energetically most unfavourable (endothermic) conformations. The percentages of exothermic and endothermic dockings, as well as the mean binding energy, were then calculated for each complex. Since the mean binding energy is derived from ensembles of low-energy docking structures rather than the optimal solution alone, it provides a better measure of the binding affinity, a prerequisite for creating functional protein complexes. This energy metric was then used as the 'affinity marker' for correlation with the substrate-reducing activities of various catalytic complexes of nitrogenase.

To evaluate the specificity between the two components in each complex, the distance between the Fe_4S_4 cluster of the Fe protein and the interface between the Fe protein and its catalytic partner was considered. Given the exponential decrease of electron tunneling/transfer probability with increasing distances, the catalytically most productive docking models should feature the smallest distances between the Fe_4S_4 cluster of the Fe

protein and the Fe protein/NifDK^{Av} or Fe protein/VnfDGK^{Av} interface. Such a distance was calculated based on the average position of the Cβ atoms of the Fe_4S_4 cluster-coordinating Cys residues of the Fe protein (Cys^{H97*}, Cys^{H132*}, Cys^{H97**} and Cys^{H132**}, where * and ** denote residues from each of the two identical subunits of the Fe protein) and the average position of the Cβ atoms of residues in a conserved hydrophobic patch, formed by Leu^{D158}, Ile^{D159}, Val^{K157} and Ile^{K158} on the surface of NifDK^{Av}, or Leu^{D142}, Ile^{D143}, Val^{K119} and Ile^{K120} on the surface of VnfDGK^{Av}. This hydrophobic batch contains the only residues of NifDK^{Av} or VnfDGK^{Av} that are located within 5 Å of the Fe_4S_4 cluster in the crystal structure of the ADP·AlF_4^--stabilized NifH^{Av}/NifDK^{Av} complex (PDB entry: 1M34) [31]. Distance computation for all solutions provided by ClusPro was automatized with a Python script that calculated the distance between groups of atoms provided by the user, and the calculated distances in the exothermic conformations were then aligned with the binding energies to reveal the relationship between the complex geometry and the binding affinity. Two energetically favourable, exothermic groups of conformations were identified based on this alignment: (*i*) a proximal group (P group) that centres at a cluster-interface distance of ~5-6 Å; and (*ii*) a distal group (D group) that centres at a distance at a cluster-interface distance of ~8-9 Å. Since the exothermic conformations in the P group are those with higher electron transfer efficiency, the average binding energy of these conformations represents an energy metric for the docking specificity of proteins within a complex. This energy metric was then used as the 'specificity marker' for correlation with the substrate-reducing activities of various catalytic complexes of nitrogenase.

Assembly complexes:

Docking calculations of the nitrogenase complexes involved in P-cluster maturation were carried out as described above except that (*i*) a SAXS-derived model of the P-cluster

precursor (designated P^P-cluster)-containing Δ*nifH* $NifDK^{Av}$ protein [40] was used as one of the complex components for the calculations; and (*ii*) the electron transfer efficiency was evaluated based on the distance calculated between the average position of the Cβ atoms of the Fe_4S_4 cluster-coordinating Cys residues of the Fe protein (Cys^{H97*}, Cys^{H132*}, Cys^{H97**} and Cys^{H132**}, where * and ** denote residues from each of the two identical subunits of the Fe protein) and the average position of the Cβ atoms of the P^P-cluster-coordinating Cys residues (Cys^{D62}, Cys^{D88}, Cys^{D154}, Cys^{K70}, Cys^{K95} and Cys^{K153}). The mean binding energy of each complex was derived from the energy landscape comprising all calculated docking models, and alignment of the cluster-cluster distances of the exothermic conformations with the corresponding binding energies revealed the presence of one or both of the P and D groups of conformations in these assembly complexes. The mean binding energy of all docking models and the average binding energy of the exothermic conformations in the P peak were then used as the markers of binding affinity and specificity, respectively, for correlation with the P-cluster maturations of the assembly complexes of nitrogenase.

2.3 Results

The NifH protein from *M. acetivorans* (termed $NifH^{Ma}$ in the following text) was heterologously co-expressed with the FeS cluster maturation machinery IscSUA in *E. coli* cells and purified via immobilized metal affinity chromatography. The protein had a size of 59.9 kDa, which is similar to the size of 63.7 kDa of NifH from *A. vinelandii* (termed $NifH^{Av}$ in the following text) (Figure 2.1) [10], [41]. The presence of the Fe_4S_4 cluster was confirmed by ICP-OES analysis. An occupancy of 3.5 ± 0.1 mol Fe/mol $NifH^{Ma}$ represents 88 % of the ideal occupancy of one Fe_4S_4 cluster/NifH protein.

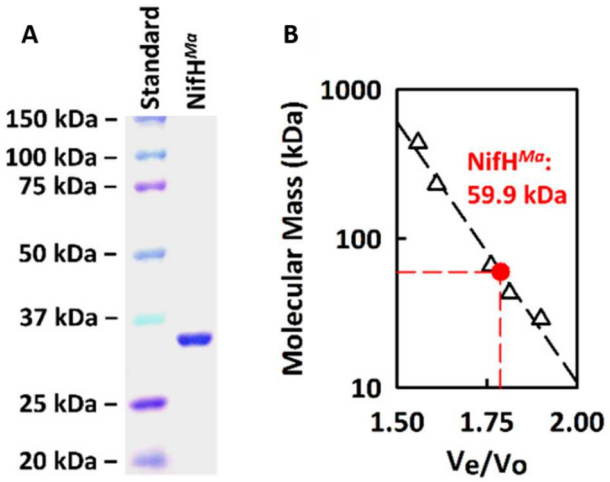

Figure 2.1 NifH^{Ma} purification and molecular weight determination: *A – Displayed is a sample of purified NifH^{Ma} ran on a 4-20 % gradient SDS-PAGE gel, stained with Coomassie Brilliant Blue. Lane 1: 15 µg pre-stained protein standard; Lane 2: 1.5 µg NifH^{Ma}. B – Molecular weight determination of NifH^{Ma} by gel filtration. V_0 = void volume; V_e = elution volume. Used protein standards (represented by open triangles): ferritin (440 kDa), catalase (232 KDa), albumin (66 kDa), ovalbumin (43 kDa), carbonic anhydrase (29 kDa).*

The Fe_4S_4 cluster on NifH^{Ma} was able to adopt the same three oxidation states as NifH^{Av}, as confirmed by electron paramagnetic (EPR) spectroscopy: the oxidized $Fe_4S_4^{2+}$ state in the presence of indigo disulfonate (IDS), which is EPR-silent (Figure 2.2A), the reduced $Fe_4S_4^{1+}$ state in the presence of dithionite (DT) (Figure 2.2B), and the super-reduced $Fe_4S_4^{0}$ state in the presence of Eu^{II} (Figure 2.2E). In contrast to the EPR-signal of NifH^{Av}, the S = 3/2 signal of NifH^{Ma} is stronger for the reduced $Fe_4S_4^{1+}$ state (Figure 2.2B). Also the g = 16.4 signal of the super-reduced $Fe_4S_4^{0}$ state shows a slight difference, with the NifH^{Ma} protein displaying a decreased magnitude, compared to NifH^{Av} (Figure 2.2B). Nucleotide binding by NifH^{Ma} caused the same line-shape change as regularly observed for NifH^{Av}: from an initial rhombic line-shape in the nucleotide-free state (Figure 2.2B), ATP binding causes a change to an axial line-shape (Figure 2.2C), while ADP binding results in an intermediary between a rhombic and axial line-shape (Figure 2.2D). However, these line-shape changes are rather moderate, compared to NifH^{Av}.

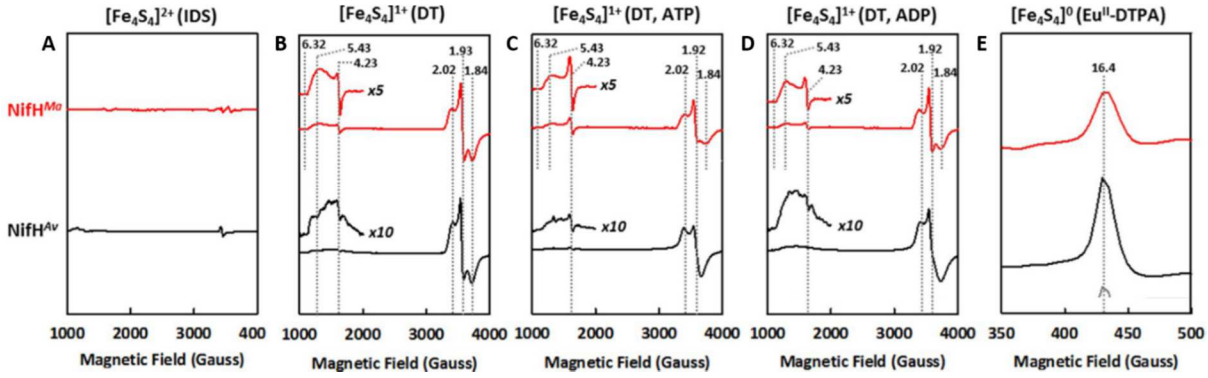

Figure 2.2 Electron paramagnetic spectroscopy analysis: *Presented are the EPR spectroscopy spectra of NifH^{Ma} (red) and NifH^{Av} (black). A – Indigo disulfonate (IDS) oxidized NifH proteins in the 2+ oxidation state. B – Nucleotide-free dithionite (DT) reduced NifH proteins in the 1+ oxidation state. C – ATP-bound dithionite reduced NifH proteins in the 1+ oxidation state. D – ADP-bound dithionite reduced NifH proteins in the 1+ oxidation state. For B-D, the S = 3/2 regions are displayed enlarged 5x (NifH^{Ma}) and 10x (NifH^{Av}) above the respective spectra. E – Nucleotide-free europium(II)-diethylenetriaminepentaacetic acid (Eu^{II}-DTPA) reduced NifH proteins in the 2+ oxidation state. The g-values are indicated by black numbers.*

The NifH^{Ma} protein was also capable of facilitating electron transfer to NifDK as well as VnfDGK from *A. vinelandii* (termed NifDK^{Av} and VnfDGK^{Av}, respectively, in the following text) and allows for the catalysis of various substrates. When combined with NifH^{Ma}, NifDK^{Av} generally displayed activities that where about 10-fold lower than when combined with the natural reductase NifH^{Av} (Table 2.1). However, a similar product profile could be observed, where NifDK^{Av} formed relatively more NH_3 than H_2 when supplied with N_2 as a substrate with both NifH^{Av} and NifH^{Ma}. Also with C_2H_2 as a substrate, the amount of formed C_2H_4 was larger than H_2 under the same conditions for both reductases. When CO was supplied as a substrate, NifDK^{Av} almost exclusively formed H_2 and only very low amounts of hydrocarbons with either NifH protein. Both NifH^{Av} and NifH^{Ma} were also able to facilitate electron transfer to the non-natural catalytic partner VnfDGK^{Av}. The use of both reductase proteins resulted in a product profile similar to that of VnfDGK^{Av}, where slightly more H_2 than NH_3 or C_2H_4 is formed with N_2 or C_2H_2 as the substrate (Table 2.1). Furthermore, NifH^{Av} and NifH^{Ma} enabled CO reduction to hydrocarbons by VnfDGK^{Av}, as it has been described previously [22], yet H_2 remains the major

product being formed under these conditions. Interestingly, the general activities of VnfDGK^{Av} are only about 3-fold lower when NifH^{Ma} is utilized, compared to NifH^{Av}. Comparing the activities of NifDK^{Av} and VnfDGK^{Av} when both were supplied with NifH^{Ma}, VnfDGK^{Av} displayed higher activity values, raising questions about the compatibility of NifH^{Ma} towards the catalytic units.

Table 2.1 Catalytic activities of reductases paired with catalytic units. *Presented are the catalytic activities of NifDK^{Av} paired with NifH^{Av} or NifH^{Ma} and VnfDGK^{Av} paired with NifH^{Av} or NifH^{Ma}. The activity values are displayed in nmol product/min/mg protein.*

Substrate Gas	N_2		CO		C_2H_2		Ar
Product	NH_3	H_2	Hydrocarbons	H_2	C_2H_4	H_2	H_2
NifDK + NifH^{Av}	1326	575	0.2	1959	1703	152	1900
NifDK + NifH^{Ma}	123	95	0.09	193	198	64	234
VnfDGK + NifH^{Av}	432	615	66	855	374	808	1335
VnfDKG + NifH^{Ma}	123	174	13	276	84	198	335

To further assess the interaction of NifH^{Ma} and NifH^{Av} with NifDK^{Av}, combined homology modelling/in silico modelling was deployed [28], [31], [35], [41]. Based on the mean binding energy of the possible conformations for each complex, an “affinity marker” was generated. A correlation between the catalytic activity and the affinity marker of the respective complex could be established, where a lower substrate reducing activity correlates with a higher mean binding energy (Figure 2.3). NifH^{Ma} showed a less favourable affinity towards NifDK^{Av} than NifH^{Av}. Both NifH proteins showed a similar affinity towards VnfDGK^{Av}. An alignment of the distances between the Fe_4S_4 cluster of the different NifH proteins and the contact surface of the catalytic NifDK^{Av} or VnfDGK^{Av}, and the exothermic binding energies resulted in the identification of a proximal and distal group of conformations for the different complex combinations. The complexes adopt a favourable binding either at a short (proximal) or long (distal) cluster-interface distance. Because the probability of electron tunnelling decreases with an increasing distance between two sites [42], the binding energy determined

for the shorter proximal site could be utilized in order to evaluate the specificity of the respective complex and to correlate the binding energies with the catalytic activities. Similar to the affinity assessment, NifH^{Ma} displays a lower specificity for the complex formation with NifDK^{Av}, compared to NifH^{Av} (Figure 2.3A). For the complex with VnfDGK^{Av}, NifH^{Ma} has only a slightly lower specificity than NifH^{Av} (Figure 2.3B).

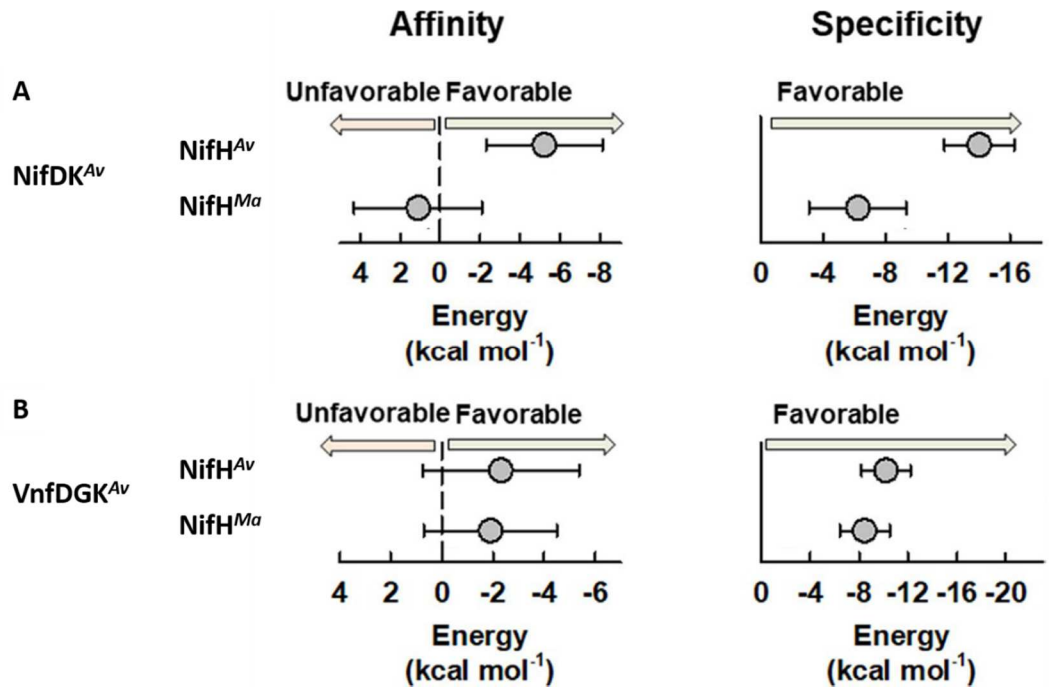

Figure 2.3 Affinity and specificity of NifH proteins towards catalytic units: *Displayed are the affinity and specificity of the interaction between NifH^{Av} and NifH^{Ma} with NifDK^{Av} or VnfDGK^{Av}. A – NifH^{Ma} shows lower affinity and specificity for NifDK^{Av} than NifH^{Av}. B – Both NifH proteins display a similar affinity and specificity for VnfDGK^{Av}.*

In addition to its ability to transfer electrons to NifDK^{Av}, NifH^{Ma} was also able to facilitate the maturation of the P-cluster on NifDK^{Av} (Δ*nifH* NifDK^{Av}) to a certain extent. The activity of the Δ*nifH* NifDK^{Av} after incubation with NifH^{Ma} corresponded to 1/3 of the activity of Δ*nifH* NifDK^{Av} after incubation with NifH^{Av} (Figure 2.4). This lower performance in P-cluster maturation aligned with lower affinity and specificity for the NifH^{Ma}-Δ*nifH* NifDK^{Av} complex for P-cluster maturation, compared to the affinity and specificity for NifH^{Av} (Figure 2.4).

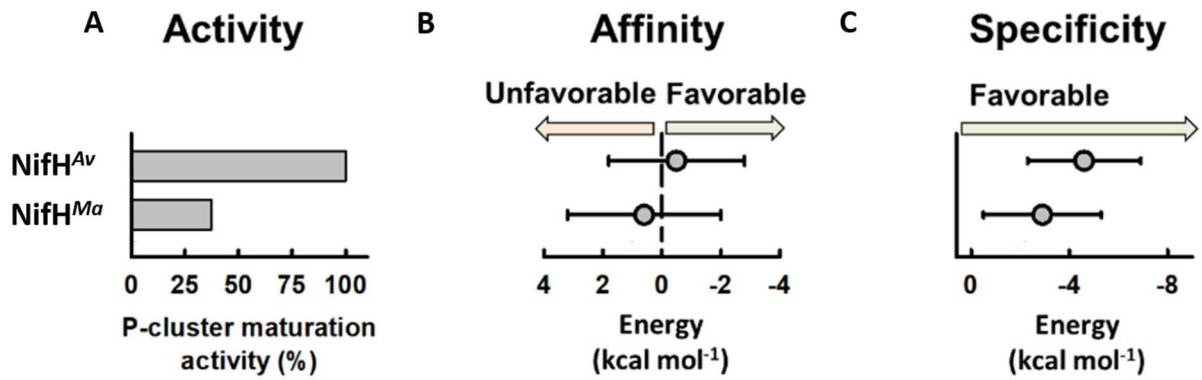

Figure 2.4 Interaction between NifH and ΔnifH NifDK^{Av} for P-cluster maturation: *Depicted are the results of the interaction between NifH^{Av} and NifH^{Ma} with ΔnifH NifDK^{Av} for P-cluster maturation. A – The resulting activity of ΔnifH NifDK^{Av} after maturation with both NifH proteins shows NifH^{Ma}-facilitated P-cluster maturation corresponds to 1/3 of the activity of NifH^{Av}-facilitated P-cluster maturation. B – NifH^{Ma} displays a lower affinity for the interaction with NifDK^{Av} during P-cluster maturation, compared to NifH^{Av}. C – Also the specificity of NifH^{Ma} for the P-cluster maturation on NifDK^{Av} is slightly lower than NifH^{Av}.*

2.4 Discussion

The presented results show evidence for the successful heterologous expression of functional nitrogenase proteins in *E. coli*. Although *E. coli* does not harbour traits similar to *A. vinelandii* that allow the bacterial cells to protect the labile Fe_4S_4 cluster from oxidative damage [43], the purified protein contained a functional Fe_4S_4 cluster. The Fe_4S_4 cluster on NifH^{Ma} is able to obtain the same oxidation states as the NifH^{Av} protein from its native host organism. The NifH^{Ma} protein can physically interact with NifDK^{Av} and VnfDGK^{Av} from *A. vinelandii* and, most importantly, form catalytically functional complexes for the reduction of N_2, CO, C_2H_2 and H^+. Combined homology modelling and *in silico* docking suggest a lower affinity and specificity of NifH^{Ma} towards NifDK^{Av} for electron transfer during catalysis, compared to NifH^{Av}, and similar affinities and specificities for both NifH proteins towards VnfDGK^{Av}. Also for P-cluster maturation on Δ*nifH* NifDK^{Av}, NifH^{Ma} displays a lower performance than NifH^{Av}, in line with lower affinity and specificity values. The calculation's success in

predicting accurate affinity and specificity values of the docking of different NifH proteins with NifDK and VnfDGK provide an opportunity for future *in silico* assessments of other NifH proteins prior to their use in *in vitro* studies. This process can save time as well as resources.

In an analogous investigation, the reductase of the vanadium-nitrogenase from *M. acetivorans*, VnfH ($VnfH^{Ma}$), has been heterologously expressed in *E. coli* [41]. The $VnfH^{Ma}$ protein was also purified with a functional Fe_4S_4 cluster, which could adopt the three oxidation states 2+, 1+ and 0 and enabled the $VnfH^{Ma}$ to transfer electrons to $NifDK^{Av}$ and $VnfDGK^{Av}$ from *A. vinelandii*. Similar to $NifH^{Ma}$, $VnfH^{Ma}$ also showed a lower affinity and specifity towards $NifDK^{Av}$ and $VnfDGK^{Av}$, compared to the natively expressed VnfH from *A. vinelandii* ($VnfH^{Av}$). Interestingly, the heterologously expressed $NifH^{Ma}$ and $VnfH^{Ma}$ showed better affinity and specificity for the respective other catalytic subunit: $VnfH^{Ma}$ paired with $NifDK^{Av}$ resulted in higher activities than $NifH^{Ma}$ with $NifDK^{Av}$ and $NifH^{Ma}$ paired with $VnfDGK^{Av}$ resulted in higher activities than $VnfH^{Ma}$ with $VnfDGK^{Av}$ [41]. This reduced activity of $VnfDGK^{Av}$ paired with $VnfH^{Ma}$ was attributed to a different binding conformation between the two proteins. The proximal position was energetically less favoured than the distal position, leading to a longer distance between the FeS clusters involved in the electron transfer process and a change from CO reduction to CO binding by $VnfDGK^{Av}$. Further evidence for CO binding without turnover came from EPR experiments [41]. This decreased binding ability of heterologously expressed NifH homologues provides an opportunity to further investigate nitrogenase substrate binding and potentially gain more insights into C-C coupling by the vanadium-nitrogenase. With *E. coli* established as a functional expression system for NifH homologues, additional variants from different diazotrophic organisms, especially those growing under anaerobic and thermophile conditions, could be explored for their compatibility with NifDK and VnfDGK. With a variety of NifH homologues the electron flow towards catalytic subunits could be tailored to specific

conditions that allow the capture of substrates or intermediates on the nitrogenase enzyme [44]–[47].

2.5 Acknowledgements

I am very grateful to Dr. Caleb Hiller for performing the EPR experiments and part of the biochemical assays and Dr. Martin Stiebritz for performing the DFT calculations presented in this chapter. I also thank Dr. Chi Chung Lee for his contribution to this project.

In addition to this, I thank Wiley-VCH GmbH for publishing these results [48] and granting me permission to reuse portions of it for this chapter.

2.6 References

[1] B. K. Burgess and D. J. Lowe, “Mechanism of molybdenum nitrogenase,” *Chem. Rev.*, vol. 96, no. 7, pp. 2983–3011, Nov. 1996.

[2] R. A. Dixon and J. R. Postgate, “Transfer of nitrogen-fixation genes by conjugation in Klebsiella pneumoniae [12],” *Nature*, vol. 234, no. 5323. Nature, pp. 47–48, 1971.

[3] R. A. Dixon and J. R. Postgate, “Genetic transfer of nitrogen fixation from klebsiella pneumoniae to escherichia coli,” *Nature*, vol. 237, no. 5350, pp. 102–103, 1972.

[4] L. Wang *et al.*, “Correction: A Minimal Nitrogen Fixation Gene Cluster from Paenibacillus sp. WLY78 Enables Expression of Active Nitrogenase in Escherichia coli,” *PLoS Genet.*, vol. 9, no. 10, Oct. 2013.

[5] J. Yang, X. Xie, M. Yang, R. Dixon, and Y. P. Wang, “Modular electron-transport chains from eukaryotic organelles function to support nitrogenase activity,” *Proc. Natl. Acad. Sci. U. S. A.*, vol. 114, no. 12, pp. E2460–E2465, Mar. 2017.

[6] J. R. Postgate and H. M. Kent, “Qualitative evidence for expression of Klebsiella pneumoniae nif in Pseudomonas putida.,” *J. Gen. Microbiol.*, vol. 133, no. 9, pp. 2563–2566, 1987.

[7] J. A. Leigh, “Nitrogen Fixation in Methanogens: The Archaeal Perspective,” 2000.

[8] M. P. Mehta and J. A. Baross, “Nitrogen fixation at 92°C by a hydrothermal vent archaeon,” *Science (80-.).*, vol. 314, no. 5806, pp. 1783–1786, Dec. 2006.

[9] M. P. Mehta, D. A. Butterfield, and J. A. Baross, “Phylogenetic diversity of nitrogenase (nifH) genes in deep-sea and hydrothermal vent environments of the Juan de Fuca Ridge,” *Appl. Environ. Microbiol.*, vol. 69, no. 2, pp. 960–970, Feb. 2003.

[10] M. M. Georgiadis, H. Komiya, P. Chakrabarti, D. Woo, J. J. Kornuc, and D. C. Rees, “Crystallographic structure of the nitrogenase iron protein from Azotobacter vinelandii,” *Science (80-.).*, vol. 257, no. 5077, pp. 1653–1659, 1992.

[11] A. C. Robinson, T. W. Chun, J. G. Li, and B. K. Burgess, “Iron-molybdenum cofactor insertion into the apo-MoFe protein of nitrogenase involves the iron protein-MgATP complex,” *J. Biol. Chem.*, vol. 264, no. 17, pp. 10088–10095, 1989.

[12] M. W. Ribbe, Y. Hu, M. Guo, B. Schmid, and B. K. Burgess, “The Femoco-deficient MoFe protein produced by a nifH deletion strain of Azotobacter vinelandii shows unusual P-cluster features,” *J. Biol. Chem.*, vol. 277, no. 26, pp. 23469–23476, Jun. 2002.

[13] Y. Hu *et al.*, “Nitrogenase Fe protein: A molybdate/homocitrate insertase,” *Proc. Natl. Acad. Sci.*, 2006.

[14] G. D. Watt and K. R. N. Reddy, “Formation of an all ferrous Fe4S4 cluster in the iron protein component of Azotobacter vinelandii nitrogenase,” *J. Inorg. Biochem.*, vol. 53, no. 4, pp. 281–294, Mar. 1994.

[15] H. C. Angove, S. J. Yoo, B. K. Burgess, and E. Münck, “Mössbauer and EPR evidence for an all-ferrous Fe4S4 cluster with S = 4 in the Fe protein of nitrogenase,” *J. Am. Chem. Soc.*, vol. 119, no. 37, pp. 8730–8731, 1997.

[16] G. A. Walker and L. E. Mortenson, “Effect of Magnesium Adenosine 5’-Triphosphate on the Accessibility of the Iron of Clostridial Azoferredoxin, a Component of Nitrogenase,” *Biochemistry*, vol. 13, no. 11, pp. 2382–2388, May 1974.

[17] T. V. Morgan, R. C. Prince, and L. E. Mortenson, “Electrochemical titration of the S = 3/2 and S = ½ states of the iron protein of nitrogenase,” *FEBS Lett.*, vol. 206, no. 1, pp. 4–8, Sep. 1986.

[18] G. D. Watt, R. R. Knotts, and Z. C. Wang, “Redox Reactions of and Nucleotide Binding to the Iron Protein of Azotobacter vinelandii,” *Biochemistry*, vol. 25, no. 25, pp. 8156–8162, 1986.

[19] A. J. Jasniewski, C. C. Lee, M. W. Ribbe, and Y. Hu, “Reactivity, Mechanism, and Assembly of the Alternative Nitrogenases,” 2020.

[20] J. G. Rebelein, M. T. Stiebritz, C. C. Lee, and Y. Hu, “Activation and reduction of carbon dioxide by nitrogenase iron proteins.,” *Nat. Chem. Biol.*, vol. 13, no. 2, pp. 147–149, 2017.

[21] Y. Hu, C. C. Lee, and M. W. Ribbe, “Extending the carbon chain: Hydrocarbon formation catalyzed by vanadium/molybdenum nitrogenases,” *Science (80-.).*, 2011.

[22] C. C. Lee, Y. Hu, and M. W. Ribbe, “Vanadium nitrogenase reduces CO,” *Science*. 2010.

[23] M. W. Ribbe, Y. Hu, M. Guo, B. Schmid, and B. K. Burgess, “The femoco-deficient MoFe protein produced by a nifH deletion strain of Azotobacter vinelandii shows

unusual P-cluster features," *J. Biol. Chem.*, vol. 277, no. 26, pp. 23469–23476, Jun. 2002.

[24] B. K. Burgess, D. B. Jacobs, and E. I. Stiefel, "Large-scale purification of high activity Azotobacter vinelandII nitrogenase.," *Biochim. Biophys. Acta*, vol. 614, no. 1, pp. 196–209, Jul. 1980.

[25] Y. Hu, A. W. Fay, P. C. Dos Santos, F. Naderi, and M. W. Ribbe, "Characterization of Azotobacter vinelandii nifZ deletion strains: Indication of stepwise MoFe protein assembly," *J. Biol. Chem.*, vol. 279, no. 52, pp. 54963–54971, Dec. 2004.

[26] N. Gavini and B. K. Burgess, "FeMo cofactor synthesis by a nifH mutant with altered MgATP reactivity," *J. Biol. Chem.*, vol. 267, no. 29, pp. 21179–21186, 1992.

[27] J. L. Corbin, "Liquid chromatographic-fluorescence determination of ammonia from nitrogenase reactions: A 2-Min assay," *Appl. Environ. Microbiol.*, vol. 47, no. 5, pp. 1027–1030, 1984.

[28] K. Arnold, L. Bordoli, J. Kopp, and T. Schwede, "The SWISS-MODEL workspace: A web-based environment for protein structure homology modelling," *Bioinformatics*, vol. 22, no. 2, pp. 195–201, Jan. 2006.

[29] F. Kiefer, K. Arnold, M. Künzli, L. Bordoli, and T. Schwede, "The SWISS-MODEL Repository and associated resources," *Nucleic Acids Res.*, vol. 37, no. SUPPL. 1, 2009.

[30] M. Biasini *et al.*, "SWISS-MODEL: Modelling protein tertiary and quaternary structure using evolutionary information," *Nucleic Acids Res.*, vol. 42, no. W1, Jul. 2014.

[31] B. Schmid *et al.*, "Biochemical and structural characterization of the cross-linked complex of nitrogenase: Comparison to the ADP-ALF4--stabilized structure," *Biochemistry*, vol. 41, no. 52, pp. 15557–15565, Dec. 2002.

[32] D. Sippel and O. Einsle, "The structure of vanadium nitrogenase reveals an unusual bridging ligand," *Nat. Chem. Biol.*, vol. 13, no. 9, pp. 956–960, Sep. 2017.

[33] D. Kozakov *et al.*, "How good is automated protein docking?," *Proteins Struct. Funct. Bioinforma.*, vol. 81, no. 12, pp. 2159–2166, Dec. 2013.

[34] D. Kozakov, R. Brenke, S. R. Comeau, and S. Vajda, "PIPER: An FFT-based protein docking program with pairwise potentials," *Proteins Struct. Funct. Genet.*, vol. 65, no. 2, pp. 392–406, Nov. 2006.

[35] S. R. Comeau, D. W. Gatchell, S. Vajda, and C. J. Camacho, "ClusPro: A fully automated algorithm for protein-protein docking," *Nucleic Acids Res.*, vol. 32, no. WEB SERVER ISS., pp. W96–W99, Jul. 2004.

[36] S. R. Comeau, D. W. Gatchell, S. Vajda, and C. J. Camacho, "ClusPro: An automated docking and discrimination method for the prediction of protein complexes," *Bioinformatics*, vol. 20, no. 1, pp. 45–50, Jan. 2004.

[37] J. van Durme, J. Delgado, F. Stricher, L. Serrano, J. Schymkowitz, and F. Rousseau, "A graphical interface for the FoldX forcefield," *Bioinformatics*, vol. 27, no. 12, pp. 1711–1712, Jun. 2011.

[38] I. E. Sánchez *et al.*, "Genome-wide prediction of SH2 domain targets using structural

information and the FoldX algorithm," *PLoS Comput. Biol.*, vol. 4, no. 4, Apr. 2008.

[39] J. Schymkowitz, J. Borg, F. Stricher, R. Nys, F. Rousseau, and L. Serrano, "The FoldX web server: An online force field," *Nucleic Acids Res.*, vol. 33, no. SUPPL. 2, Jul. 2005.

[40] M. C. Corbett *et al.*, "Conformational differences between Azotobacter vinelandii nitrogenase MoFe proteins as studied by small-angle X-ray scattering," *Biochemistry*, vol. 46, no. 27, pp. 8066–8074, Jul. 2007.

[41] C. J. Hiller, M. T. Stiebritz, C. C. Lee, J. Liedtke, and Y. Hu, "Tuning Electron Flux through Nitrogenase with Methanogen Iron Protein Homologues.," *Chemistry*, vol. 23, no. 64, pp. 16152–16156, Nov. 2017.

[42] C. C. Page, C. C. Moser, X. Chen, and P. L. Dutton, "Natural engineering principles of electron tunnelling in biological oxidation-reduction," *Nature*, vol. 402, no. 6757, pp. 47–52, Nov. 1999.

[43] W. Sabra, A. P. Zeng, H. Lunsdorf, and W. D. Deckwer, "Effect of oxygen on formation and structure of Azotobacter vinelandii alginate and its role in protecting nitrogenase," *Appl. Environ. Microbiol.*, vol. 66, no. 9, pp. 4037–4044, Sep. 2000.

[44] C. C. Lee *et al.*, "Uncoupling binding of substrate CO from turnover by vanadium nitrogenase," *Proc. Natl. Acad. Sci. U. S. A.*, vol. 112, no. 45, pp. 13845–13849, Nov. 2015.

[45] H. I. Lee *et al.*, "Electron inventory, kinetic assignment (En), structure, and bonding of nitrogenase turnover intermediates with C2H2 and CO," *J. Am. Chem. Soc.*, vol. 127, no. 45, pp. 15880–15890, Nov. 2005.

[46] T. Spatzal, K. A. Perez, O. Einsle, J. B. Howard, and D. C. Rees, "Ligand binding to the FeMo-cofactor: Structures of co-bound and reactivated nitrogenase," *Science (80-.).*, vol. 345, no. 6204, pp. 1620–1623, Sep. 2014.

[47] B. Tyree and D. A. Webster, "The binding of cyanide and carbon monoxide to cytochrome o purified from Vitreoscilla. Evidence for subunit interaction in the reduced protein," *J. Biol. Chem.*, vol. 253, no. 19, pp. 6988–6991, 1978.

[48] C. J. Hiller, M. T. Stiebritz, C. C. Lee, J. Liedtke, and Y. Hu, "Tuning Electron Flux through Nitrogenase with Methanogen Iron Protein Homologues," *Chem. - A Eur. J.*, vol. 23, no. 64, pp. 16152–16156, Nov. 2017.

Chapter 3: Effect of Specific Point Mutations on CO_2-binding to the Nitrogenase Iron Protein

3.1 Introduction

The bacterial enzyme nitrogenase is best known for its ability to reduce N_2 to NH_3 [1]. A study by Seefeldt *et al.* gave a first indication that Mo-nitrogenase could also reduce carbon dioxide (CO_2) and carbonyl sulphide (COS) to carbon monoxide (CO) [2]. Later, the V-nitrogenase was shown to reduce CO to hydrocarbons, suggesting that nitrogenase can perform reactions similar to the Fischer-Tropsch synthesis [3], [4]. This led to investigations of nitrogenase's ability to also reduce CO_2 to hydrocarbons, which was successfully shown for a variant of the Mo-nitrogenase (α-V70A, α-H195Q) as well as the wildtype Mo-, V- and Fe-nitrogenases among which the V-nitrogenase showed the most promising potential for Fischer-Tropsch-like catalysis [5]–[9]. The reduction of CO_2 to methane (CH_4) and H_2O requires the input of, at least, 8 e^-, which is the same requirement as for the reduction of N_2 to 2 NH_3 (see equation 3.1 and 3.2).

$$CO_2 + 8\ e^- + 8\ H^+ \rightarrow CH_4 + 2\ H_2O \qquad \text{(Equation 3.1)}$$

$$N_2 + 8\ e^- + 8\ H^+ \rightarrow 2\ NH_3 + H_2 \qquad \text{(Equation 3.2)}$$

This multi-step reaction is facilitated by the complex cluster at the active site of the respective catalytic nitrogenase component. The conversion of CO_2 to CO or hydrocarbons, a complex multi-step reaction process, made the discovery of CO_2 reduction by various NifH homologues even more interesting, as NifH only contains a single Fe_4S_4 cluster [10], [11]. Initially, NifH ($NifH^{Av}$) and VnfH ($VnfH^{Av}$) from *Azotobacter vinelandii* (*A. vinelandii*) were shown to reduce CO_2 to CO in the presence of dithionite and europium (II) diethylenetriaminepentaacetic acid (Eu^{II}-DTPA) as reductants, whereby the activity with Eu^{II}-DTPA was significantly higher than with dithionite [10]. NifH ($NifH^{Ma}$) and VnfH ($VnfH^{Ma}$) from *Methanosarcina acetivorans* (*M. acetivorans*) have previously been expressed heterologously

in *Escherichia coli* (*E. coli*) and were shown to support the same oxidation states of the cluster (2+, 1+ and 0) as NifH^{Av}, as well as the electron transfer to NifDK and VnfDGK from *A. vinelandii* [12]. The NifH^{Ma} was then also investigated for the ability to reduce CO_2 and was found to facilitate the reduction to CO, like NifH^{Av} [11]. In addition to this, NifH^{Ma} was able to perform further reduction steps, forming various hydrocarbons from CO_2 as well.

The bacterial NifH^{Av} and archaeal NifH^{Ma} share 59 % sequence identity and 72 % sequence similarity, both contain a Fe_4S_4 cluster and have a molecular weight of about 60 kDa [12]. Although both proteins can also obtain the same oxidation states, their electron paramagnetic resonance (EPR) spectra show deviations: NifH^{Ma} displays a stronger S = 3/2 signal in the reduced 1+ state than NifH^{Av} and a lower intensity of the g =16.4 signal in the parallel mode in the super-reduced 0 state [12]. Furthermore, the reduction potential of the $Fe_4S_4^{1+/2+}$ redox pair of NifH^{Ma} (E^0 = -395 mV) is lower than that of the respective $Fe_4S_4^{1+/2+}$ redox pair of NifH^{Av} (E^0 = -301 mV) [11]. However, the reduction of CO_2 in this state with dithionite as the reductant is majorly decreased compared to the $Fe_4S_4^{1+/0}$ state with Eu^{II}-DTPA as a reductant for both proteins [10], [11].

Crystallization of NifH^{Ma} in the presence of bicarbonate, an alternative CO_2 source, resulted in a structure with a small electron density in close proximity to the Fe_4S_4 cluster, which could be modelled as CO_2 [13]. Two conserved arginine (Arg) residues in close proximity to the Fe_4S_4 cluster (position 100 for NifH^{Av}, position 98 for NifH^{Ma}) are potentially involved in the binding and subsequent reduction of CO_2 on the NifH protein. The interaction could be facilitated by hydrogen bonding and electrostatic interactions. The following results provide an insight into the role of the two Arg residues by investigations of NifH^{Ma} variants containing

point mutations at the respective position and density functional theory (DFT) calculations, leading to a plausible model for the reduction of CO_2 by the NifH protein.

3.2 Materials and Methods

Reagents and chemicals were purchased from Sigma-Aldrich and Fisher Scientific, unless stated otherwise. Protein work was performed in an argon atmosphere, with an oxygen concentration of < 5 ppm.

Strain Construction

Strains expressing NifH^{Ma}R98H and NifH^{Ma}R98G variants were constructed via site-directed mutagenesis of the wild-type *M. acetivorans nifH* sequence carried out on a pET14b vector [14], followed by co-transformation of the resultant plasmids together with a plasmid carrying *iscSUA* into *E. coli* strain BL21(DE3).

Cell Growth

The strains were grown in a BIOFLO 415 fermenter (New Brunswick Scientific), using Difco LB medium containing 100 mg/L ampicillin (BD Biosciences) and 34 mg/L chloramphenicol at 37 °C with 10 L/min airflow and 200 rpm agitation. Bacterial growth was analysed by measuring the cell density at 600 nm using a Spectronic 20 Genesys spectrometer (Spectronic Instruments). Once the OD_{600} reached 0.5, the expression of the respective NifH^{Ma} (variant) was induced by addition of 25 µM IPTG and the temperature was changed to 25 °C. The bacteria were grown for an additional 16 h and subsequently harvested by centrifugation using a Thermo Fisher Scientific Legend XTR centrifuge.

Protein Purification

Protein purification was performed anaerobically using Schlenk techniques. Immobilized metal affinity chromatography was used to purify His-tagged NifH^{Ma}, NifH^{Ma}R98H and NifH^{Ma}R98G, as previously described [14].

SDS-PAGE Analysis

A 4-20 % Mini-PROTEAN TGX precast gel (BioRad) was used to perform SDS-PAGE analysis. The gel was run at 100 V for 1 h in TGX running buffer and subsequently stained with Coomassie Brilliant Blu (BioRad).

Iron Determination

Inductively coupled plasma optical emission spectroscopy (ICP-OES) was used to determine the iron content of NifH^{Ma} and variant proteins, utilizing a Thermo Scientific iCAP7000. Addition of 100 µL of concentrated nitric acid (HNO_3) and 100 µL of concentrated sulfuric acid (H_2SO_4) to each protein sample was followed by incubation at 250 °C for 30 min. Acid addition and heating steps were repeated until the solution became colourless. The samples were cooled to room temperature and diluted to a total volume of 10 mL with 2 % HNO_3 (vol/vol). A stock solution of elemental iron (1 mg/mL, Thermo Fisher Scientific) was used for serial dilutions to make standard solutions for calibration.

Activity Analysis

The in vitro CO_2-reduction assays were carried out in 9.4-ml assay vials with crimped butyl rubber serum stoppers. Each assay contained, in a total volume of 1.0 ml, 500 mM Tris-HCl (pH 10.0), 0.5 mg Fe protein (NifH^{Ma}, NifH^{Ma}R98H or NifH^{Ma}R98G), and 100 mM Eu^{II}-DTPA. In addition, the headspace of each assay contained 100 % CO2 (for reactions) or 100 % Ar (for controls). The assays were assembled without protein and Eu^{II}-DTPA and repeatedly flushed

and exchanged with CO_2, followed by equilibration for 30 min until pH stabilized at ~8.0. The reaction was initiated upon addition of $NifH^{Ma}$, followed immediately by addition of Eu^{II}-DTPA and incubation with continuous shaking at 30 °C for 300 min until the reaction was complete. Following the quenching of each assay by 100 µL of 30 % trichloroacetic acid, the headspace sample was examined for the production of CO and hydrocarbons as described previously [11].

EPR Analysis

The EPR samples were prepared in a Vacuum Atmospheres glove box and flash-frozen in liquid nitrogen prior to analysis. The DT-reduced samples contained 2 mM DT, 50 mM Tris-HCl (pH 8.0), 500 mM NaCl, and 10 % (vol/vol) glycerol. EPR spectra were recorded by an ESP 300 Ez spectrophotometer (Bruker) interfaced with an ESR-9002 liquid-helium continuous-flow cryostat (Oxford Instruments) using a microwave power of 50 mW, a gain of 5×10^4, a modulation frequency of 100 kHz, and a modulation amplitude of 5 G. Five scans were recorded for each EPR sample at a temperature of 10 K and a microwave frequency of 9.62 GHz.

3.3 Results

The importance of the physiochemical character of the Arg residues in close proximity to the Fe_4S_4 cluster on $NifH^{Ma}$ was investigated by exchanging the respective residue (R98) by histidine (His; R98H) and glycine (Gly; R98G). Deploying His in this position preserves the hydrogen bonding ability of the original amino acid, however at the price of shortening the chain length as compared to Arg. Replacing Arg with Gly results in the loss of any form of interaction between a bound CO_2 and the amino acid in this location.

Both NifH^{Ma} variants as well as the wildtype protein were constructed on plasmid DNA, co-transformed together with the FeS-cluster-forming machinery IscSUA into *E. coli*, expressed and purified using a His-tag. All three proteins have the same molecular weight (Figure 3.1 A). Inductively coupled plasma optical emission spectroscopy (ICP-OES) showed that the NifH^{Ma}R98H protein contained 2.83 Fe atoms per dimer and the NifH^{Ma}R98G contained 3.07 Fe atoms per dimer, which corresponds to 80 % and 87 % of the Fe content of the wildtype NifH^{Ma}, respectively (Figure 3.1 B). EPR analysis of all three proteins resulted in the same *S* = 1/2 EPR signal for the variants as for the wildtype NifH^{Ma} in the 1+ dithionite-reduced state (Figure 3.1 C). These results indicate that the mutations R98H and R98G do not affect the ability of NifH^{Ma} to hold the Fe_4S_4 cluster within the dimer, nor does it perturb the oxidation state in the dithionite-reduced form.

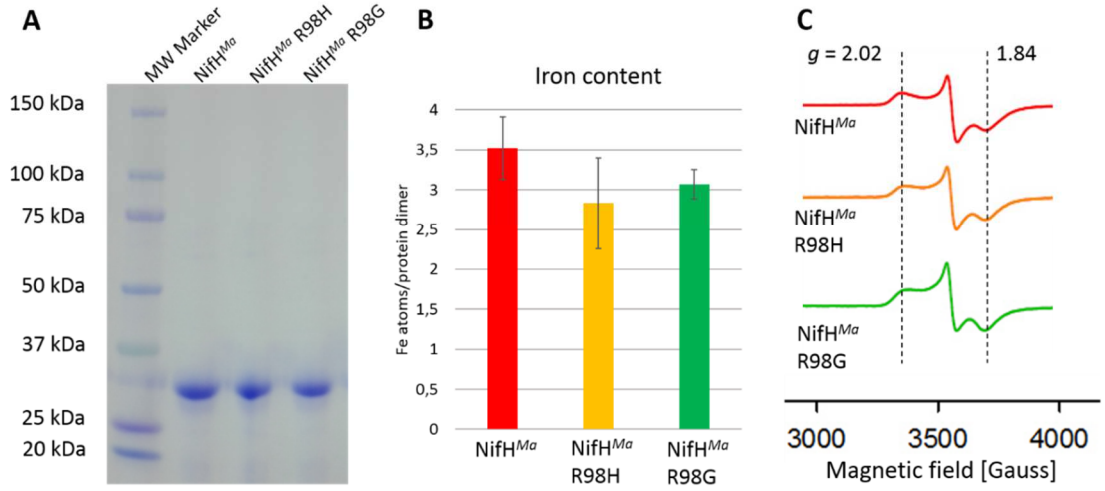

Figure 3.1 Properties of NifH^{Ma}, NifH^{Ma}R98H and NifH^{Ma}R98G: *Displayed is a general assessment of the wildtype NifH^{Ma} along with the two point-mutant variants NifH^{Ma}R98H and NifH^{Ma}R98G. A – SDS-PAGE of all three proteins (lanes 2-4) along with a molecular weight (MW) marker. All three proteins show the same molecular weight. B – ICP-OES analysis resulted in 3.52 Fe atoms/protein dimer for NifH^{Ma}, 2.83 Fe atoms/protein dimer for NifH^{Ma}R98H and 3.07 Fe atoms/protein dimer for NifH^{Ma}R98G. C – EPR spectroscopy of all three proteins in the dithionite-reduced 1+ state showed the characteristic S = 1/2 signal for each protein variant.*

The NifH^{Ma}R98H variant displays about 80 % of the CO_2-reducing capability of the wildtype NifH^{Ma} (Figure 3.2). While the amount of CO formed by NifH^{Ma}R98H is very similar to that produced by NifH^{Ma}, the amount and size distribution of the formed hydrocarbons has changed. NifH^{Ma}R98H forms generally less of each C_1 to C_3 hydrocarbon product and no butane (C_4H_8), which can be observed as a product when NifH^{Ma} is used. This leads to a slightly changed product ratio of hydrocarbons:CO from CO_2-reduction of 1.9 for NifH^{Ma}R98H vs. 2.7 for NifH^{Ma}, which means that the former generates relatively more CO from CO_2 (Figure 3.2). Both findings can potentially be explained by the shorter chain length of the His residue at position 98 that limits its ability to directly interact with the CO_2-species at the cluster and thereby conceivably weakens hydrogen-bonding interactions and lowers the efficiency of possible proton-transfer steps. The NifH^{Ma}R98G variant displays about 15 % of the CO_2-reducing capability of NifH^{Ma} (Figure 3.2). CO and CH_4 are the major products formed by NifH^{Ma}R98G, with very small amounts of C_2- and C_3-products. Analogous to NifH^{Ma}R98H, NifH^{Ma}R98G does not form any C_4 products. These findings may be explained by the inability of glycine to act as a donor for both hydrogen-bonding interactions and proton-transfer reactions and highlight the importance of the Arg residue at position 98 for the CO_2-reducing activity of NifH^{Ma}.

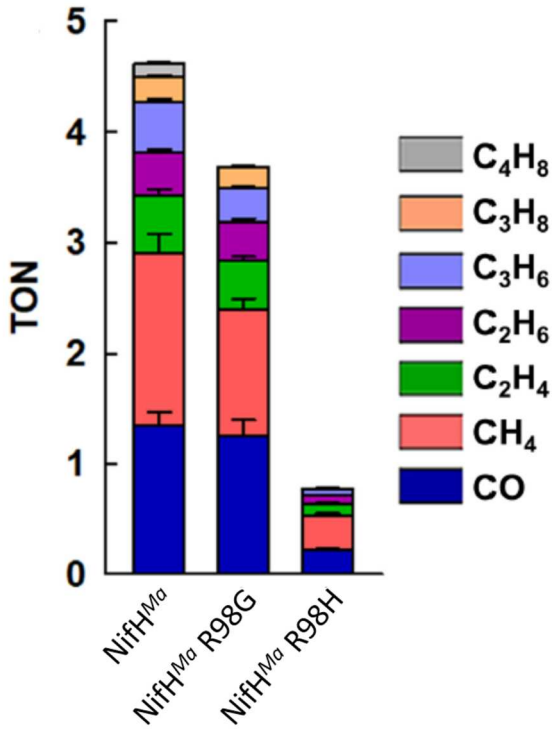

Figure 3.2 CO_2-reduction by wildtype and variant NifH^{Ma} proteins: *Displayed is the CO_2-reduction capability, calculated based on the total amount (in nmol) of reduced carbon atoms (TON = turnover number). Overall, NifH^{Ma}R98H retains ~80 % of the CO_2-reducing capability of wildtype NifH^{Ma}. While the amounts of CO formed by NifH^{Ma} and NifH^{Ma}R98H are similar, the latter forms less hydrocarbons and only up to C_3-products, thus changing the ratio of formed hydrocarbons:CO from 2.7 for NifH^{Ma} to 1.9 for NifH^{Ma}R98H. NifH^{Ma}R98G displays only ~15 % of the CO_2-reduction capability of wildtype NifH^{Ma}, with mainly CO and CH_4 being formed.*

3.4 Discussion

The initial discovery of NifH^{Av} facilitating the reduction of CO_2 to CO provided the first insight into NifDK-independent catalytic capabilities of NifH proteins [10]. The utilization of NifH^{Ma} then further extended the range of NifH-facilitated CO_2-reduction [11]. The mutation of two Arg residues in close proximity to the Fe_4S_4 cluster presented here now gave additional insights into the mechanistic details of CO_2-reduction, without affecting the electronic properties of the Fe_4S_4 cluster. Preserving the hydrogen-bonding and proton-donating abilities of the residue by utilizing His in the respective position 98 of NifH^{Ma} resulted in a slightly reduced capability of the protein to form hydrocarbons. This can be attributed to a shorter

side chain which may worsen the hydrogen-bonding and proton-donating abilities of NifH^{Ma}R98H. A complete removal of a potential interaction between the substrate CO_2 and the amino acid at position 98 significantly decreased the reduction of CO_2 by NifH^{Ma}R98G. Thus, a hydrogen-bond-donating and proton-donating residue appears to be sufficient for significant CO_2-reduction, while a sufficient range of the residue is required for the formation of extended hydrocarbons by NifH.

Comparing the crystal structures of dithionite-reduced NifH^{Av} (PDB 1G5P) [15] and CO_2-bound NifH^{Ma} (PDB 6NZJ) [13] can provide further mechanistic ideas of the CO_2-reduction by NifH proteins. While NifH^{Av} and NifH^{Ma} share 59 % sequence identity and 72 % sequence similarity, the C_α root-mean-square deviation (RMSD) between the A and B subunits of both proteins amounts to only 0.599 and 0.616 Å, respectively [13]. Comparing the position of the Fe_4S_4 clusters in both structures reveals a slightly higher surface exposure of the cluster of NifH^{Ma} which goes in concert with a flatter protein surface, compared to NifH^{Av} (Figure 3.3). In the case of NifH^{Ma}, the helices C^A and C^B adopt a more linearized confirmation (in the top-view perspective) with the Fe_4S_4 cluster located in between them (Figure 3.3). The Arg residues under investigation ($R98^A$ and $R98^B$) are located proximally with respect to the Fe_4S_4 cluster and oriented towards it (Figure 3.3). In NifH^{Av} the respective helices are almost parallel to each other (in the top-view perspective) and the Arg residues ($R100^A$ and $R100^B$) are oriented away from the Fe_4S_4 cluster (Figure 3.3). This slightly different conformation of the secondary structure could facilitate the CO_2-reception at the Fe_4S_4 cluster due to its increased surface exposure. The supposedly crucial Arg residues could further hold the CO_2 at the active site by stabilizing the activated CO_2 via hydrogen-bonding. These differences in NifH^{Ma} could be a reason for the advanced CO_2-reduction to hydrocarbons by this NifH homologue and highlight the importance of the role of the two Arg residues investigated above. However, the observed

conformation could also be altered by the CO_2 trapped on $NifH^{Ma}$ in the $Fe_4S_4^{1+}$-state which changed the protein into a turnover-like state. Furthermore, differences in non-conserved charged residues between $NifH^{Ma}$ and $NifH^{Av}$ also contribute to a general difference in electrode potential. Here, $NifH^{Av}$ has an elementary charge of -16, while $NifH^{Ma}$ has an elementary charge of -7. This difference might also contribute to differences in the reduction abilities of the two proteins.

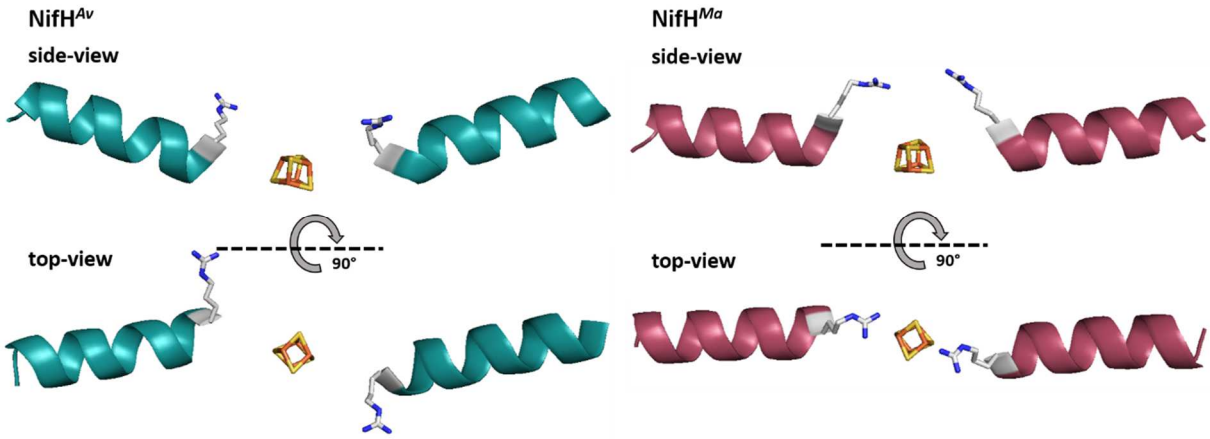

Figure 3.3 Comparative view of $NifH^{Av}$ and $NifH^{Ma}$: *Displayed are the helices C^A and C^B and the Fe_4S_4 cluster (Fe = orange, S = yellow) in-between them of $NifH^{Av}$ (left, marine blue) and $NifH^{Ma}$ (right, raspberry red). The Arg residues (R100 for $NifH^{Av}$, R98 for $NifH^{Ma}$) are displayed as sticks in grey with the nitrogen atoms in blue. The R100 residues of $NifH^{Av}$ are facing away from the central Fe_4S_4 cluster and the helices C^A and C^B are oriented in a parallel manner. The R98 residues of $NifH^{Ma}$ are facing towards the Fe_4S_4 cluster and the helices C^A and C^B are oriented in a linear manner. The side-view shows that the Fe_4S_4 cluster of $NifH^{Av}$ is less solvent-exposed due to more acute angle of the helices C^A and C^B.*

Based on DFT calculations performed on active-site models of $NifH^{Av}$, CO_2-binding in the active site could be facilitated by an interaction between a Fe atom from the Fe_4S_4 cluster in the super-reduced 0 oxidation-state and the carbon atom of the substrate molecule [10]. The coordination and activation of CO_2 is accompanied by the accumulation of negative charge at its two oxygen atoms, one of which interacts with the positively charges guanidinium group of one of the two Arg100 residues. This interaction stabilizes the bound CO_2 and enables the

proton transfer necessary for the release of a first H_2O. The binding energy for this interaction was calculated to be slightly exothermic with about -5 kcal/mol [10]. The need for a stabilizing residue in the respective position (100 for NifH^{Av}, 98 for NifH^{Ma}) was also shown by the biochemical assessment of NifH^{Ma} variants performed for this thesis, which further validates the proposed model. These calculations however do not account for the CO_2-reduction by NifH^{Av} in presence of dithionite, which only allows the reduced 1+ state of the Fe_4S_4 cluster [10]. Under these DT-reduced conditions, the amount of formed CO from CO_2 by NifH^{Av} is two orders of magnitude lower than under super-reduced conditions with Eu^{II}-DTPA. However, the super-reduced state might also be acquired temporarily by a small population of Fe_4S_4 clusters on NifH when DT is used as a reductant.

The reversible reduction of CO_2 to CO is also catalysed by the enzyme CO dehydrogenase (CODH), which contains a $NiFe_4S_4$ cluster, termed cluster C, in its active site [16], [17]. During catalysis, the carbon atom of CO_2 coordinates to the Ni of cluster C. One of the two oxygen atoms coordinates to a Fe of cluster C, with a lysine and a histidine residue in close proximity, which are both crucial for catalysis by CODH [16], [18]. The need for a residue with hydrogen bonding and proton donating abilities near the substrate CO_2 in two independent CO_2-reducing enzymes indicates the importance of such interactions during catalysis.

3.5 Acknowledgements

I am very grateful to Dr. Lee Rettberg for his accompanying structural research and Dr. Martin Stiebritz for his DFT calculation results. I also would like to thank Dr. Caleb Hiller, Dr. Wonchull Kang and Dr. Chi Chung Lee for their contributions to this project.

Furthermore, I am grateful to the American Society for Microbiology for publishing the results [13] and giving me permission to reuse parts of the publication for this chapter.

3.6 References

[1] B. K. Burgess and D. J. Lowe, “Mechanism of molybdenum nitrogenase,” *Chem. Rev.*, vol. 96, no. 7, pp. 2983–3011, Nov. 1996.

[2] L. C. Seefeldt, S. A. Ensign, and M. E. Rasche, “Carbonyl Sulfide and Carbon Dioxide as new Substrates, and Carbon Disulfide as a new Inhibitor, of Nitrogenase,” *Biochemistry*, vol. 34, no. 16, pp. 5382–5389, Apr. 1995.

[3] C. C. Lee, Y. Hu, and M. W. Ribbe, “Vanadium nitrogenase reduces CO,” *Science*. 2010.

[4] C. K. Rofer-DePoorter, “A Comprehensive Mechanism for the Fischer-Tropsch Synthesis,” *Chem. Rev.*, vol. 81, no. 5, pp. 447–474, 1981.

[5] Z. Y. Yang, V. R. Moure, D. R. Dean, and L. C. Seefeldt, “Carbon dioxide reduction to methane and coupling with acetylene to form propylene catalyzed by remodeled nitrogenase,” *Proc. Natl. Acad. Sci. U. S. A.*, vol. 109, no. 48, pp. 19644–19648, Nov. 2012.

[6] J. G. Rebelein, Y. Hu, and M. W. Ribbe, “Differential Reduction of CO2 by Molybdenum and Vanadium Nitrogenases,” *Angew. Chemie - Int. Ed.*, vol. 53, no. 43, pp. 11543–11546, Oct. 2014.

[7] A. J. Jasniewski, C. C. Lee, M. W. Ribbe, and Y. Hu, “Reactivity, Mechanism, and Assembly of the Alternative Nitrogenases,” 2020.

[8] Y. Zheng *et al.*, “A pathway for biological methane production using bacterial iron-only nitrogenase,” *Nat. Microbiol.*, vol. 3, no. 3, pp. 281–286, Mar. 2018.

[9] J. G. Rebelein, Y. Hu, and M. W. Ribbe, “Widening the Product Profile of Carbon Dioxide Reduction by Vanadium Nitrogenase,” *ChemBioChem*, vol. 16, no. 14, pp. 1993–1996, Sep. 2015.

[10] J. G. Rebelein, M. T. Stiebritz, C. C. Lee, and Y. Hu, “Activation and reduction of carbon dioxide by nitrogenase iron proteins.,” *Nat. Chem. Biol.*, vol. 13, no. 2, pp. 147–149, 2017.

[11] M. T. Stiebritz *et al.*, “Ambient conversion of CO2 to hydrocarbons by biogenic and synthetic [Fe4S4] clusters,” *Nat. Catal.*, vol. 1, no. 6, pp. 444–451, Jun. 2018.

[12] C. J. Hiller, M. T. Stiebritz, C. C. Lee, J. Liedtke, and Y. Hu, “Tuning Electron Flux through Nitrogenase with Methanogen Iron Protein Homologues.,” *Chemistry*, vol. 23, no. 64, pp. 16152–16156, Nov. 2017.

[13] L. A. Rettberg *et al.*, “Structural analysis of a nitrogenase iron protein from

methanosarcina acetivorans: Implications for CO2 capture by a surface-exposed [Fe4S4] cluster," *MBio*, vol. 10, no. 4, p. 2020, Jul. 2019.

[14] C. J. Hiller, M. T. Stiebritz, C. C. Lee, J. Liedtke, and Y. Hu, "Tuning Electron Flux through Nitrogenase with Methanogen Iron Protein Homologues," *Chem. - A Eur. J.*, vol. 23, no. 64, pp. 16152–16156, Nov. 2017.

[15] J. L. Schlessman, D. Woo, L. Joshua-Tor, J. B. Howard, and D. C. Rees, "Conformational variability in structures of the nitrogenase iron proteins from Azotobacter vinelandii and Clostridium pasteurianum," *J. Mol. Biol.*, vol. 280, no. 4, pp. 669–685, Jul. 1998.

[16] J. Fesseler, J. H. Jeoung, and H. Dobbek, "How the [NiFe4S4] Cluster of CO Dehydrogenase Activates CO2 and NCO-," *Angew. Chemie - Int. Ed.*, vol. 54, no. 29, pp. 8560–8564, Jul. 2015.

[17] M. Can, F. A. Armstrong, and S. W. Ragsdale, "Structure, function, and mechanism of the nickel metalloenzymes, CO dehydrogenase, and acetyl-CoA synthase," *Chemical Reviews*, vol. 114, no. 8. American Chemical Society, pp. 4149–4174, 23-Apr-2014.

[18] E. J. Kim, J. Feng, M. R. Bramlett, and P. A. Lindahl, "Evidence for a Proton Transfer Network and a Required Persulfide-Bond-Forming Cysteine Residue in Ni-Containing Carbon Monoxide Dehydrogenases," *Biochemistry*, vol. 43, no. 19, pp. 5728–5734, May 2004.

Chapter 4: Characterization of a Mo-Nitrogenase Variant Containing a Citrate-Substituted Cofactor

4.1 Introduction

Nitrogenase is a versatile metalloenzyme that catalyses the reduction of N_2 to NH_3, and CO to hydrocarbons (e.g., C_2H_6, C_3H_8 and C_4H_{10}), concomitant with the formation of H_2 [1]–[7]. The two nitrogenase reactions mirror two important industrial processes: the Haber-Bosch process, which combines N_2 and H_2 into NH_3; and the Fischer-Tropsch process, which combines CO and H_2 into hydrocarbons [8], [9]. However, the industrial processes use the syngas H_2 to reduce N_2 or CO at high temperatures and pressures; whereas in contrast, the reactions catalysed by nitrogenase use H^+/e^- to reduce N_2 or CO under ambient conditions, and they generate H_2 as an abundant side product. The ability of nitrogenase to effect ambient reduction of N_2 or CO makes this enzyme an attractive subject for studying small molecule activation and developing cost-efficient strategies for the production of useful chemical commodities in the future.

The "classic" Mo-dependent nitrogenase is the best characterized member of the nitrogenase enzyme family, which utilizes a reductase component to specifically donate electrons to a catalytic component for substrate reduction [1]–[3], [6], [7]. Designated the Fe protein (or NifH), the reductase component of Mo-nitrogenase is a homodimer of ~60 kDa that contains a Fe_4S_4 cluster at the subunit interface and a MgATP-binding site within each subunit. Designated the MoFe protein (or NifDK), the catalytic component of Mo-nitrogenase is an $\alpha_2\beta_2$-tetramer of ~230 kDa that contains a pair of complex metalloclusters in each αβ-dimer: a P-cluster ($[Fe_8S_7]$) that is located at each α/β-subunit interface; and an M-cluster (or cofactor; [(*R*-homocitrate)$MoFe_7S_9C$]) that is housed within each α-subunit. Catalysis by the Mo-nitrogenase is believed to involve repeated complex association/dissociation between NifH and NifDK, during which process electrons are transferred concomitantly with ATP

hydrolysis from the Fe_4S_4 cluster of NifH, via the P-cluster, to the M-cluster of NifDK, where substrate reduction eventually takes place.

Arguably one of the most complex metallocofactors found in biological systems, the M-cluster underlies the diverse catalytic capabilities of Mo-nitrogenase. Other than N_2, the Mo-nitrogenase is capable of reducing a wide range of alternative substrates, such as C_2H_2, CN^- and CO, at ambient conditions. Of these alternative substrates, CO is the most interesting one because it is isoelectronic to N_2. Considered mainly as an inhibitor for the Mo-nitrogenase, CO was shown to be reduced by the M-nitrogenase to short-chain hydrocarbons (up to C4 products) at ~0.02 nmol reduced C/nmol of protein/min [5]. This activity is only marginal relative to that of the Mo-nitrogenase in the reduction of its physiological substrate, N_2. Such a drastic discrepancy in the activities of N_2- and CO-reduction points to a clear distinction between the mechanisms of the two reactions despite the isoelectronic properties of N_2 and CO and the apparent "common denominator" of H_2 evolution that occurs in both N_2- and CO-reduction by Mo-nitrogenase.

Intimately associated with the reduction of substrates, the shuttling of protons by nitrogenase during catalysis is one key aspect of the mechanistic investigation of enzyme. The homocitrate ligand of the cofactor is an excellent target for this line of investigation given the proposed role of this organic ligand in proton delivery during substrate reduction [10]–[12]. Homocitrate is synthesized by the nifV-encoded homocitrate synthase (or NifV) in the cell [13], [14]. Previously, a Mo-nitrogenase variant was expressed upon deletion of nifV in *Klebsiella pneumoniae* (*K. pneumoniae*) [15], [16]. Subsequent crystallographic analysis revealed the presence of a citrate-substituted M-cluster at the active site of the NifDK component of this Mo-nitrogenase variant. Activity analysis further demonstrated a substantial decrease in the

activity of N_2 reduction by this NifDK variant, as well as an inhibition of its activity in H_2 evolution by CO [17], [18]. The inhibition of H_2 evolution upon citrate substitution is particularly interesting, as it may imply a re-distribution of protons/electrons from H_2-evolution toward hydrocarbon-formation in CO reduction as previously observed in the case of the V-nitrogenase, a homolog to the Mo-nitrogenase [4]. More importantly, substitution of the organic ligand of the cofactor seems to impact the catalytic behaviour of nitrogenase toward both N_2 and CO via alteration of proton supplies, pointing to the utility of this approach in probing the reaction mechanism of nitrogenase [19].

4.2 Materials and Methods

Strain construction and cell growth.

Azotobacter vinelandii strain YM13A, which expresses a His-tagged form of wildtype NifDK ($NifDK^{WT}$) [20], was used to construct a *nifV*-deletion strain. Specifically, using a previously described protocol [21], a DNA fragment carrying a 1.3-kb kanamycin resistance cartridge between the flanking sequences of *nifV* on the chromosome of *A. vinelandii* was transformed into YM13A and used to replace *nifV* with the kanamycin resistance cassette via homologous recombination. The resulting *A. vinelandii* strain, designated YM81A, expresses a His-tagged, citrate-substituted variant of NifDK ($NifDK^{Cit}$) due to the absence of the *nifV*-encoded homocitrate synthase. Strains YM13A [20], YM81A, YM7A [22], DJ1165 [23], and DJ1041 [24], which express His-tagged $NifDK^{WT}$, $NifDK^{Cit}$, $NifDK^{apo}$, $NifDK^{\Delta nifH}$, and NifEN respectively, were grown in 180 L batches in a 200 L New Brunswick fermenter (New Brunswick Scientific) in Burke's minimal medium supplemented with 2 mM ammonium acetate as described earlier [20]–[24]. Cells were harvested in the late exponential phase by a

flowthrough centrifugal harvester (Cepa), and the cell paste was washed with a buffer containing 50 mM Tris-HCl (pH 8.0). Published methods were then used for the purification of His-tagged NifDK proteins and nontagged NifH protein [20]–[24].

Protein characterization

The subunit compositions of His-tagged $NifDK^{WT}$ and $NifDK^{Cit}$ proteins were determined by SDS-PAGE analysis on a 4-20 % precast Tris-glycine gel (Bio-Rad). The metal contents of the proteins were determined by inductively coupled plasma-optical emission spectroscopy (ICP-OES) based on previously established protocols [25]. The native molecular masses of His-tagged $NifDK^{WT}$ and $NifDK^{Cit}$ proteins were determined by size exclusion chromatography using an Ultrogel ACA 34 column (Pall Life Science; ID: 2.5 cm, Length: 1.4 m) at a flow rate of 0.5 mL/min. Conalbumin (75 kDa), aldolase (158 kDa), ferritin (440 kDa) and thyroglobulin (669 kDa) were used as protein standards (GE Healthcare Biosciences). A native molecular mass of 241 kDa was determined for $NifDK^{Cit}$, consistent with an $\alpha_2\beta_2$-subunit composition.

Organic acid determination

Protein samples were evaporated to dryness under Ar and resuspended in pyridine prior to incubation at 70 °C for 14 h under Ar with bis-trimethylsilyl) trifluoroacetamide (BSTFA) and 30 % trimethylchlorosilane (TMCS), the derivatizing agents that convert the alcohol functional groups to trimethylsilyl (TMS) groups. The derivatized products were then extracted with oxygen-free hexanes prior to being analysed by GC-MS. For GC-MS analysis, 1 µL of the hexane extraction layer was injected into a GC-MS (Thermo Scientitific, Trace 1300 GC and ISQ single quadrupole MS) with a split injector set at 120 °C. The flow rate of high purity He carrier gas was set at 12 mL/min with a split ratio of 2. A 4 mm ID liner with glass

wool was used to protect the column from unreacted silylating reagent and inorganic components of the derivatization reaction mixture. Derivatized products were separated on a VF-5ms 30 m x 0.25 mm capillary column (Agilent Technologies), which was held at 120 °C for 3 min, heated to 200 °C at a rate of 10 °C/min, and held at 200°C for another 19 min. The mass spectrometer was operated in electron impact (EI) ionization and positive ion modes. Silylated products were identified by using both the scan mode and the selected ion monitoring (SIM) mode of GC-MS.

EPR spectroscopy

EPR samples were prepared in a Vacuum Atmospheres dry box at an oxygen level of <4 ppm. All reduced samples contained 0.5 mM protein, 25 mM Tris-HCl (pH 8.0), 10 % glycerol and 2 mM sodium dithionite ($Na_2S_2O_4$). The oxidized samples were prepared by adding excess IDS (from a 5 mM stock solution) to the dithionite-reduced sample until the sample turned dark blue, followed by incubation of the sample for 10 min. The EPR spectra were taken in perpendicular mode using a Bruker ESP 300 Ez spectrophotometer (Bruker) interfaced with an Oxford Instruments ESR-9002 liquid helium continuous flow cryostat. All perpendicular mode spectra were recorded at temperatures indicated in Figure 2A and B, using a microwave power of 1 mW, a gain of 5×10^4, a modulation frequency of 100 kHz, and a modulation amplitude of 5 G. A microwave frequency of 9.62 GHz was used to collect five scans for each sample. The parallelmode spectra shown in Figure 2C were recorded at a temperature of 10 K, a microwave power of 50 mW, and otherwise identical conditions to those described above for the collection of perpendicular-mode spectra.

Activity assays

All nitrogenase activity assays were carried out as described earlier [21], [26]. The hydrocarbon products were analysed as described elsewhere [4], [5], [25]. Ammonium was determined by a high-performance liquid chromatography fluorescence method [27], and hydrogen was analysed as described previously [28]. The *in vitro* NifEN-based cluster maturation assays and the *in vitro* reconstitution of $NifDK^{apo}$ with clusters donated by NifEN were carried out as described earlier [29]–[31].

4.3 Results and Discussion

Using a similar strategy applied previously to *K. pneumoniae* [18], we constructed an *Azotobacter vinelandii* (*A. vinelandii*) *nifV*-deletion strain expressing a His-tagged NifDK variant, cultivated the strain under N_2-fixing conditions, and subsequently isolated this NifDK variant using affinity chromatography. Designated $NifDK^{Cit}$, this NifDK variant has the same $\alpha_2\beta_2$-subunit composition (Figure 1A) and the same Mo/Fe ratio of the metal clusters (Figure 1B) as the wildtype NifDK (designated $NifDK^{WT}$). However, the Mo content of $NifDK^{Cit}$ is only ~31% of that of $NifDK^{WT}$, suggesting a partial occupancy of the cofactor sites in $NifDK^{Cit}$ (Figure S1A). Consistent with this suggestion, the as-isolated $NifDK^{Cit}$ can be further activated by ~4 fold upon reconstitution with the isolated M-clusters (Figure S1B). Results from the GC-MS analysis reveal the presence of citrate in place of homocitrate in the cofactor of $NifDK^{Cit}$ (Figure 1C, D) and, together with the data from metal analysis, these results establish this cofactor species as a citrate-substituted M-cluster analogue (designated M-$cluster^{Cit}$).

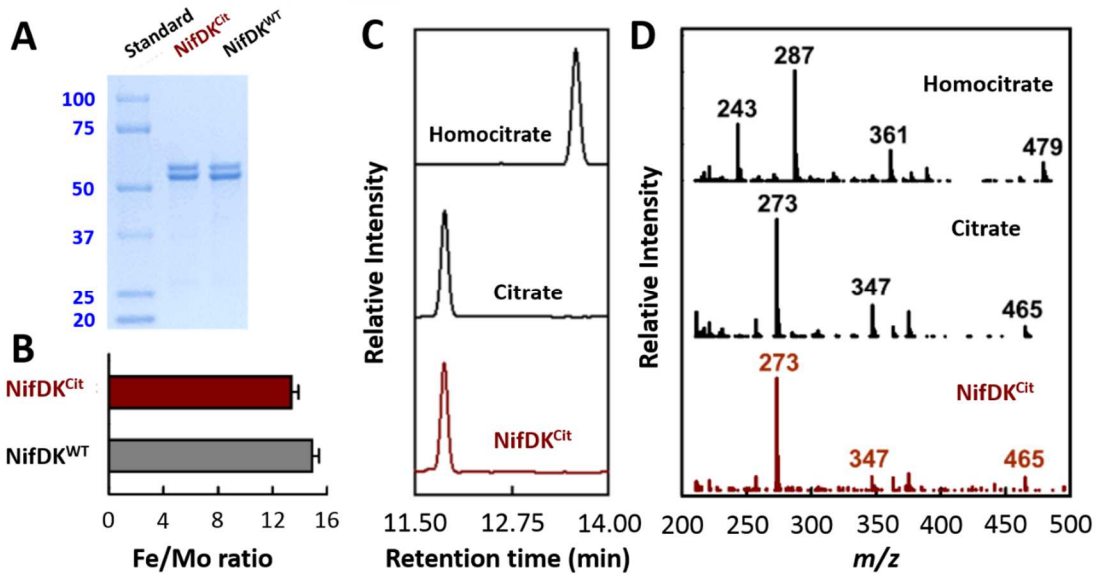

Figure 4.1 Subunit composition, metal content and organic ligand of NifDK^{Cit}: *(A) SDS-PAGE of NifDK^{Cit} and NifDK^{WT}. The molecular masses (in kilodaltons) of the protein standards are shown on the left of the gel. (B) Fe/Mo ratios of NifDK^{Cit} and NifDK^{WT}. The Mo contents of NifDK^{Cit} and NifDK^{WT} are 0.62+0.03 and 1.95+0.10 mol Mo/mol protein, respectively. (C) GC and (D) GC-MS chromatography of NifDK^{Cit} using homocitrate and/or citrate as the standard. The m/z ratios of the derivatized homocitric and/or citric acid fragments used for the identification of the organic compound are indicated in the GC-MS fragmentation patterns (D).*

EPR analyses of NifDK^{Cit} provide important insights into the electronic and spin properties of its associated cluster species (Figure 2). In the dithionite-reduced state, NifDK^{Cit} displays an S = 3/2 signal that is nearly indistinguishable in g-values and temperature-dependency from the signal displayed by NifDK^{WT} (Figure 2A, B upper, brown vs. black). However, compared to the S = 3/2 signal of NifDK^{WT}, the S = 3/2 signal of NifDK^{Cit} is clearly broadened in line-shape and significantly decreased in signal intensity (~40 % relative to the S = 3/2 signal of NifDK^{WT} upon normalization of the Mo-content), pointing to an impact of citrate substitution on the spin properties of the M-cluster. Other than the S = 3/2 signal, NifDK^{Cit} also displays an S = 1/2 at g = 2.05 and 1.93, which is nearly identical to the S = 1/2 signal displayed by the NifDK variant isolated from a *nifH*-deletion strain of *A. vinelandii* (designated NifDK$^{\Delta nifH}$) [23] in terms of g-values and temperature-dependency (Figure 2A, B lower, brown vs. blue).

This signal was shown to originate from a P-cluster precursor in NifDKΔ^{nifH}, which consists of a Fe_4S_4 cluster pair instead of a mature Fe_8S_7 structure [23], [32]. The presence of this cluster species in NifDK^{Cit} (~26 % relative to that in NifDK$^{\Delta nifH}$) (Figure 2A, brown), along with a fully matured P-cluster species (reflected by the *g* = 11.8 signal of the IDS-oxidized P-cluster) (Figure 2C, brown), suggests a certain structural instability of NifDK^{Cit} at the α/β-subunit interface where the P-cluster resides. Such an instability likely originates from the "incompatibility" of the altered M-cluster^{Cit} with its binding site, leading to the partial occupancy of the M-cluster^{Cit} within the α-subunit and the ensuing instability of the P-cluster at the α/β-subunit interface.

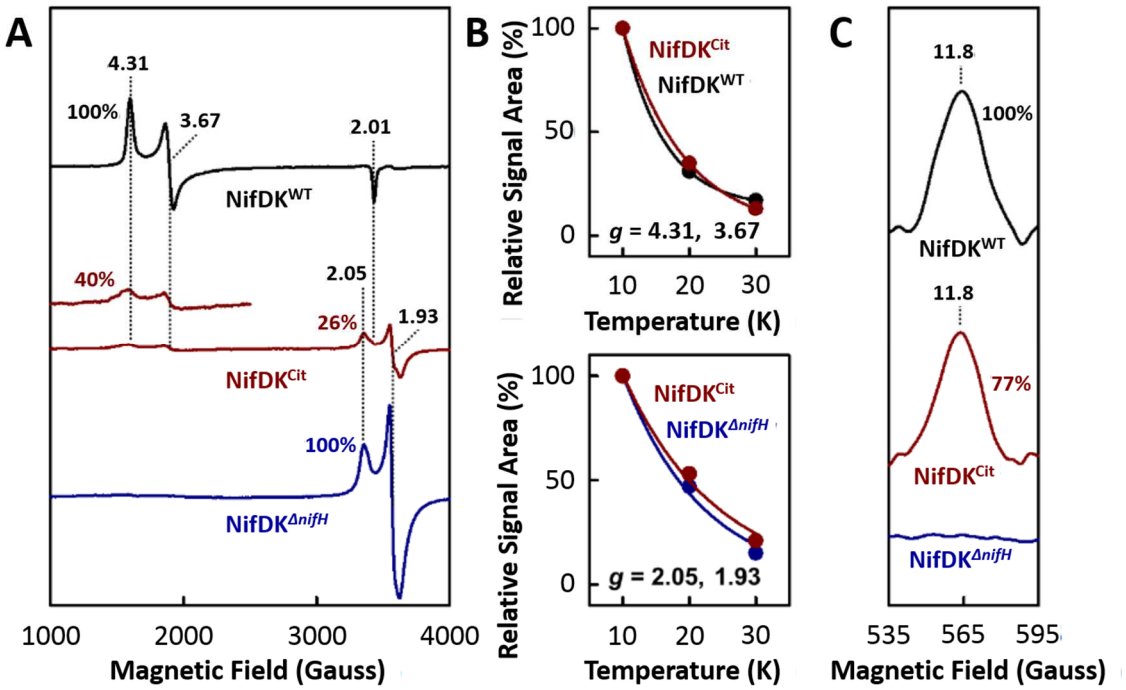

Figure 4.2 EPR spectroscopic properties of NifDK^{Cit}: *(A) EPR spectra (perpendicular-mode) of dithionite reduced NifDK^{WT} (upper, black), NifDK^{Cit} (middle, brown) and NifDK$^{\Delta nifH}$ (lower, blue). The relative signal intensities of the M-cluster-specific S = 3/2 species at g = 4.31 and 3.67, normalized based on the Mo content, are shown for NifDK^{Cit} and NifDK^{WT}, with the value of NifDK^{WT} set as 100 %. The relative signal intensities of the P-cluster precursor-specific S = 1/2 species at g = 2.05 and 1.93 are shown for NifDK^{Cit} and NifDK$^{\Delta nifH}$, with the value of NifDK$^{\Delta nifH}$ set as 100 %. The EPR spectra were collected at 1 mW and 10 K. (B) Temperature dependence of the M-cluster-specific S=3/2 species at g=4.31 and 3.67 (upper) and the P-cluster precursor-specific S = 1/2 species at g = 2.05 and 1.93 (lower). The signal intensities are expressed as relative signal areas, with the total signal areas set as 100 %. The plots in B are coloured the same way as the corresponding EPR traces in A. (C) EPR spectra (parallel-mode) of IDS-oxidized NifDK^{WT} (upper, black), NifDK^{Cit} (middle, brown) and NifDK$^{\Delta nifH}$ (lower, blue). The EPR spectra were collected at 50 mW and 10 K. The relative signal intensities of the P-cluster-specific species at g = 11.8 are shown for NifDK^{WT} and NifDK^{Cit}, with the value of NifDK^{WT} set as 100 %. Data in this figure were collected on the as-isolated NifDK^{Cit}, NifDK^{WT} and NifDK$^{\Delta nifH}$.*

Results from the Mo K-edge XAS analysis of NifDK^{Cit} align well with those from the EPR analysis. The Mo K-edge XAS/EXAFS spectra of NifDK^{WT} and NifDK^{Cit} are very similar to each other, suggesting a similar Mo environment in the cofactor species of these proteins (Figure 3A-C). Consistent with this observation, NifDK^{WT} and NifDK^{Cit} closely resemble each other in the EXAFS-derived Mo-S, Mo-O/N, Mo···Fe and Mo···C distances of their respective cofactors (Figure 3D). However, there is a difference in the Mo K-edge energies of NifDK^{WT} (20011.3 eV)

and NifDK^{Cit} (20012.0 eV), which could result from a difference in the oxidation state, spin state and/or ligand identity of the cofactors in these proteins (Figure 3A). Since the O-donor ligands of homocitrate and citrate that bind to the respective Mo centres in NifDK and NifDK^{Cit} are very similar to each other, the observed K-edge difference of 0.7 eV between these proteins likely originates from a change in the oxidation state or spin properties. Given the observed difference between NifDK^{Cit} and NifDK^{WT} in their cofactor-originated S = 3/2 signals (see Figure 2A), the difference in the K-edge energies of their XAS spectra again points to a possible impact of citrate substitution on the spin properties of the M-cluster.

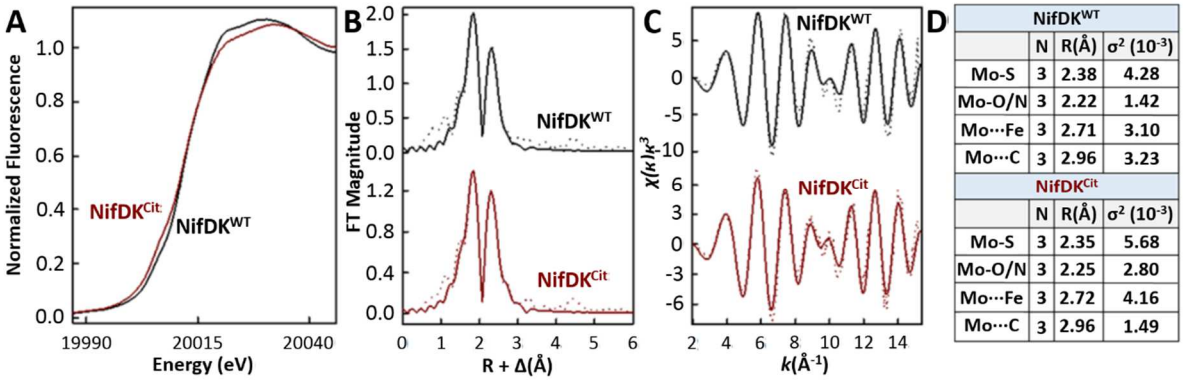

NifDK^{WT}			
	N	R(Å)	σ^2 (10^{-3})
Mo-S	3	2.38	4.28
Mo-O/N	3	2.22	1.42
Mo···Fe	3	2.71	3.10
Mo···C	3	2.96	3.23
NifDK^{Cit}			
	N	R(Å)	σ^2 (10^{-3})
Mo-S	3	2.35	5.68
Mo-O/N	3	2.25	2.80
Mo···Fe	3	2.72	4.16
Mo···C	3	2.96	1.49

Figure 4.3 Mo K-edge XAS/EXAFS analysis of NifDK^{WT} and NifDK^{Cit}: *(A) XAS analysis of NifDK^{WT} (black) and NifDK^{Cit} (brown). (B) Fourier transforms and (C) k3-weighted EXAFS data (dotted) and the best fits of data (solid) of NifDK^{WT} (black, upper) and NifDK^{Cit} (brown, lower). (D) Best fits of the experimental data with parameters between k = 2–15.3 Å-1. Data in this figure were collected on the as-isolated NifDK^{Cit} and NifDK^{WT}.*

Concomitant with a change in the spin properties of its cofactor, NifDK^{Cit} also demonstrates an alteration of its substrate-reducing behaviour. Compared to NifDK^{WT}, NifDK^{Cit} shows substantially reduced activities in H^+-, N_2-, C_2H_2- and CO-reduction (Figure S2A), which could be accounted for by the partial occupancy of the cofactor (i.e., M-cluster^{Cit}) in NifDK^{Cit} and an overall decrease of the electron flux (calculated from the number of electrons that appear in products) through this protein. Interestingly, compared to NifDK^{WT}, NifDK^{Cit}

shows a shift from NH_3- or C_2H_4-formation toward H_2-evolution in the reaction of N_2- or C_2H_2-reduction (Figure 4A), and an opposite shift from H_2-evolution toward hydrocarbon-formation in the reaction of CO-reduction (Figure 4B). To further verify these results, an *in vitro* maturation assay was used to incorporate Mo along with citrate and homocitrate, respectively, into an M-cluster precursor on the assembly protein, NifEN [30], [33]. This step was followed by reconstitution of the M-cluster deficient NifDK with the M-cluster or M-cluster^{Cit} donated by NifEN [30], [31], [33], which resulted in the *in vitro* equivalents of NifDK^{WT} and NifDK^{Cit}. A comparison between the substrate-reducing activities of the two proteins derived from the *in vitro* approach (Figure S2B; Figure 4C, D) shows the same results as those when their in vivo equivalents are compared (Figure S2A; Figure A, B), confirming the effect of citrate substitution on the activity of NifDK. Taken together, these results illustrate a perturbance of the proton supply and, consequently, the electron flux that is closely affiliated with proton delivery, in substrate reduction by NifDK upon citrate substitution. The disparate effects of such a substitution on the reduction of different substrates, particularly N_2 and CO, could very well reflect a mechanistic difference between the two reactions.

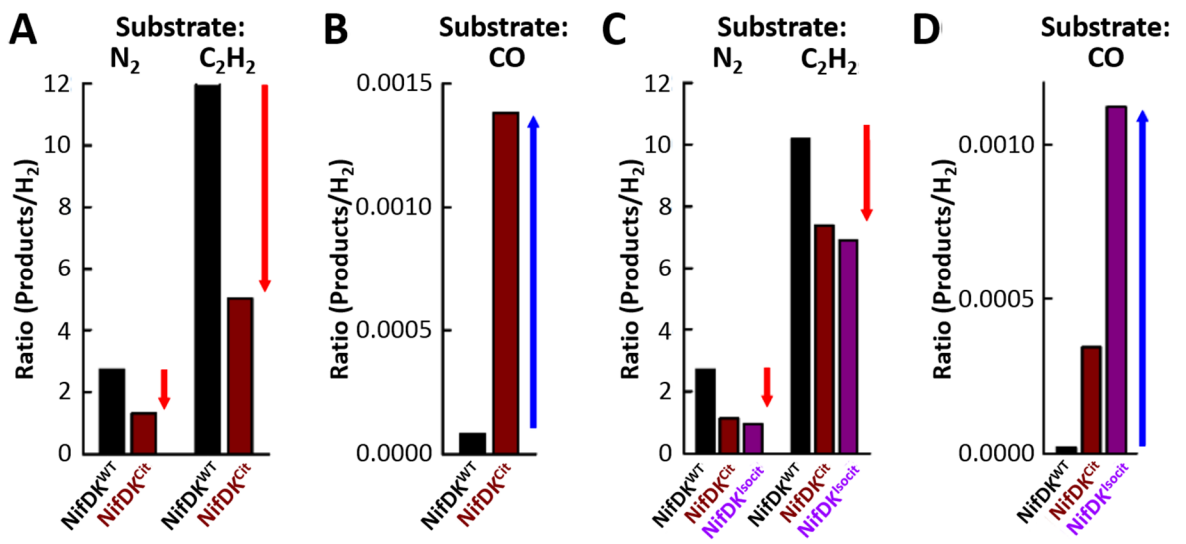

Figure 4.4 Products/H_2 ratios of N_2-, C_2H_2-, and CO-reduction by the various NifDK species generated by (A, B) in vivo and (C, D) in vitro approaches: *$NifDK^{WT}$, $NifDK^{Cit}$ and $NifDK^{Isocit}$ are coloured black, brown and purple, respectively. The increase or decrease of products/H_2 ratios are indicated by red or blue arrows. The products/H_2 ratios were calculated based on the numbers of electrons that appeared in the products (other than H_2) and H_2, respectively, using the values of substrate-reducing activities presented in Figure S2. In addition to H_2, the products of N_2-, C_2H_2- and CO-reduction are NH_3, C_2H_4 and hydrocarbons (C_2H_4 and C_2H_6), respectively.*

The *in vitro* approach presented an opportunity to generate additional M-cluster analogues with homocitrate replaced by other organic ligands, such as isocitrate, for further evaluation of the impact of organic ligand substitution on the catalytic properties of NifDK. Like $NifDK^{Cit}$, the isocitrate-substituted NifDK (designated $NifDK^{Isocit}$) displays decreased substrate-reducing activities in N_2-, C_2H_2- and CO-reduction, as well as a shift toward H_2-evolution in the reactions of N_2- and C_2H_2-reduction and an opposite shift toward hydrocarbon-formation in the reaction of CO-reduction (Figure S2B; Figure 4C, D). Strikingly, the shift toward hydrocarbon-formation in CO-reduction by $NifDK^{Isocit}$ is much more dramatic than that by $NifDK^{Cit}$ (Figure 4D). Given that isocitrate is a structural isomer of citrate, the similarity and distinction between the citrate- and isocitrate-substituted NifDK proteins

implies a stereospecific effect of the organic ligand in proton delivery while again pointing to the role of this ligand in shuttling protons for substrate reduction by nitrogenase.

Structural insights into the role of homocitrate in nitrogenase catalysis were obtained through our recent structural analysis of an N_2-bound conformation of NifDK [34]. Generated under limited electron fluxes, this conformation has the belt sulphurs (designated S2B, S5A and S3A) asymmetrically displaced with distinct dinitrogen species in the two M-clusters (i.e., S2B in one and S3A/S5A in the other) concomitant with oxidation of both P-clusters to the P_{OX} state in the two αβ-dimers of NifDK. Interestingly, in the αβ-dimer of NifDK where the belt sulphur S2B is displaced by a dinitrogen species, the Mo-O7 (hydroxyl) distance between Mo and homocitrate is substantially elongated; whereas in the αβ-dimer of NifDK where the belt sulphurs S3A and S5A are displaced by dinitrogen species, the Mo-O5 (carboxyl) distance between Mo and homocitrate is substantially elongated. Such an alternate elongation/breaking of the Mo-O7 and Mo-O5 bonds switches the coordination of Mo by homocitrate from bidentate to monodentate, which plausibly facilitates the rotation of the M-cluster around the Mo-C-Fe1 axis during substrate turnover. These observations have led to the proposal of a mechanism that involves the initial binding of N_2 at the S3A site, followed by cluster rotation and stepwise reduction of N2 at the S2B and S5A sites, and the release of NH_3 from S5A [34]. This proposal is consistent with a catalysis-dependent migration of belt sulphur as suggested by a previous crystallographic pulse-chase study [35], and it could explain why substitution with citrate or isocitrate has such a dramatic impact on substrate reduction, as such a cluster-rotation mechanism seems to be (stereo)specifically configured for R-homocitrate. It is possible that the alternate elongation/breaking of the Mo-O7 and Mo-O5 bonds, which results from an alternate protonation of these bonds, not only facilitates the

rotation of the M-cluster, but also participates in the delivery of protons (concomitant with electrons) to the bound substrate/intermediate to enable substrate reduction.

A survey of the difference between the N_2- and CO-bound structures of NifDK provides some clues to the disparate impact of organic ligand substitution on N_2- and CO-reduction. Contrary to the dinitrogen species that appear at all three belt sulphur sites of the M-cluster, CO was shown to bind only to the S2B site of the M-cluster in both dimers of NifDK [36][37]. Moreover, a switch of the Mo-homocitrate ligation from bidentate to monodentate was not observed in the crystal structure of the CO-bound NifDK [37]. The observation that CO tends to be "stuck" at the S2B site implies that (i) the cluster-rotation mechanism that is proposed for the efficient reduction of N_2 works, at best, extremely poorly for the reduction of CO and (ii) C-C coupling may occur mainly at the S2B site, where the "first" CO molecule is "stuck" long enough to be coupled with the "next" CO molecule. In this scenario, while substitution with citrate or isocitrate disrupts proton delivery and causes a significant decrease in H_2 production in both N_2- and CO-reduction (see Figure S2), it will have a differential impact on the reactions of N_2- and CO-reduction. In the case of N2 reduction, the impairment of cluster rotation upon organic ligand substitution causes a substantial decrease of NH_3 formation, so much so that it outweighs the decrease of H_2 evolution, resulting in a decreased NH_3/H_2 ratio (see Figure 4). In the case of CO reduction, however, the disruption of cluster rotation results in the cluster being "stuck" at S2B even longer to promote C-C coupling, resulting in an increased C_2 hydrocarbons/H_2 ratio.

Although the cluster rotation mechanism provides one plausible explanation for our experimental observables, evidence is yet to be obtained in support of this hypothesis. Additionally, altered binding modes of the ligand, impact of citrate substitution on proton

delivery, and conformational dynamics of citrate-like molecules and cognate model compounds should be explored as alternative explanations for the observed effect of organic ligand substitution on substrate reduction by nitrogenase. While the mechanistic details of nitrogenase and the specific actions of the organic ligand during catalysis require further investigation, the current study points to a crucial role of homocitrate in substrate reduction by nitrogenase. Moreover, the modulating effect of the organic ligand on the catalytic properties of nitrogenase suggests a distinct possibility to alter the product profiles of nitrogenase catalysed reactions upon substitution of this ligand, which could prove instrumental in future development of nitrogenase-based applications for the production of useful chemical commodities.

4.4 Acknowledgements

I am very grateful to Dr. Megan Newcomb who determined the identity of the organic compound and provided help with the activity assays as well. I would like to thank Dr. Andrew Jasniewski for his XAS/EXAFS analysis. I also thank John Quitangon for his help with the strain construction. I thank Dr. Kazuki Tanifuji and Dr. Chi Chung Lee for their contribution to this project.

Additionally, I would like to thank Wiley-VCH GmbH for publishing these results [38] and providing me permission to reuse the material for this chapter.

4.5 Appendix

Supporting Figures

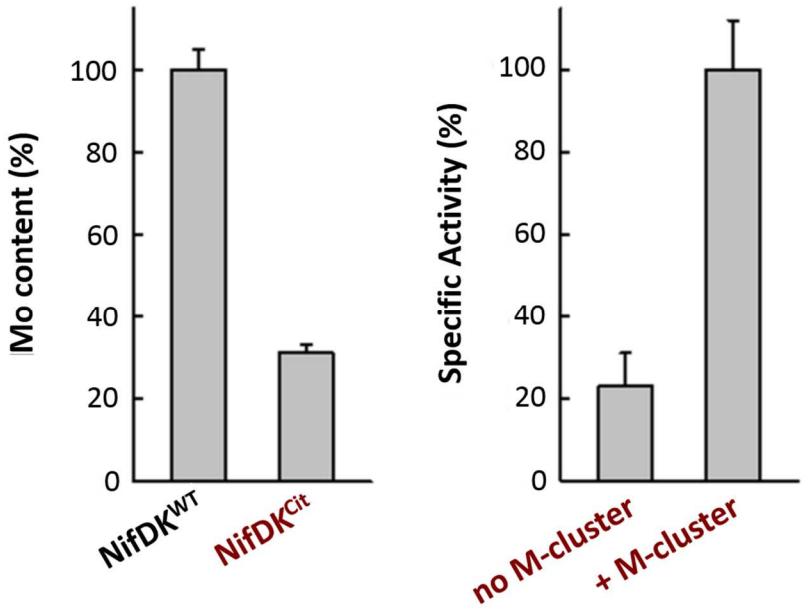

Figure S4.1 Cluster contents of NifDK^{WT} and NifDK^{Cit}*: (A) Mo contents of NifDK^{WT} and NifDK^{Cit}. The Mo content of NifDK^{Cit} is 0.62 ± 0.03 mol Mo/mol protein, which is 31% relative to that of NifDK^{WT}. (B) Specific activities of the as-isolated NifDK^{Cit} ("no M-cluster") and NifDK^{Cit} upon reconstitution with the isolated M-clusters ("+M-cluster"). The specific activity of C_2H_2-reduction by the as-isolated NifDK^{Cit} is 60 ± 13 nmol C_2H_4/nmol protein/min; whereas upon reconstitution with the isolated M-clusters, the specific activity of C_2H_2-reduction by NifDK^{Cit} is increased by ~4 fold.*

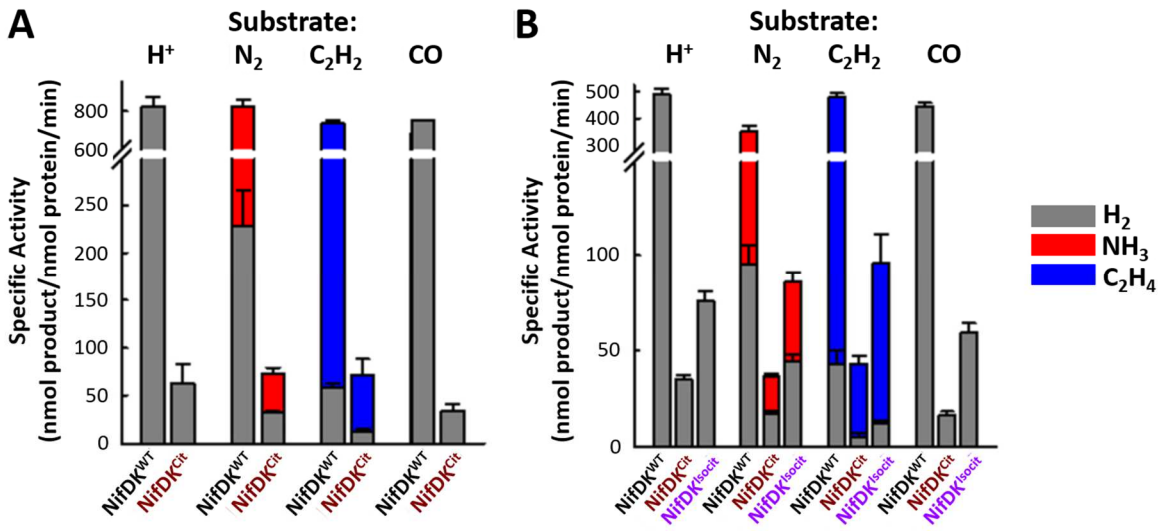

Figure S4.2 Specific activities of N_2-, C_2H_2- and CO-reduction by NifDK^{WT}, NifDK^{Cit}, and NifDK^{Isocit} proteins generated by (A) in vivo and (B) in vitro approach*: The amounts of hydrocarbons (C_2H_4 and C_2H_6) generated by CO-reduction, expressed as nmol products per assay, are as follows: 2.7 (A, NifDK^{WT}), 2.3 (A, NifDK^{Cit}), 0.4 (B, NifDK^{WT}), 0.3 (B, NifDK^{Cit}), and 3.0 (B, NifDK^{Isocit}). The amounts of products were calculated based on the numbers of electrons that appeared in the products.*

4.6 References

[1] B. K. Burgess and D. J. Lowe, "Mechanism of molybdenum nitrogenase," *Chem. Rev.*, vol. 96, no. 7, pp. 2983–3011, Nov. 1996.

[2] H. L. Rutledge and F. A. Tezcan, "Electron Transfer in Nitrogenase," *Chem. Rev.*, vol. 120, no. 12, pp. 5158–5193, 2020.

[3] A. J. Jasniewski, C. C. Lee, M. W. Ribbe, and Y. Hu, "Reactivity, Mechanism, and Assembly of the Alternative Nitrogenases," 2020.

[4] C. C. Lee, Y. Hu, and M. W. Ribbe, "Vanadium nitrogenase reduces CO," *Science*. 2010.

[5] Y. Hu, C. C. Lee, and M. W. Ribbe, "Extending the carbon chain: Hydrocarbon formation catalyzed by vanadium/molybdenum nitrogenases," *Science (80-.).*, 2011.

[6] D. C. Rees *et al.*, "Structural basis of biological nitrogen fixation."

[7] L. C. Seefeldt *et al.*, "Reduction of Substrates by Nitrogenases," 2020.

[8] C. K. Rofer-DePoorter, "A Comprehensive Mechanism for the Fischer-Tropsch Synthesis," *Chem. Rev.*, vol. 81, no. 5, pp. 447–474, 1981.

[9] C. C. Lee, Y. Hu, and M. W. Ribbe, "Tracing the Hydrogen Source of Hydrocarbons

Formed by Vanadium Nitrogenase," *Angew. Chemie Int. Ed.*, vol. 50, no. 24, pp. 5545–5547, Jun. 2011.

[10] I. Dance, "The controlled relay of multiple protons required at the active site of nitrogenase," *Dalt. Trans.*, vol. 41, no. 25, pp. 7647–7659, Jul. 2012.

[11] I. Dance, "The pathway for serial proton supply to the active site of nitrogenase: Enhanced density functional modeling of the Grotthuss mechanism," *Dalt. Trans.*, vol. 44, no. 41, pp. 18167–18186, Oct. 2015.

[12] K. D. Demadis, S. M. Malinak, and D. Coucouvanis, "Catalytic reduction of hydrazine to ammonia with MoFe3S4-polycarboxylate clusters. Possible relevance regarding the function of the molybdenum-coordinated homocitrate in nitrogenase," *Inorg. Chem.*, vol. 35, no. 13, pp. 4038–4046, 1996.

[13] L. Zheng, R. H. White, and D. R. Dean, "Purification of the Azotobacter vinelandii nifV-encoded homocitrate synthase," *J. Bacteriol.*, vol. 179, no. 18, pp. 5963–5966, 1997.

[14] T. R. Hoover *et al.*, "Identification of the V factor needed for synthesis of the iron-molybdenum cofactor of nitrogenase as homocitrate," *Nature*, vol. 329, no. 6142, pp. 855–857, 1987.

[15] J. Liang, M. Madden, V. K. Shah, and R. H. Burris, "Citrate Substitutes for Homocitrate in Nitrogenase of a nifV Mutant of Klebsiella pneumoniae," *Biochemistry*, vol. 29, no. 37, pp. 8577–8581, Sep. 1990.

[16] S. M. Mayer, C. A. Gormal, B. E. Smith, and D. M. Lawson, "Crystallographic analysis of the MoFe protein of nitrogenase from a nifV mutant of Klebsiella pneumoniae identifies citrate as a ligand to the molybdenum of iron molybdenum cofactor (FeMoco)," *J. Biol. Chem.*, vol. 277, no. 38, pp. 35263–35266, Sep. 2002.

[17] P. A. McLean and R. A. Dixon, "Requirement of nifV gene for production of wild-type nitrogenase enzyme in Klebsiella pneumoniae.," *Nature*, vol. 292, no. 5824, pp. 655–6, Aug. 1981.

[18] P. A. McLean, B. E. Smith, and R. A. Dixon, "Nitrogenase of Klebsiella pneumoniae nifV mutants.," *Biochem. J.*, vol. 211, no. 3, pp. 589–597, Jun. 1983.

[19] M. P. Newcomb *et al.*, "A V-Nitrogenase Variant Containing a Citrate-Substituted Cofactor," *ChemBioChem*, vol. 21, no. 12, pp. 1742–1748, Jun. 2020.

[20] Y. Hu, A. W. Fay, B. Schmid, B. Makar, and M. W. Ribbe, "Molecular insights into nitrogenase FeMoco insertion: TRP-444 of MoFe protein α-subunit locks FeMoco in its binding site," *J. Biol. Chem.*, vol. 281, no. 41, pp. 30534–30541, Oct. 2006.

[21] Y. Hu, A. W. Fay, P. C. Dos Santos, F. Naderi, and M. W. Ribbe, "Characterization of Azotobacter vinelandii nifZ deletion strains: Indication of stepwise MoFe protein assembly," *J. Biol. Chem.*, vol. 279, no. 52, pp. 54963–54971, Dec. 2004.

[22] Y. Hu *et al.*, "Nitrogenase reactivity with P-cluster variants," *Proc. Natl. Acad. Sci.*, 2005.

[23] M. W. Ribbe, Y. Hu, M. Guo, B. Schmid, and B. K. Burgess, “The femoco-deficient MoFe protein produced by a nifH deletion strain of Azotobacter vinelandii shows unusual P-cluster features,” *J. Biol. Chem.*, vol. 277, no. 26, pp. 23469–23476, Jun. 2002.

[24] Y. Hu, A. W. Fay, and M. W. Ribbe, “Identification of a nitrogenase FeMo cofactor precursor on NifEN complex,” *Proc. Natl. Acad. Sci. U. S. A.*, vol. 102, no. 9, pp. 3236–3241, Mar. 2005.

[25] N. S. Sickerman *et al.*, “Reduction of C1, substrates to hydrocarbons by the homometallic precursor and synthetic mimic of the nitrogenase cofactor,” *J. Am. Chem. Soc.*, vol. 139, no. 2, pp. 603–606, Jan. 2017.

[26] B. K. Burgess, D. B. Jacobs, and E. I. Stiefel, “Large-scale purification of high activity Azotobacter vinelandII nitrogenase.,” *Biochim. Biophys. Acta*, vol. 614, no. 1, pp. 196–209, Jul. 1980.

[27] J. L. Corbin, “Liquid chromatographic-fluorescence determination of ammonia from nitrogenase reactions: A 2-Min assay,” *Appl. Environ. Microbiol.*, vol. 47, no. 5, pp. 1027–1030, 1984.

[28] N. Gavini and B. K. Burgess, “FeMo cofactor synthesis by a nifH mutant with altered MgATP reactivity,” *J. Biol. Chem.*, vol. 267, no. 29, pp. 21179–21186, 1992.

[29] Y. Hu *et al.*, “FeMo cofactor maturation on NifEN,” *Proc. Natl. Acad. Sci.*, 2006.

[30] J. M. Yoshizawa *et al.*, “Optimization of FeMoco maturation on NifEN,” *J. Am. Chem. Soc.*, vol. 131, no. 26, pp. 9321–9325, Jul. 2009.

[31] B. Schmid *et al.*, “Structure of a cofactor-deficient nitrogenase MoFe protein,” *Science (80-.).*, vol. 296, no. 5566, pp. 352–356, Apr. 2002.

[32] M. C. Corbett, Y. Hu, F. Naderi, M. W. Ribbe, B. Hedman, and K. O. Hodgson, “Comparison of iron-molybdenum cofactor-deficient nitrogenase MoFe proteins by x-ray absorption spectroscopy. Implications for P-cluster biosynthesis,” *J. Biol. Chem.*, vol. 279, no. 27, pp. 28276–28282, Jul. 2004.

[33] Y. Hu *et al.*, “FeMo cofactor maturation on NifEN,” *Proc. Natl. Acad. Sci. U. S. A.*, vol. 103, no. 46, pp. 17119–17124, Nov. 2006.

[34] W. Kang, C. C. Lee, A. J. Jasniewski, M. W. Ribbe, and Y. Hu, “Structural evidence for a dynamic metallocofactor during N2 reduction by Mo-nitrogenase,” *Science (80-.).*, vol. 368, no. 6497, pp. 1381–1385, Jun. 2020.

[35] T. Spatzal, K. A. Perez, J. B. Howard, and D. C. Rees, “Catalysis-dependent selenium incorporation and migration in the nitrogenase active site iron-molybdenum cofactor,” *Elife*, vol. 4, no. DECEMBER2015, Dec. 2015.

[36] T. Spatzal, K. A. Perez, O. Einsle, J. B. Howard, and D. C. Rees, “Ligand binding to the FeMo-cofactor: Structures of co-bound and reactivated nitrogenase,” *Science (80-.).*, vol. 345, no. 6204, pp. 1620–1623, Sep. 2014.

[37] T. Spatzal *et al.*, “Evidence for interstitial carbon in nitrogenase FeMo cofactor,” *Science*, vol. 334, no. 6058. American Association for the Advancement of Science, p. 940, 18-Nov-2011.

[38] J. Liedtke, C. C. Lee, K. Tanifuji, A. Jasniewski, M. W. Ribbe, and Y. Hu, “Characterization of a Mo-nitrogenase variant containing a citrate-substituted cofactor,” *ChemBioChem*, p. cbic.202000598, Sep. 2020.

Chapter 5: Assessment of Small Organic Acids for Their Incorporation into Nitrogenase's M-cluster

5.1 Introduction

Nitrogenase's ability to reduce N_2, C_2H_2 and CO has been well described in this work and elsewhere [1]–[5]. For these reactions, nitrogenase relies on its unique cofactors to reduce substrates at the active site [6], [7]. When nitrogenase is expressed in a genetic background lacking the *nifB* gene, the resulting NifDK protein lacks the M-cluster within the active site. This apo-NifDK enzyme is incapable of any substrate reduction. Electron paramagnetic resonance (EPR) spectroscopic analysis of apo-NifDK shows a S = 1/2 signal instead of the characteristic S = 3/2 signal of wild-type enzyme [6], [8]. However the apo-nitrogenase can be reconstituted with M-cluster isolated from functional NifDK protein or *in vitro* from NifEN [9]–[13], enabling the enzyme to carry out catalysis and re-establish the S = 3/2 EPR-signal [6], [8].

The extracted M-cluster can also support catalysis independent of the protein scaffold [14]. Under these isolated conditions, the M-cluster is capable of forming hydrocarbons in the range of methane (CH_4) to pentene (C_5H_{10}) from CO [14], [15], while NifDK-bound M-cluster can only form hydrocarbons ranging from methane (CH_4) to propane (C_3H_8) [3]. This suggests that the nitrogenase protein has an effect on the reactive capability of the cluster within its active site. Further evidence for the role of the protein scaffold comes from a hybrid V-nitrogenase that contains the M-cluster instead of the typical V-cluster [16]. This hybrid V-nitrogenase showed an increased reactivity towards CO, which resembled the catalytic profile of wild-type V-nitrogenase containing V-cluster. Furthermore, EPR features of the hybrid V-nitrogenase and the wild-type V-nitrogenase are similar and lack the characteristic S = 3/2 signal the M-cluster usually displays [16].

Recent investigations of the organic ligand for both the M- and V-cluster suggest that the organic ligand has an impact on the catalytic profile of Mo- and V-nitrogenase [17], [18]. In order to further investigate the role of the organic ligand during nitrogenase catalysis, we tested additional small organic acids for their ability to form an active M-cluster in *in vitro* experiments. Based on the coordination of (*R*)-homocitrate and citrate to Mo via two hydroxyl groups [19], [20], we selected organic molecules with hydroxyl groups in varying orientation for this screening process. Finally, we analysed the reconstitution of apo-NifDK with extracted M-cluster containing citrate or isocitrate using biochemical and spectroscopic methods.

5.2 Materials and Methods

Reagents and chemicals were purchased from Sigma-Aldrich and Fisher Scientific, unless stated otherwise. Protein work was performed in an argon atmosphere, with an oxygen concentration of < 5 ppm.

Strains and cell growth

A. vinelandii strains expressing His-tagged $NifDK^{WT}$ (YM13A) [21], His-tagged apo-NifDK (Δ*nifB* NifDK; YM7A) [7] and His-tagged NifEN (DJ1041) [22] were previously constructed. The bacteria were grown in 180 L batches using a 250 L New Brunswick fermenter (New Brunswick Scientific) in Burke's minimal medium, containing additional 2 mM ammonium acetate as described elsewhere [21], [23], [24]. The bacteria were allowed to grow into the late exponential phase, when they were harvested using a flowthrough centrifugal harvester (Cepa). The cell mass was washed using a 50 mM Tris-HCl (pH 8.0) buffer. The His-tagged proteins were purified using immobilized metal affinity chromatography, while the non-

tagged NifH protein was purified using anion-exchange and size-exclusion chromatography. Both procedures were previously published [21]–[23].

Activity assays

The *in vitro* maturation of M-cluster variants on NifEN as well as the reconstitution of Δ*nifB* NifDK were performed as previously described [13], [25], [26]. All activity assays were performed as published in the past [27]. Hydrocarbon products were assessed as previously described [2], [28]. Formed hydrogen was assessed as published earlier [29].

M-cluster extraction

In vitro maturation of M-cluster variants on NifEN was performed as previously reported [12], [13]. The His-tagged NifEN protein was subsequently purified using immobilized metal affinity chromatography. The M-cluster variants were extracted from NifEN by using DEAE-cellulose and DMF, as described previously [11]. The sodium dithionite ($Na_2S_2O_4$) concentration in all buffers was kept at 0.5 mM.

EPR spectroscopy

EPR sample preparation was performed in a Vacuum Atmospheres dry box at oxygen levels < 4 ppm. All samples were prepared in buffer containing 25 mM Tris-HCl (pH 8.0), 10 % glycerol and 2 mM sodium dithionite ($Na_2S_2O_4$). The M-cluster variants were added to the Δ*nifB* NifDK protein and the samples were incubated for 40 min at room temperature. After spin concentration at 6,000 x *g*, 10 °C for 15 min, the reconstituted protein samples were adjusted to a concentration of 20 mg/mL and subsequently flash frozen in liquid nitrogen. EPR spectra were taken using a Bruker ESP 300 Ez spectrophotometer (Bruker) interfaced with an Oxford Instruments ESR-9002 liquid helium continuous flow cryostat. All spectra were taken in perpendicular mode at a temperature of 10 K and a microwave power of 5 mW.

5.3 Results

Utilizing a modified *in vitro* maturation of M-cluster on NifEN, a series of small organic acids were provided separately to the solution along with Mo, enabling the formation of M-cluster variants containing different organic ligands (Scheme 5.1, A; where X = organic acid tested) [13], [17], [25]. Subsequently, these M-cluster variants on NifEN could be used to reconstitute apo-NifDK, potentially enabling the reduction of C_2H_2 to C_2H_4 (Scheme 5.1, B). The organic acids selected for the reduction reaction were: (*R*)-homocitrate, isocitrate, α-ketoglutarate, malate, malonate, tartrate, and mandelate (Figure 5.1). Of these, only (*R*)-homocitrate, isocitrate, and mandelate showed C_2H_4 formation from reconstitution with apo-NifDK and the modified NifEN species (Table 5.1)

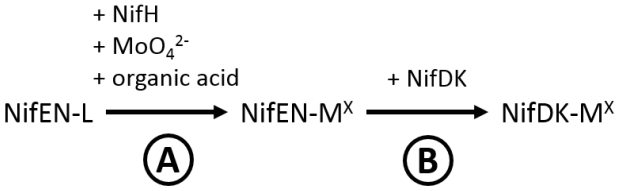

Scheme 5.1

Table 5.1 In vitro screening of organic ligands for M-cluster maturation: *Presented are the results of C_2H_2-reduction by reconstituted NifDK after M-cluster maturation on NifEN, using different organic acids during the maturation. Samples contained 0.15 mg reconstituted NifDK in a total volume of 1 mL with 25 mM Tris-HCl pH 8. Samples were incubated at 30 °C for 8 minutes. The C_2H_4 formation is displayed in nmol C_2H_4 x min^{-1} x mg $protein^{-1}$.*

Organic ligand	nmol C_2H_4/min/mg protein
(*R*)-homocitrate	307 ± 9.2
isocitrate	14.3 ± 2.7
α-ketoglutarate	0.5 ± 1.4
malonate	0.12 ± 0.34
malate	0.1 ± 0.06
tartrate	0.1 ± 0.04
mandelate	3.9 ± 0.19

These data alone are not conclusive. An absence of C_2H_2-reduction by NifDK could be attributed to either an incomplete M-cluster, lacking any organic ligand, or the incapability of

the reconstituted NifDK to reduce C_2H_2 with the respective organic molecule. However, a more general assessment of the compatibility of the organic molecules to form an active M-cluster can be made. α-ketoglutarate and malonate both possess multiple hydroxyl groups (Figure 5.1), but were not able to enable formation of catalytically active M-cluster. One potential explanation is that both hydroxyl groups of these ligands are part of carboxyl groups. In both (*R*)-homocitrate and citrate, only one hydroxyl group that coordinates the ligand to Mo is part of a carboxyl group, while the second hydroxyl group is not (Figure 5.1) [19], [20]. Malate, tartrate and mandelate all contain at least one carboxyl group with a hydroxyl group on the neighbouring C-atom, the same pattern found on (*R*)-homocitrate and citrate (Figure 5.1). Yet, malate and tartrate do not allow for a catalytically active M-cluster to be formed. Inclusion of mandelate resulted in a minor C_2H_2-reduction by NifDK. This activity was still lower than those measured with (*R*)-homocitrate and isocitrate and could potentially be attributed to the bulky phenyl-group of mandelate which might impede the insertion of the formed M-cluster (M-cluster^{Man}) into the active site of NifDK.

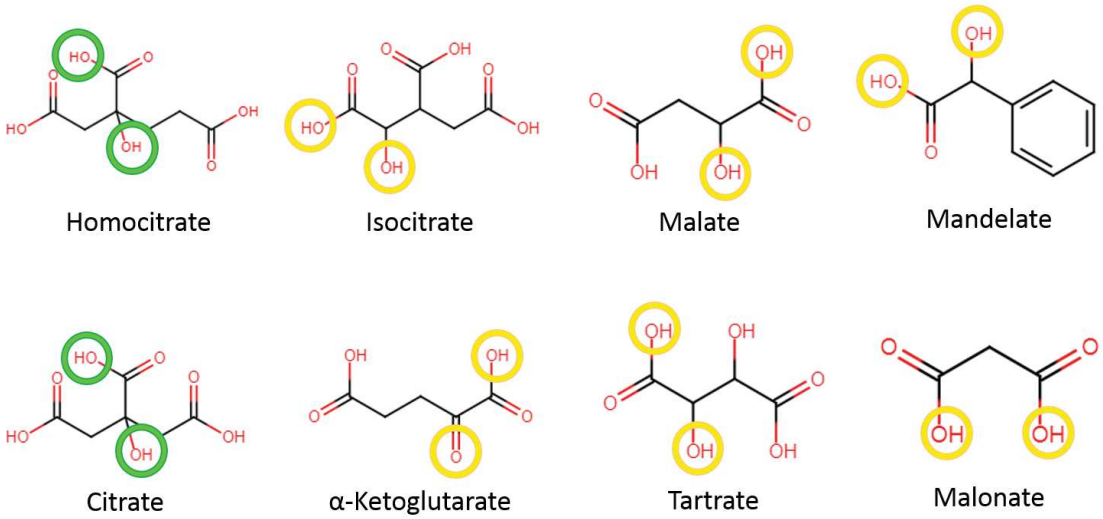

Figure 5.1 Organic acids used in M-cluster maturation: *Displayed are the structures of the small organic acids used in this study for M-cluster maturation. The hydroxyl-groups of (R)-homocitrate and citrate previously shown to coordinate to the Mo-atom are highlighted in green* [19], [20]. *The reactive groups of other organic acids hypothesised to potentially coordinate to the Mo-atom of the M-cluster are highlighted in yellow.*

The insertion funnel for the M-cluster on NifDK is relatively narrow and gated by two histidine (His) residues (His-α247 and His-α451) [26], [30]. These His residues provide a positive charge to the insertion funnel, attracting the negatively charged M-cluster, containing the negatively charged organic ligand (*R*)-homocitrate (or citrate under special circumstances) [26], [31]. Mandelate possess a lower overall charge (-1) compared to (*R*)-homocitrate and citrate (-3 for both). This charge difference results in a less negatively charged M-cluster^{Man}, which could impede the reception of this cluster by the positively charged His residues. Furthermore, the phenyl ring of mandelate would pose a steric challenge compared to (*R*)-homocitrate when the insertion funnel region has critical large His residue.

In an attempt to facilitate the incorporation of mandelate-containing M-cluster into apo-NifDK, a protein variant that contained the mutations αH247A and αH451A (Δ*nifB* NifDK$^{\alpha H247A/\alpha H451A}$) was used for reconstitution experiments. Analysis of this protein variant

previously showed lower M-cluster incorporation into apo-NifDK and consequently lower activity rates of the reconstituted NifDK enzyme [30]. The effect of the double mutation Δ*nifB* NifDK$^{\alpha H247A/\alpha H451A}$ on the capability to incorporate M-cluster variants with different organic ligands was assessed analogously to the previous experiments [13], [17], [25]. The resulting activities of the reconstituted Δ*nifB* NifDK$^{\alpha H247A/\alpha H451A}$ are presented in Table 5.2.

Table 5.2 C_2H_2-redcution by reconstituted Δ*nif*B NifDK$^{\alpha H247A/\alpha H451A}$ with M-cluster variants: *Presented are the rates of C_2H_4-formation from C_2H_2 by Δ*nifB *NifDK$^{\alpha H247A/\alpha H451A}$ after reconstitution with M-cluster containing (R)-homocitrate, isocitrate or mandelate as the organic ligand. Samples contained 0.15 mg reconstituted NifDK in a total volume of 1 mL with 25 mM Tris-HCl pH 8. Samples were incubated at 30 °C for 8 minutes. The C_2H_4 formation is displayed in nmol C_2H_4 x min^{-1} x mg protein^{-1}.*

Organic ligand	nmol C_2H_4/min/mg protein
(*R*)-homocitrate	37.3 ± 0.62
isocitrate	10.6 ± 0.31
mandelate	2.7 ± 0.05

All three organic ligands used resulted in lower activity than observed in previous experiments with Δ*nifB* NifDK (Table 5.1). This can be attributed to either the His residues' crucial role in the incorporation of M-cluster in general or the role both His residues play in retaining the M-cluster within the active site of NifDK. The low activity of Δ*nifB* NifDK$^{\alpha H247A/\alpha H451A}$ reconstituted with M-cluster^{Man} indicates that the cluster is not getting inserted or is not being retained. This suggests that a steric hindrance of αH247 and αH451 is not critically affecting the insertion of M-cluster^{Man} and that there are other factors which prevent effective catalysis of Δ*nifB* NifDK reconstituted with M-cluster^{Man}. Because citrate and isocitrate provided the best results from the screening, these two molecules will be used for the following investigations of alternative organic ligands for M-cluster maturation.

Previous *in vitro* maturation experiments with different organic ligands contained both His-tagged NifEN and His-tagged Δ*nifB* NifDK [17], complicating a spectroscopic analysis of the

reconstituted NifDK enzyme because the separation of NifDK from NifEN is difficult due to the similar size of both proteins (NifD: 55 kDa, NifK: 50 kDa; NifE: 52 kDa, NifN: 49 kDa). While NifDK containing wild-type M-cluster (with (*R*)-homocitrate) or M-cluster^{Cit} (with citrate) can be formed *in vivo* and isolated from *Azotobacter vinelandii* (*A. vinelandii*) from wildtype or Δ*nifV* background, respectively, the NifDK containing M-cluster^{Isocit} has only been formed in *in vitro* experiments [1], [17]. A large scale *in vitro* maturation of M-cluster with (*R*)-homocitrate, citrate or isocitrate on NifEN was performed, followed by isolation of the formed M-cluster variants, as described by Wink *et al.* [11]. The isolated M-cluster variants, M-cluster^{Homocit}, M-cluster^{Cit} and M-cluster^{Isocit}, were used for reconstitution of Δ*nifB* NifDK with subsequent activity assessment. All three variants of the *in vitro* matured M-cluster facilitated the reduction of C_2H_2 to C_2H_4 (Table 5.3). Only Δ*nifB* NifDK reconstituted with M-cluster^{Isocit} was able to reduce C_2H_2 to C_2H_6, at a low rate (Table 5.3). This reaction is usually only observed with the alternative V- and Fe-nitrogenases, but not with Mo-nitrogenase [4].

Table 5.3 C_2H_2 reduction by ΔnifB NifDK, reconstituted with isolated M-cluster variants: *Presented are the rates of formed C_2H_4 (ethylene), C_2H_6 (ethane) and H_2 (hydrogen) in an argon atmosphere containing 10 % C_2H_2 (acetylene). The rates are presented as nmol product x min^{-1} x mg protein^{-1}. The M-cluster variants were formed by L-cluster maturation on NifEN with (R)-homocitrate, citrate or isocitrate as the organic ligand. The M-cluster variants were then extracted from re-purified NifEN and used for reconstitution of ΔnifB NifDK. M-cluster extracted from NifDK was used as a positive control. Samples contained 0.15 mg reconstituted NifDK in a total volume of 1 mL with 25 mM Tris-HCl pH 8. Samples were incubated at 30 °C for 8 minutes.*

	Acetylene[a]		
	Ethylene[b]	Ethane[b]	Hydrogen[b]
Δ*nifB* NifDK + M-cluster^{WT}	1450 ± 20	0 ± 0	156.5 ± 3.5
Δ*nifB* NifDK + M-cluster^{Homocit}	144.3 ± 0.3	0 ± 0	70.1 ± 3.3
Δ*nifB* NifDK + M-cluster^{Cit}	82.4 ± 2.74	0 ± 0	62.2 ± 4.6
Δ*nifB* NifDK + M-cluster^{Isocit}	100.1 ± 3.75	1.7 ± 0.1	141.6 ± 2.3

a: Denotes substrate (10 % C_2H_2, balance Ar)
b: Denotes product

The Δ*nifB* NifDK enzyme, reconstituted with the M-cluster variants, was also analysed by EPR spectroscopy (Figure 5.2). The addition of M-cluster^{Homocit} led to a shift from an *S* = 1/2 signal of the Δ*nifB* NifDK protein (Figure 5.2, green spectrum) to a *S* = 3/2 signal, which is characteristic for nitrogenase containing M-cluster (Figure 5.2, purple spectrum) [6], [8]. M-cluster^{Cit}-reconstituted Δ*nifB* NifDK also displays an *S* = 3/2 signal with the same *g*-values of 4.31 and 3.67, however at a lower intensity (Figure 5.2, blue spectrum). The presence of the *S* = 1/2 signal with *g*-values of 2.06 and 1.94 is similar to that observed from Δ*nifB* NifDK. The M-cluster^{Isocit} in Δ*nifB* NifDK barely changes the spectrum and results in an *S* = 1/2 signal with the same *g*-values as Δ*nifB* NifDK (Figure 5.2, red spectrum).

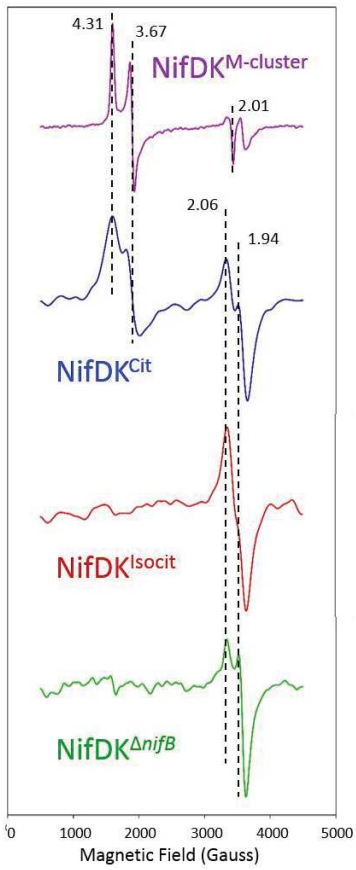

Figure 5.2 EPR analysis of ΔnifB NifDK reconstituted with M-cluster variants: *Displayed are the EPR spectra of ΔnifB NifDK reconstituted with M-cluster (purple), M-cluster^{Cit} (blue), and M-cluster^{Isocit}. An EPR spectrum of untreated ΔnifB NifDK (green) is shown at the bottom. The spectra were collected in perpendicular-mode at 10 K and 5 mW. The g-values are indicated by dashed lines and labelled at the top of the respective dashed line.*

5.4 Discussion

This chapter explores the effects that the organic ligand has on the reactivity and properties of the M-cluster of nitrogenase. The coordination pattern by which (*R*)-homocitrate and citrate are ligated to the Mo-atom of the M-cluster is the same for both ligands: two hydroxyl-groups, one as part of a carboxyl-group and the other bound to a neighbouring C-atom [19], [20]. The results previously obtained with isocitrate as part of the M-cluster indicate that the incorporation of other ligands into the M-cluster is generally possible [17]. Based on this, small organic acids were selected to assess their potential to be integrated into the M-cluster in *in vitro* maturation experiments. Tartrate, malate and mandelate all possess a carboxyl-group with a hydroxyl-group on the neighbouring C-atom, the same pattern by which (*R*)-homocitrate and citrate coordinate to the Mo-atom of the M-cluster (Figure 5.1). Tartrate even possess this pattern twice within the molecule. These groups were expected to allow an interaction with the Mo-atom and the formation of a reactive M-cluster. α-ketoglutarate possesses a carboxyl-group with a ketone-group on the neighbouring C-atom. This varies from the established coordination pattern of (*R*)-homocitrate and citrate and provides a control for the requirement of a neighbouring hydroxyl-group to the carboxyl-group of the ligand (Figure 5.1). Malonate offers two carboxyl-groups, spaced by one C-atom, for potential coordination to the Mo-atom. It thereby displays another control that does not contain a reactive group immediately next to a carboxyl-group (Figure 5.XX).

Among the selected candidate molecules, α-ketoglutarate, malonate, tartrate, and malate all failed to enable reactivity of Δ*nifB* NifDK. Both α-ketoglutarate and malonate might be unable to accommodate binding to the M-cluster. For malonate, the lack of a hydroxyl-group on the neighbouring C-atom of the carboxyl-group could here be the reason (Figure

5.1). The two terminal carboxyl-groups combined are unable to facilitate the binding of the ligand to the M-cluster. α-ketoglutarate does possess a ketone-group on the neighbouring C-atom of the carboxyl-group (Figure 5.1). Although ketone-groups are polar, with a nucleophilic O-atom and an electrophilic C-atom, and able to form hydrogen-bonds, the interaction via this group, together with the hydroxyl-group of the neighbouring carboxyl-group, appears to be insufficient to coordinate to the Mo-atom of the M-cluster. Therefore, it is likely that both, α-ketoglutarate and malonate, were excluded from incorporation into M-cluster on NifEN during the maturation process.

Malate offers a carboxyl-group with a hydroxyl-group on the neighbouring C-atom (Figure 5.1), yet it is also unable to accommodate appropriate binding to the M-cluster. The reason could be not enough additional reactive groups within the molecule to allow interactions with surrounding amino acids of NifDK. (*R*)-homocitrate not only coordinates to the Mo-atom of the M-cluster, but is also close enough to a glutamine residue (αQ191; 2.9 Å) and a backbone N-atom of an isoleucine residue (αI425; 2.8 Å) to form hydrogen-bonds via two additional carboxyl-groups (Figure 5.3). Malate only possesses one additional carboxyl-group to form hydrogen-bonds with either αQ191 or αI425. Which of these two hydrogen-bonds is established would depend on the conformation malate takes within the M-cluster-binding pocket. However, this conformation does not enable reactivity of reconstituted Δ*nifB* NifDK. Both carboxyl-groups of tartrate have a hydroxyl-group on the neighbouring C-atom, which would allow either side of the molecule to interact with the M-cluster. But similar to malate, only one other carboxyl-group is then able establish hydrogen-bonds with either αQ191 or αI425. Ultimately, also for tartrate, neither conformation enables reactivity of reconstituted Δ*nifB* NifDK. However, it cannot be ruled out that incorporation of any of these

two molecules, malate and tartrate, into the M-cluster has prohibited the insertion of the M-cluster variant into apo-NifDK.

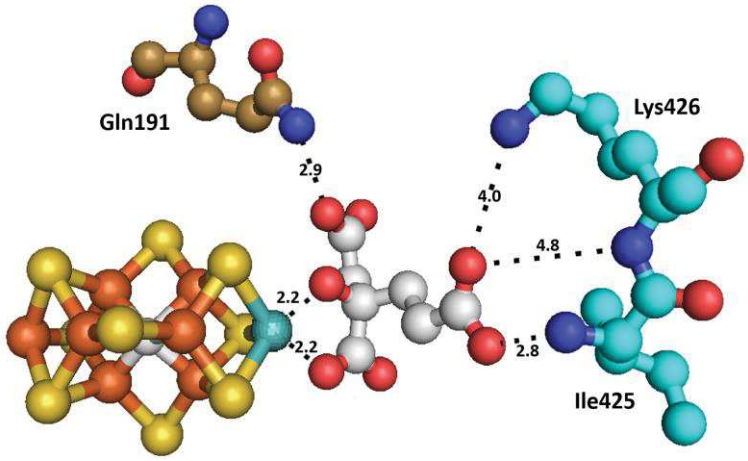

Figure 5.3 (R)-homocitrate interactions within the active site of NifDK: *Displayed is the M-cluster within the active site of NifDK together with three amino acids in close proximity to (R)-homocitrate. Potential interactions of (R)-homocitrate with the amino acids and the Mo-atom are indicated by dashed lines, labelled with the distances in Å. Elements are presented in different colours: carbon (grey), nitrogen (blue), oxygen (red), sulphur (yellow), iron (dark orange) molybdenum (teal); I425 and K426 at the back of the active site are presented in light blue, Q191 above the M-cluster is presented in brown.*

The inclusion of mandelate in the *in vitro* maturation of M-cluster resulted in low C_2H_2-reducing activity of reconstituted Δ*nifB* NifDK. The carboxyl-group and the hydroxyl-group on the neighbouring C-atom would be the obvious reactive groups to coordinate to the Mo-atom of the M-cluster. The remaining phenyl-group of the molecule is not conducive for hydrogen-bond formation with either αQ191 or αI425, but the electron density of its π-system could be enough to stabilise the molecule within the M-cluster-binding pocket. One potential way to improve the interaction with αQ191 and αI425 is the halogenation of the phenyl-group. This would establish a greater negative charge and allow for stronger interactions with αQ191 and αI425. Depending on the position of the halogen on the phenyl-group, either of the two amino acids could be targeted for interactions, which could give further insights into the relevance of the individual interactions. Furthermore, the αH247A and αH451A mutations did not affect

the C_2H_2-reducing activity of M-cluster^{Man}-reconstituted Δ*nifB* NifDK. This suggests that the two His residues are not sterically preventing the M-cluster^{Man} from being inserted into the active site of NifDK.

The ability of Δ*nifB* NifDK reconstituted with extracted M-cluster^{Cit} or M-cluster^{Isocit} to reduce C_2H_2 to C_2H_4 is in line with previous results of *in vitro* formed NifDK^{Cit} and NifDK^{Isocit} [17]. Also the reduction of C_2H_2 to C_2H_6 could be observed after reconstitution with extracted M-cluster^{Isocit}. These results indicate that functional M-cluster^{Cit} and M-cluster^{Isocit} can be extracted from NifEN and that these M-cluster variants can be integrated into apo-nitrogenase.

The *S* = 3/2 signal of the M-cluster^{Cit}-reconstituted NifDK displays the same *g*-values as regular NifDK (4.31 and 3.67). This indicates that the inclusion of citrate in the M-cluster leads to spin properties similar to those of regular M-cluster with homocitrate. This has also been observed for NifDK^{Cit}, formed *in vivo* in a Δ*nifV* background in *A. vinelandii* [17]. The *S* = 1/2 signal with *g*-values of 2.06 and 1.94 resembles the pattern found in Δ*nifB* NifDK, hinting at an incomplete reconstitution of the Δ*nifB* NifDK population in the sample. The *S* = 1/2 itself could emerge from unmatured P-cluster, remaining in the state of two Fe_4S_4 clusters, or subpopulations of the P-cluster in a different oxidation state than the diamagnetic DT-reduced P^N state [8], [23], [32]. This highlights that M-cluster^{Cit} is not the ideal cofactor for NifDK and is inserted with a lower efficiency than regular M-cluster.

Reconstitution of Δ*nifB* NifDK with M-cluster^{Isocit} resulted only in an *S* = 1/2 signal with the same *g*-values as M-cluster^{Cit}-reconstituted NifDK and Δ*nifB* NifDK (2.06 and 1.94). No *S* = 3/2 signal is observed under these conditions. This could be attributed to a reconstitution rate that is even lower than the one of M-cluster^{Cit} or spin properties of the M-cluster^{Isocit} that

render it diamagnetic and thereby EPR-silent. A combination of EPR-spectroscopy, inductively-coupled-plasma-optical-emission-spectroscopy (ICP-OES), and protein concentration analysis can be utilized to determine the M-cluster^{Isocit}-incorporation rate relative to the protein concentration. From this, conclusions about the contribution of the M-cluster^{Isocit} to the EPR-spectrum can be drawn to further understand the effect the organic ligand has on the electronic properties of the protein. The remaining S = 1/2 signal could stem from unmatured P-cluster or P-cluster in oxidation states other than P^N, as described above [8], [23], [32]. Taking together this difference in the EPR spectrum with the ability of NifDK^{Isocit} to reduce C_2H_2 to C_2H_6, further than regular NifDK or NifDK^{Cit}, and to reduce CO to more and longer hydrocarbons than NifDK and NifDK^{Cit} [17], hint at different properties of the M-cluster^{Isocit} overall. These properties could be due to a different conformation of isocitrate as the organic ligand around the M-cluster. Density functional theory (DFT) calculations suggest that isocitrate orients itself towards the M-cluster (Figure 5.4), instead of αI425 at the opposite end of the binding pocket (M. Stiebritz, personal communication). In this conformation, one carboxyl-group reaches towards a proposed substrate binding site on the M-cluster [33]. This additional reactive group in close proximity to the substrate could provide an improved proton delivery during the catalysis of C_2H_2 and allow the advanced reduction to C_2H_6. This reaction is usually not observed with Mo-nitrogenase, but V- and Fe-nitrogenase [34], [35]. Further research on the mechanism of alternative nitrogenases is required to unravel the reason for the different reductive abilities of the enzymes. The finding of C_2H_6 formation from C_2H_2 and an increased hydrocarbon formation from CO by a Mo-nitrogenase variant containing M-cluster^{Isocit} hints at the general ability of the Mo-nitrogenase protein scaffold to support these reactions [17]. Results from EPR-spectroscopy of Δ*nifB* NifDK reconstituted with M-cluster^{Isocit} showed different electronic properties, compared to wild-type NifDK. Additional analysis of

Δ*nifB* NifDK reconstituted with M-cluster^{Isocit} is necessary to confirm the conformation of isocitrate within the active site and its contribution to a changed reductive ability of nitrogenase.

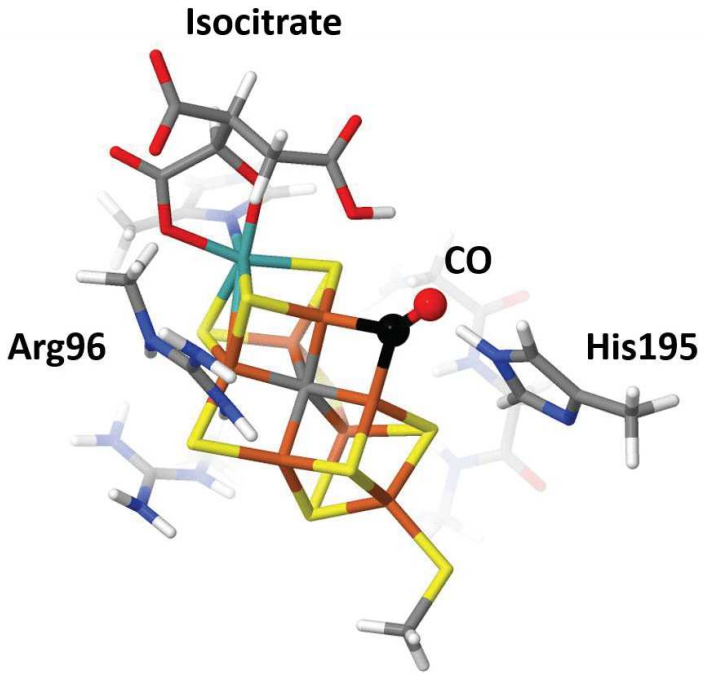

Figure 5.4 Prediction of isocitrate conformation at the M-cluster by DFT-calculations: *Displayed is a potential conformation isocitrate at the M-cluster, based on DFT-calculations (Calculations based on PDB: 4TKU* [33]*; structural optimization, DFT: TPSS/def-SV(P), performed by Dr. Martin Stiebritz (personal communication)). Elements are presented in different colours: carbon (grey), carbon of bound CO-moiety (black), nitrogen (blue), oxygen (red), hydrogen (white), sulphur (yellow), iron (dark orange) molybdenum (teal).*

5.5 Acknowledgments

I want to thank Dr. Kazuki Tanifuji for his technical help throughout this project. I also thank Dr. Martin Stiebritz for performing and allowing me to use the DFT calculations included in the discussion section.

5.6 References

[1] B. K. Burgess and D. J. Lowe, “Mechanism of molybdenum nitrogenase,” *Chem. Rev.*, vol. 96, no. 7, pp. 2983–3011, Nov. 1996.

[2] C. C. Lee, Y. Hu, and M. W. Ribbe, “Vanadium nitrogenase reduces CO,” *Science*. 2010.

[3] Y. Hu, C. C. Lee, and M. W. Ribbe, “Extending the carbon chain: Hydrocarbon

formation catalyzed by vanadium/molybdenum nitrogenases," *Science (80-.).*, vol. 333, no. 6043, pp. 753–755, Aug. 2011.

[4] A. J. Jasniewski, C. C. Lee, M. W. Ribbe, and Y. Hu, "Reactivity, Mechanism, and Assembly of the Alternative Nitrogenases," 2020.

[5] L. C. Seefeldt *et al.*, "Reduction of Substrates by Nitrogenases," 2020.

[6] T. D. Paustian, V. K. Shah, and G. P. Roberts, "Apodinitrogenase: Purification, Association with a 20-Kilodalton Protein, and Activation by the Iron-Molybdenum Cofactor in the Absence of Dinitrogenase Reductase," *Biochemistry*, vol. 29, no. 14, pp. 3515–3522, Apr. 1990.

[7] Y. Hu *et al.*, "Nitrogenase reactivity with P-cluster variants," *Proc. Natl. Acad. Sci. U. S. A.*, vol. 102, no. 39, pp. 13825–13830, Sep. 2005.

[8] J. Christiansen, P. J. Goodwin, W. N. Lanzilotta, L. C. Seefeldt, and D. R. Dean, "Catalytic and biophysical properties of a nitrogenase apo-MoFe protein produced by a nifB-deletion mutant of Azotobacter vinelandii," *Biochemistry*, 1998.

[9] A. W. Fay, C. C. Lee, J. A. Wiig, Y. Hu, and M. W. Ribbe, "Protocols for cofactor isolation of nitrogenase," *Methods Mol. Biol.*, vol. 766, pp. 239–248, 2011.

[10] S.-S. Yang *et al.*, "Iron-Molybdenum Cofactor from Nitrogenase - Modified Extraction Methods as Probes for Composition," 1982.

[11] D. A. Wink, P. A. McLean, A. B. Hickman, and W. H. Orme-Johnson, "A New Method for Extraction of Iron-Molybdenum Cofactor (FeMoco) from Nitrogenase Adsorbed to DEAE-cellulose. 2. Solubilization of FeMoco in a Wide Range of Organic Solvents," *Biochemistry*, vol. 28, no. 24, pp. 9407–9412, 1989.

[12] Y. Hu *et al.*, "FeMo cofactor maturation on NifEN," *Proc. Natl. Acad. Sci.*, 2006.

[13] J. M. Yoshizawa *et al.*, "Optimization of FeMoco maturation on NifEN," *J. Am. Chem. Soc.*, vol. 131, no. 26, pp. 9321–9325, Jul. 2009.

[14] C. C. Lee, Y. Hu, and M. W. Ribbe, "Catalytic reduction of CN-, CO, and CO2by nitrogenase cofactors in lanthanide-driven reactions," *Angew. Chemie - Int. Ed.*, vol. 54, no. 4, pp. 1219–1222, Jan. 2015.

[15] C. C. Lee, Y. Hu, and M. W. Ribbe, "ATP-independent formation of hydrocarbons catalyzed by isolated nitrogenase cofactors," *Angew. Chemie - Int. Ed.*, vol. 51, no. 8, pp. 1947–1949, Feb. 2012.

[16] J. G. Rebelein, C. C. Lee, M. Newcomb, Y. Hu, and M. W. Ribbe, "Characterization of an M-cluster-substituted nitrogenase VFe protein," *MBio*, 2018.

[17] J. Liedtke, C. C. Lee, K. Tanifuji, A. Jasniewski, M. W. Ribbe, and Y. Hu, "Characterization of a Mo-nitrogenase variant containing a citrate-substituted cofactor," *ChemBioChem*, p. cbic.202000598, Sep. 2020.

[18] M. P. Newcomb *et al.*, "A V-Nitrogenase Variant Containing a Citrate-Substituted Cofactor," *ChemBioChem*, vol. 21, no. 12, pp. 1742–1748, Jun. 2020.

[19] S. M. Mayer, C. A. Gormal, B. E. Smith, and D. M. Lawson, "Crystallographic analysis of

the MoFe protein of nitrogenase from a nifV mutant of Klebsiella pneumoniae identifies citrate as a ligand to the molybdenum of iron molybdenum cofactor (FeMoco)," *J. Biol. Chem.*, vol. 277, no. 38, pp. 35263–35266, Sep. 2002.

[20] J. Kim and D. C. Rees, "Crystallographic structure and functional implications of the nitrogenase molybdenum-iron protein from Azotobacter vinelandii," *Nature*, vol. 360, no. 6404, pp. 553–560, 1992.

[21] Y. Hu, A. W. Fay, B. Schmid, B. Makar, and M. W. Ribbe, "Molecular insights into nitrogenase FeMoco insertion: TRP-444 of MoFe protein α-subunit locks FeMoco in its binding site," *J. Biol. Chem.*, vol. 281, no. 41, pp. 30534–30541, Oct. 2006.

[22] Y. Hu, A. W. Fay, and M. W. Ribbe, "Identification of a nitrogenase FeMo cofactor precursor on NifEN complex," *Proc. Natl. Acad. Sci. U. S. A.*, vol. 102, no. 9, pp. 3236–3241, Mar. 2005.

[23] M. W. Ribbe, Y. Hu, M. Guo, B. Schmid, and B. K. Burgess, "The Femoco-deficient MoFe protein produced by a nifH deletion strain of Azotobacter vinelandii shows unusual P-cluster features," *J. Biol. Chem.*, vol. 277, no. 26, pp. 23469–23476, Jun. 2002.

[24] Y. Hu *et al.*, "Nitrogenase reactivity with P-cluster variants," *Proc. Natl. Acad. Sci.*, 2005.

[25] Y. Hu *et al.*, "FeMo cofactor maturation on NifEN," *Proc. Natl. Acad. Sci. U. S. A.*, vol. 103, no. 46, pp. 17119–17124, Nov. 2006.

[26] B. Schmid *et al.*, "Structure of a cofactor-deficient nitrogenase MoFe protein," *Science (80-.).*, vol. 296, no. 5566, pp. 352–356, Apr. 2002.

[27] B. K. Burgess, D. B. Jacobs, and E. I. Stiefel, "Large-scale purification of high activity Azotobacter vinelandII nitrogenase.," *Biochim. Biophys. Acta*, vol. 614, no. 1, pp. 196–209, Jul. 1980.

[28] N. S. Sickerman *et al.*, "Reduction of C1, substrates to hydrocarbons by the homometallic precursor and synthetic mimic of the nitrogenase cofactor," *J. Am. Chem. Soc.*, vol. 139, no. 2, pp. 603–606, Jan. 2017.

[29] N. Gavini and B. K. Burgess, "FeMo cofactor synthesis by a nifH mutant with altered MgATP reactivity," *J. Biol. Chem.*, vol. 267, no. 29, pp. 21179–21186, 1992.

[30] A. W. Fay, Y. Hu, B. Schmid, and M. W. Ribbe, "Molecular insights into nitrogenase FeMoco insertion - The role of His 274 and His 451 of MoFe protein α subunit," *J. Inorg. Biochem.*, vol. 101, no. 11–12, pp. 1630–1641, Nov. 2007.

[31] J. Liang, M. Madden, V. K. Shah, and R. H. Burris, "Citrate Substitutes for Homocitrate in Nitrogenase of a nifV Mutant of Klebsiella pneumoniaet," 1990.

[32] N. Gavini, L. Ma, G. Watt, and B. K. Burgess, "Purification and Characterization of a FeMo Cofactor-Deficient MoFe Protein," *Biochemistry*, vol. 33, no. 39, pp. 11842–11849, Oct. 1994.

[33] T. Spatzal, K. A. Perez, O. Einsle, J. B. Howard, and D. C. Rees, "Ligand binding to the FeMo-cofactor: Structures of co-bound and reactivated nitrogenase," *Science (80-.).*,

vol. 345, no. 6204, pp. 1620–1623, Sep. 2014.

[34] R. N. Pau, M. E. Eldridge, D. J. Lowe, L. A. Mitchenall, and R. R. Eady, “Molybdenum-independent nitrogenases of Azotobacter vinelandii: A functional species of alternative nitrogenase-3 isolated from a molybdenum-tolerant strain contains an iron-molybdenum cofactor,” *Biochem. J.*, vol. 293, no. 1, pp. 101–107, Jul. 1993.

[35] D. Sippel *et al.*, “Production and isolation of vanadium nitrogenase from Azotobacter vinelandii by molybdenum depletion,” *J. Biol. Inorg. Chem.*, vol. 22, no. 1, pp. 161–168, Jan. 2017.